

**THE EFFECT OF SPATIAL RESOLUTION IN REMOTE
SENSING ESTIMATES OF TOTAL EVAPORATION IN THE
UMNGENI CATCHMENT**

C Shoko

Submitted in fulfilment of the requirements for the degree of Msc Bioresources Systems

Supervisor: DJ Clark

Co-supervisors: H Bulcock and MG Mengistu

Centre for Water Resources Research

School of Engineering

University of KwaZulu-Natal

Pietermaritzburg

December 2014

ABSTRACT

The estimation of total evaporation plays a vital role in water resources monitoring and management, especially in water-limited environments. In South Africa, the increasing water demand, due to population growth and economic development, threatens the long-term water supply. This, therefore, underscores the need to account for water by different consumers, for well-informed management, allocation and future planning. Currently, there are different methods (*i.e.* ground-based and remote sensing-based methods), which have been developed and implemented to quantify total evaporation at different spatial and temporal scales. However, previous studies have shown that ground-based methods are inadequate for understanding the spatial variations of total evaporation, within a heterogeneous landscape; they only represent a small area, when compared to remotely sensed methods. The advent of remote sensing therefore provides an invaluable opportunity for the spatial characterization of total evaporation at different spatial scales.

This study is primarily aimed at estimating variations of total evaporation across a heterogeneous catchment in KwaZulu-Natal, South Africa, using remote sensing data. The first part provides an overview of total evaporation, its importance within the water balance and consequently in the management of water resources. It also covers various methods developed to estimate total evaporation, highlighting their applications, limitations, and finally, the need for further research.

Secondly, the study determines the effect of sensor spatial resolution in estimating variations of total evaporation within a heterogeneous uMngeni Catchment. Total evaporation estimates were derived, using multispectral 30 m Landsat 8 and 1000 m MODIS, based on the Surface Energy Balance (SEBS) model. The results have shown that different sensors, with varying spatial resolutions, have different abilities in representing variations of total evaporation at catchment scale. It was found that Landsat-based estimates were significantly different ($p < 0.05$) from MODIS.

The study finally estimates spatial variations of total evaporation from Landsat 8 and MODIS datasets for the uMngeni Catchment. It was found that the Landsat 8 dataset has greater potential for the detection of spatial variations of total evaporation, when compared to the

MODIS dataset. For instance, MODIS-based daily total evaporation estimates did not show any significant difference across different land cover types (One way ANOVA; $F_{1,924} = 1.412$, $p = 0.186$), when compared to the 30 m Landsat 8, which yielded significantly different estimates between different land cover types (One way ANOVA; $F_{1,993} = 5.185$, $p < 0.001$). The validation results further indicate that Landsat-based estimates were more comparable to ground-based eddy covariance measurements ($R^2 = 0.72$, with a RMSE of 32.34 mm per month (30.30% of the mean)). In contrast, MODIS performed poorly ($R^2 = 0.44$), with a RMSE of 93.63 mm per month (87.74% of the mean). In addition, land cover-based estimates have shown that, not only does the land cover type have an effect on total evaporation, but also the land cover characteristics, such as areal extent and patchiness.

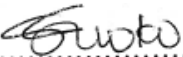
Overall, findings from this study underscore the importance of the sensor type, especially spatial resolution, and land cover type characteristics, such as areal extent and patchiness, in accurately and reliably estimating total evaporation at a catchment scale. It is also evident from the study that the spatial and temporal variations in SEBS inputs (*e.g.*, LAI, NDVI and FVC) and energy fluxes (*e.g.*, R_n) calculated by SEBS for the two sensors can affect the spatial and temporal variations in total evaporation estimates. For instance, spatial variations in total evaporation reflected similar spatial variations in R_n . Areas with high NDVI, FVC and LAI (which denotes dense vegetation cover) tend to have higher total evaporation estimates, compared to areas with lower vegetation cover. In addition, the MODIS sensor at 1000 m spatial resolution showed lower estimates of SEBS inputs with less variability across the catchment. This resulted in lower total evaporation estimates, with less variability, compared to the 30 m Landsat 8.


In addition, with regard to inputs derived from remote sensing, it was found that the spatial variations in total evaporation are not determined by individual variables (*e.g.*, LST), but are influenced by a combination of many biophysical variables, such as LAI, FVC and NDVI. These findings lay a foundation for a better approach to estimate total evaporation using remote sensing for use in the management and allocation of water.


DECLARATION – PLAGIARISM

I *Cletah Shoko*, declare that:

- (i) The research reported in this thesis except where otherwise indicated is my original work,
- (ii) This thesis has not been submitted for any degree or examination at any other University,
- (iii) This thesis does not contain other persons' data, pictures, graphs or other information unless specifically acknowledged as being sourced from other persons.
This thesis does not contain other persons' writing, unless specifically acknowledged as being sourced from other researchers
- (iv) Where other written sources have been quoted, then:
 - (a) their words have been rewritten but the general information attributed to them has been referenced;
 - (b) where their exact words have been used, their writing has been placed inside quotation marks, and referenced.
- (v) Where I have reproduced a publication of which I am an author, co-author or editor, I have indicated in detail which part of the publication was actually written by myself alone and have fully referenced such publications.
- (vi) This thesis does not contain text, graphics or tables copied and pasted from the internet, unless specifically acknowledged, and the source being detailed in the thesis and in the reference section.

Signed: 
Cletah Shoko

Signed: 
Mr DJ Clark
Supervisor

Signed: 
Dr H Bulcock
Co-supervisor

Signed: 
Dr MG Mengistu
Co-supervisor

DECLARATION – PUBLICATIONS

Details of the contribution of publications that form part and/or include research presented in this dissertation including publications in preparation, submitted, in press and published, and details of the contributions of each author to the experimental work and writing of each publication.

Publication 1 – Chapter 4

Shoko C*, Clark DJ, Bulcock H and Mengistu MG (In preparation). The effect of sensor spatial resolution on remote sensing estimates of total evaporation in the uMngeni Catchment, South Africa.

Research for this publication was conducted by C Shoko under the supervision of second, third and fourth authors. This publication was written in its entirety by C Shoko and all data tables, graphs and photos were produced by the same, unless otherwise referenced in the text of the paper. Editing and advice regarding data interpretation was provided by co-authors.

Publication 2 - Chapter 5

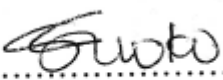
C Shoko*, Clark DJ, Bulcock, H and Mengistu MG. (In preparation). Estimating spatial variations in total evaporation, using multispectral remote sensing data in the uMngeni Catchment, South Africa.

Research for this publication was conducted by C Shoko under the supervision and guidance of second, third and fourth author. This publication was written in its entirety by C Shoko and all data tables, graphs and photos were produced by the same unless otherwise referenced in the text of the paper. Editing and advice regarding data interpretation was provided by co-authors.

PREFACE

The work described in this thesis was carried out within the Centre for Water Resources Research, School of Engineering, University of KwaZulu-Natal, Pietermaritzburg, from July 2013 to November 2014, under the supervision of Mr DJ Clark and co-supervision of Dr H Bulcock and Dr MG Mengistu.

The study represents the original work of the author and has not otherwise been submitted in any form for any degree or diploma to any tertiary institution. Where use has been made of the work of others, it is duly acknowledged in the text.

Signed:.....
Cletah Shoko

ACKNOWLEDGEMENTS

My sincere gratitude goes to my Supervisor, Mr DJ Clark, for the guidance, critical comments and support throughout the study. I appreciate it. I would also like to appreciate the effort of Dr H Bulcock and Dr MG Mengistu, for the assistance, time and guidance they devoted to this research.

More so, I am grateful to the Water Research Commission (WRC), for funding the project, and the Centre for Water Resources Research (CWRR) and School of Engineering within which this research was conducted.

It is my pleasure to extend my gratitude to the South African Weather Services and South African Sugarcane Research Institute, for the provision of meteorological data, as well as Ezemvelo KZN Wildlife, for providing KwaZulu-Natal land cover data. I am grateful to Mr A Clulow for the provision of ground-based total evaporation measurements.

I would like to thank the National Aeronautics Space Administration (NASA) and the United States Geological Survey for the provision of MODIS and Landsat 8 remote sensing data.

Special thanks go to my family, for all the love, moral support and encouragement they gave me throughout my study. To my sister Karen, thank you for your prayers. To my uncle Tinashe, you always tell me that the sky is the limit. I will always cherish it.

To Shadeen Gokool, from UKZN Hydrology and my colleagues at the Dept. of Geography UKZN, Sibanda Mbulisi, Victor Bangamwabo and everyone who have contributed to the completion of this research, thank you very much. To Timothy Dube, my best friend, you always encourage me to work hard and never loss hope. That kept me going. Also many thanks go to Dr Masocha and Prof. Murwira (Geo Dept, UZ) for scientifically grooming me during my undergraduate studies.

Above all, I give thanks to the Almighty God, who gave me the strength and brought this research to completion.

DEDICATION

To my mother

TABLE OF CONTENTS

	Page
ABSTRACT.....	i
DECLARATION – PLAGIARISM.....	iii
DECLARATION – PUBLICATIONS	iv
PREFACE.....	v
ACKNOWLEDGEMENTS.....	vi
DEDICATION.....	vii
TABLE OF CONTENTS.....	viii
LIST OF TABLES.....	xii
LIST OF FIGURES	xiii
ACRONYMS AND ABBREVIATIONS	xv
1. GENERAL INTRODUCTION.....	1
1.1 Aims and Objectives	3
1.2 Thesis Outline	3
1.3 References.....	6
2. REVIEW OF METHODS FOR ESTIMATING TOTAL EVAPORATION.....	8
Abstract	8
2.1 Introduction.....	8
2.2 Estimating Total Evaporation	9
2.2.1 Meteorological methods	9
2.2.2 Remote sensing methods	13
2.2.3 Vegetation indices	14
2.2.4 Surface Energy Balance Index	15
2.2.5 Simplified Surface Energy Balance Index	15
2.2.6 Surface Energy Balance System for Land.....	17
2.2.7 Mapping EvapoTranspiration at High Resolution with Internalized Calibration ...	19
2.2.8 Surface Energy Balance System.....	19
2.2.9 The influence of spatial heterogeneity on total evaporation estimates using remote sensing	25

2.3	Discussion and conclusion.....	27
2.4	References.....	29
3.	OVERVIEW OF METHODOLOGY.....	41
3.1	Introduction.....	41
3.2	SEBS Remote Sensing Inputs.....	41
3.3	SEBS Meteorological Inputs.....	50
3.4	SEBS Outputs.....	55
3.5	Reference Evaporation Estimates.....	61
3.6	Spatial Heterogeneity.....	62
3.7	Validation of Remote Sensing Estimates.....	63
3.8	Discussion and Conclusion.....	63
3.9	References.....	65
4.	THE EFFECT OF SPATIAL RESOLUTION ON REMOTE SENSING ESTIMATES OF TOTAL EVAPORATION IN THE UMNGENI CATCHMENT, SOUTH AFRICA...	67
	Abstract.....	67
4.1	Introduction.....	68
4.2	Materials and Methods.....	70
4.2.1	Study area description.....	70
4.2.2	Surface Energy Balance System model.....	72
4.2.3	Landsat 8 and MODIS data acquisition and calibration.....	72
4.2.4	Atmospheric correction.....	73
4.2.5	SEBS meteorological and ancillary data.....	73
4.2.6	Validation of remote sensing total evaporation estimates.....	74
4.2.7	Statistical analysis.....	74
4.3	Results.....	75
4.3.1	Land cover types within the uMngeni Catchment.....	75
4.3.2	Spatial and temporal variability of total evaporation.....	76
4.3.3	Total evaporation variation between different land cover types.....	80
4.3.4	Validation results.....	83

4.4	Discussion	83
4.4.1	Spatio-temporal variability of total evaporation	84
4.4.2	Total evaporation variations between different land cover types.....	85
4.5	Conclusion	86
4.6	References.....	87
5.	ESTIMATING SPATIAL VARIATIONS OF TOTAL EVAPORATION USING MULTISPECTRAL SENSORS WITHIN THE UMNGENI CATCHMENT, SOUTH AFRICA.....	90
	Abstract	90
5.1	Introduction.....	91
5.2	Materials and Methods.....	93
5.2.1	Study site	93
5.2.2	Data acquisition and pre-processing.....	94
5.2.3	Determination of monthly and annual total evaporation estimates	95
5.2.4	Statistical Analysis	96
5.2.5	Determining spatial characteristics of different land cover types	97
5.3	Results.....	97
5.3.1	Land cover types and distribution within the uMngeni Catchment	98
5.3.2	Spatial characteristics of different land cover types.....	99
5.3.3	Monthly total evaporation estimates	104
5.3.4	Spatial variation of seasonal and annual total evaporation	105
5.3.5	Seasonal total evaporation from different land cover types	108
5.3.6	Annual total evaporation from different land cover types	109
5.3.7	Validation results.....	113
5.4	Discussion.....	113
5.4.1	Seasonal and annual total evaporation estimates	114
5.4.2	Spatial variations of total evaporation across the catchment	114
5.5	Conclusion	116
5.6	References.....	117

6. SYNTHESIS AND RECOMMENDATION.....	122
6.1 Introduction.....	122
6.2 The Effect of Sensor Spatial Resolution on Estimating Total Evaporation.....	122
6.3 Estimating the Spatial Variations in Total Evaporation across a Heterogeneous Catchment using Multispectral Remote Sensing Data.....	123
6.4 Recommendations for Future Studies.....	126
6.5 References.....	127
APPENDIX A Total evaporation estimation flowcharts using MODIS L1B images	128
APPENDIX B Total evaporation estimation flowcharts using Landsat 8 images	131

LIST OF TABLES

	Page
Table 2.1 Summary of the data requirements by different meteorological-based methods ..	10
Table 2.2 Summary of micro-meteorological methods to estimate total evaporation.....	12
Table 2.3 Summary of SEBS applications at different spatial scales.....	22
Table 2.4 Primary landscape metrics used to determine spatial heterogeneity	27
Table 3.1 Meteorological data acquired and used in the study.....	51
Table 3.2 Meteorological data corresponding to satellite overpass used in SEBS model.....	53
Table 3.3 Values used to determine land cover Z_{om} for uMngeni Catchment (after Brutsaert, 2005; Pardalos <i>et al.</i> , 2014; Ramli <i>et al.</i> , 2009; Su, 2006; WMO, 2008)	63
Table 4.1 Estimated total evaporation statistics for the uMngeni Catchment (mm)	76
Table 5.1 Spatial characteristic of different land cover types	100
Table 5.2 Summary of seasonal and annual total evaporation statistics (mm).....	106
Table 5.3 Summary of land cover-based annual total evaporation statistics (mm).....	111

LIST OF FIGURES

	Page
Figure 1.1	Flowchart of thesis structure5
Figure 2.1	S-SEBI principle for deriving evaporative fraction and total evaporation 16
Figure 3.1	SEBS remote sensing inputs for 24 June 2013 (dry season).....43
Figure 3.2	SEBS remote sensing inputs for 23 March 2014 (wet season)46
Figure 3.3	Location of meteorological stations and the validation site.....54
Figure 3.4	DEM for the uMngeni catchment54
Figure 3.5	Average transmissivity of the uMngeni catchment55
Figure 3.6	SEBS outputs for the 24 th of June 201357
Figure 3.7	SEBS outputs for the 23 rd of March 2014.....59
Figure 3.8	Spatial variations of reference evaporation across the catchment 61
Figure 3.9	Spatial variations of reference evaporation across the catchment62
Figure 4.1	Location of the study area.....71
Figure 4.2	Main land cover types within the uMngeni Catchment, EKZNW (2013).....75
Figure 4.3	Spatial and temporal variability of total evaporation from the two sensors79
Figure 4.4	Mean total evaporation between different land cover types82
Figure 4.5	Comparison between remotely-sensed estimates and ground-based measurements.....83
Figure 5.1	Location of the study area and mean annual rainfall (Schulze <i>et al.</i> , 2008).....94
Figure 5.2	Main land cover types within the uMngeni Catchment, EKZNW (2013).....98
Figure 5.3	Land cover types areal extent, EKZNW (2013)99
Figure 5.4	Z_{om} for uMngeni Catchment, derived on the 23 rd of May 2013 from: (a) Landsat 8, (b) MODIS and (c) land cover map 102
Figure 5.5	Landsat 8 (a) and MODIS (b) total evaporation estimates for the 23 rd of May 2013 using Z_{om} derived by SEBS, and Landsat (c) and MODIS (d) total evaporation estimates using Z_{om} derived from uMngeni land cover map 103
Figure 5.6	Monthly mean total evaporation estimates for the catchment for the hydrological year 2013/14 105
Figure 5.7	Spatial variation of seasonal and annual total evaporation 107
Figure 5.8	Land cover-based mean seasonal total evaporation estimates from the two sensors a) Dry season (2013) and (b) Wet season (2013/14)..... 109

Figure 5.9	Land cover-based mean annual total evaporation from the two sensors for the period 2013-2014.....	110
Figure 5.10	Mean annual total evaporation for selected land cover types from the two sensors.....	112
Figure 5.11	Validation of remotely-sensed mean monthly total evaporation with eddy covariance	113

ACRONYMS AND ABBREVIATIONS

AATSR	Advanced Along-Track Scanning Radiometer
AERONET	Aerosol Robotic Network
ANOVA	Analysis Of Variance
ASL	Atmospheric Surface Layer
ASTER	Advanced Spaceborne Thermal Emission and Reflection Radiometer
AVHRR	Advanced Very High Resolution Radiometer
CWSI	Crop Water Stress Index
EVI	Enhanced Vegetation Index
EROS	Earth Resources Observation Systems
EKZNV	Ezemvelo KwaZulu-Natal Wildlife
ETM+	Enhanced Thematic Mapper plus
FVC	Fractional Vegetation Cover
ILWIS	Integrated Land and Water Information System
LAI	Leaf Area Index
MERIS	Medium Resolution Imaging Spectrometer
METRIC	Mapping EvapoTranspiration at High Resolution with Internalized Calibration
MODIS	Moderate Resolution Imaging Spectroradiometer
MOST	Monin-Obukhov Similarity Theory
MSS	Multispectral Scanner
NASA	National Aeronautics and Space Administration
NDVI	Normalized Difference Vegetation Index
NIR	Near Infrared
SAVI	Soil Adjusted Vegetation Index
SAWS	South Africa Weather Services
SASRI	South African Sugarcane Research Institute
SEBI	Surface Energy Balance Index
S-SEBI	Simplified-Surface Energy Balance Index
SEBS	Surface Energy Balance System
SEBAL	Surface Energy Balance Algorithm for Land
SMAC	Simplified Method for Atmospheric Correction

SRTM	Shuttle Radar Topography Mission
SWPN	Strategic Water Partners Network
TM	Thematic Mapper
USGS	United States Geological Survey
VITT	Vegetation Index Temperature Trapezoid
WMA	Water Management Areas

1. GENERAL INTRODUCTION

Water availability has been recognized as a global issue and needs to be consistently quantified to support sustainable use (Doll *et al.*, 2003). Despite the importance of water, the world is far from being water secure, with demand already outstripping supply in many regions (Oki and Kanae, 2006; Zhuwakinyu, 2012). In addition, climate change is posing a threat to global water resources and the projected increase in temperature is most likely to impact the availability of already limited water resources (Doll *et al.*, 2003). In southern Africa, water is increasingly becoming scarce, due to population growth and development (Lange *et al.*, 2007; Zhuwakinyu, 2012). In South Africa, the growing demand for water, coupled with the mostly arid nature of the country has, in some cases, resulted in demand exceeding natural availability (Molobela and Sinha, 2011). Consequently, in more than 50% of the 19 Water Management Areas (WMAs), demand exceeds supply (DWA, 2004). The water disclosure South Africa report (Zhuwakinyu, 2012), predicted that some of the country's most economically important catchment areas will be affected (Zhuwakinyu, 2012), notably the Luvuvhu, Upper Breede and uMngeni Catchments (Summerton *et al.*, 2010; Warburton *et al.*, 2012). In addition, the Strategic Water Partners Network (SWPN) estimates that water demand in South Africa will rise by 52% in the next three decades, while water supply will deteriorate (Zhuwakinyu, 2012). This will increase the competition for water resources within different economic sectors. Therefore, there is a need for sustainable water resource management practices, without jeopardizing economic growth and development.

In order to manage water resources, water accounting plays a fundamental role. Molden (1997) describes water accounting as a method that analyses water consumption, depletion and production within a catchment. This method uses the water balance approach (Molden *et al.*, 2001). Consequently, different water balance components are measured for the analysis of water use, depletion and productivity. The hydrological cycle comprises various components, such as precipitation, runoff, storage and total evaporation. Total evaporation, which is also widely known as evapotranspiration, is one of the key components (second largest after precipitation) in a water balance (Maeda *et al.*, 2011). Total evaporation is one of the processes by which water is depleted from a catchment (Molden and Sakthivadivel, 1999), hence it has an effect on water availability. The accurate spatial and temporal estimation of total evaporation is required for water resources monitoring, management and

planning. In addition, Ershadi *et al.* (2013) also emphasize that there have been on-going efforts in the hydrological and related sciences to accurately estimate total evaporation. More specifically, Jarman *et al.* (2009a) highlighted that, in a semi-arid and water-scarce country like South Africa, which has a large number of consumers of water, it is important to estimate total evaporation with a high degree of accuracy. This becomes fundamental in order to save, secure and guarantee the distribution of water to different consumers in a more sustainable manner. Moreover, water quality is increasingly deteriorating, which may negatively impact on the supply of water (Jarman *et al.*, 2009b). Different methods have therefore been developed to quantify total evaporation at various spatial and temporal scales, based on meteorological observations, micro-meteorological techniques, such as the eddy covariance system and A-Pan, as well as remote sensing.

Although different methods have been developed, the choice of a method depends on the availability of the method or model, data requirements and reliability, as well as its accuracy in mapping the spatial variability of total evaporation. The ground-based methods of estimating total evaporation, although accurate, are impractical for large-scale implementation (Drexler *et al.*, 2004; Li *et al.*, 2009). They are useful for the verification of total evaporation by specific land cover types, but cannot represent the spatial variations of total evaporation (Gibson *et al.*, 2013; Lott and Hunt, 2001). Remote sensing techniques therefore, offer robust, instantaneous and efficient spatial and temporal data useful for the large-scale estimation of total evaporation for the improved management of water resources (Li *et al.*, 2009; Ruhoff *et al.*, 2012).

Although remote sensing products provide a reliable method of estimating total evaporation, the ability of satellite sensors to detect spatial variations of total evaporation within a catchment characterized by various land cover types and climatic conditions requires further investigation. Total evaporation varies spatially and temporally, due to the variations of land cover characteristics and climatic conditions. Understanding the performance of remote sensing datasets and their ability to discriminate spatial variations of total evaporation across a catchment provides an integrated approach for the better management and allocation of water. There is also a need to determine the effect of different land cover types and their contributions to total evaporation within a catchment, for the long-term sustainability of water and its allocation to various consumers within different sectors. It is in the light of this,

that the present study aims to understand spatial variations of total evaporation within a catchment characterized by various land cover types and climatic conditions, using multispectral remote sensing data.

1.1 Aims and Objectives

The main aim of this research was to estimate the spatial variations of total evaporation, using remotely sensed data across the uMngeni Catchment in KwaZulu-Natal, South Africa. More specifically the objectives were to:

- i. determine the effect of varying sensor spatial resolutions (*i.e.* 30-m Landsat 8 and 1000-m MODIS data) on estimating variations of total evaporation for the heterogeneous uMngeni Catchment, and
- ii. determine the spatial variations of total evaporation estimates, using multispectral remote sensing data and the effect of varying land cover characteristics in estimating total evaporation within the uMngeni Catchment.

1.2 Thesis Outline

The structure of this dissertation is presented in six chapters as shown in Figure 1.1. Chapter One provides an introduction to the study, as well as highlighting the main aim of the study.

Chapter Two contains a detailed review of literature on total evaporation estimation. This highlights the various methods of estimating total evaporation, as well as their strengths and weaknesses in the management of water resources. Remote sensing-based approaches for the accurate monitoring of total evaporation and their various challenges are discussed in detail and possible solutions are also suggested.

Chapter Three highlights the general overview of the methodological approach, including data used during the study. It also contains some of the interim results, which are further given in details in chapters Four and Five.

Chapter Four is the first publishable paper, in which the effect of varying sensor spatial resolution on the remote sensing estimates of total evaporation in the uMngeni Catchment is investigated. This determines if there are any significant differences in total evaporation estimates between two different sensors with varying spatial resolutions across the catchment.

Chapter Five constitutes the second publishable paper, which further investigates spatial variations of total evaporation estimates, using multispectral remote sensing data, within the uMngeni Catchment. The study specifically investigates the spatial variations of total evaporation estimates from two different sensors, as well as determining the effect of land cover characteristics in estimating seasonal and annual total evaporation across the catchment.

Finally, Chapter Six provides a synthesis of the study. This constitutes a summary of major findings and conclusions derived from the preceding chapters. The Chapter also presents the limitations of the study and some relevant recommendations for future studies on the applications of remote sensing for estimating total evaporation.

As encouraged by UKZN, this dissertation has been structured as a set of papers, preceded by a general introduction chapter, overview of methodology and followed by a synthesis chapter. Hence, there may be repetition in some sections, since chapters constitute stand-alone papers, which are intended for submission to different journals for publication.

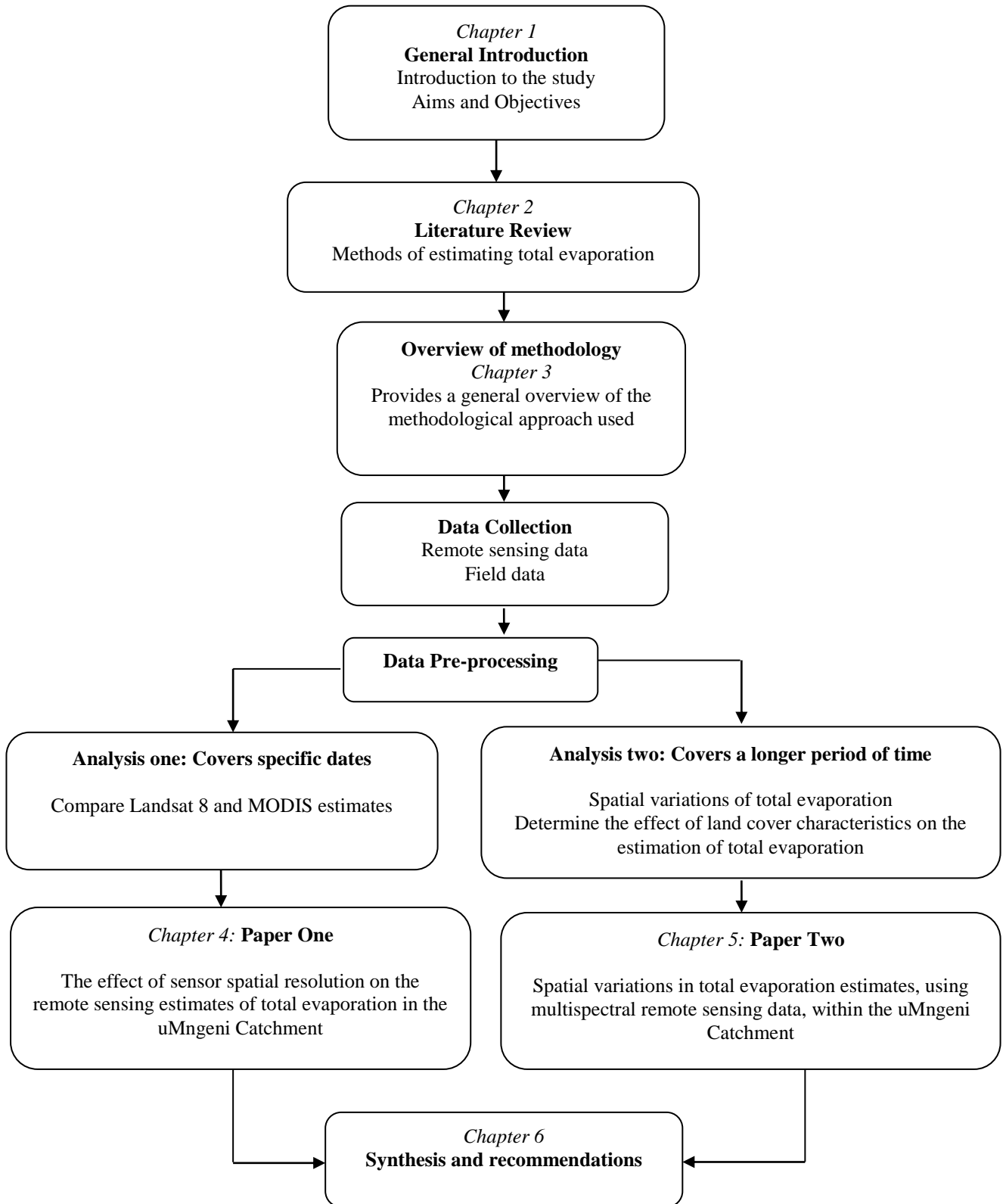


Figure 1.1 Flowchart of thesis structure

1.3 References

- Doll, P, Kaspar, F, Lehner, B. 2003. A global hydrological model for deriving water availability indicators: model tuning and validation. *Journal of Hydrology* 270: 105–134.
- Drexler, J, Snyder, R, Spano, D, Paw, KT. 2004. A review of models and micrometeorological methods used to estimate wetland evapotranspiration. *Hydrological Processes* 18(11): 2071-2101.
- DWAF. 2004. *Integrated Water Resource Management*. Department of Water Affairs and Forestry, Pretoria, South Africa.
- Ershadi, A, McCabe, M.F., Evans, JP, Walker, JP. 2013. Effects of spatial aggregation on the multi-scale estimation of evapotranspiration. *Remote Sensing of Environment* 131: 51–62.
- Gibson, LA, Jarman, C, Su, Z, Eckardt, FE. 2013. Estimating evapotranspiration using remote sensing and the Surface Energy Balance System – A South African perspective. *Water SA* 39(4): 477-484.
- Jarman, C, Bastiaanssen, W, Mengistu, M, Jewitt, G, Kongo, V. 2009a. *A Methodology for Near-Real Time Spatial Estimation of Evaporation*. Report No. 1751/1/09 Water Research Commission, Pretoria, South Africa.
- Jarman, C, Everson, C, Savage, M, Mengistu, M, Clulow, A, Walker, S, Gush, M. 2009b. *Refining tools for evaporation monitoring in support of water resources management*. Report No. 1567/1/08 Water Research Commission, Pretoria, South Africa.
- Lange, G-M, Mungatana, E, Hassan, R. 2007. Water accounting for the Orange River Basin: An economic perspective on managing a transboundary resource. *Ecological Economics* 61(4): 660-670.
- Li, Z, Tang, R, Wan, Z, Bi, Y, Zhou, C, Tang, B, Yan, G, Zhang, X. 2009. A review of current methodologies for regional evapotranspiration estimation from remotely sensed data. *Sensors* 9: 3801-3853.
- Lott, RB, Hunt, RJ. 2001. Estimating evapotranspiration in natural and constructed wetlands. *Wetlands* 21(4): 614–628.
- Maeda, EE, Wiberg, DA, Pellikka, PKE. 2011. Estimating reference evapotranspiration using remote sensing and empirical models in a region with limited ground data availability in Kenya. *Applied Geography* 31: 251-258.

- Molden, D. 1997. *Accounting for Water Use and Productivity*. 1 SWIM Paper 1. International Irrigation Management Institute. Colombo, Sri Lanka
- Molden, D, Sakthivadivel, R. 1999. Water Accounting to Assess Use and Productivity of Water. *Water Resources Development* 15(1/2): 55-71.
- Molden, D, Sakthivadivel, R, Habib, Z. 2001. *Basin-Level Use and Productivity of Water: Examples from South Asia*. International Water Management Institute, Colombo, Sri Lanka.
- Molobela, IP, Sinha, P. 2011. Management of water resources in South Africa: A Review. *African Journal of Environmental Science and Technology* 5(12): 993-1002.
- Oki, T, Kanae, S. 2006. Global Hydrological Cycles and World Water Resources. *Science* 313: 1068-1072.
- Ruhoff, AL, Paz, AR, Collischonn, W, Aragao, LEOC, Rocha, HR, Malhi, YS. 2012. A MODIS-based energy balance to estimate evapotranspiration for clear-sky days in Brazilian Tropical Savannas. *Remote Sensing* 4: 703-725.
- Summerton, M, Schulze, RE, Graham, PL. 2010. Impacts of a changing climate on hydrology and water supply in the Mgeni catchment, South Africa. *Third International Symposium, Managing Consequences of a Changing Global Environment*. Newcastle.
- Warburton, ML, Schulze, RE, Jewitt, GPW. 2012. Hydrological impacts of land use change in three diverse South African catchments. *Journal of Hydrology* 414–415(0): 118-135.
- Zhuwakinyu, M, 2012. *A review of South Africa's water sector*. Johannesburg, South Africa.

2. REVIEW OF METHODS FOR ESTIMATING TOTAL EVAPORATION

Abstract

Different approaches have been developed, to understand variations of total evaporation at various spatial and temporal scales. However, it has been observed that estimates using ground-based meteorological and micro-meteorological methods are inadequate for representing large-scale spatial variations of total evaporation. Remote sensing offers timely, up-to-date and relatively accurate spatial estimates of total evaporation for the sustainable and effective management of water resources. This paper, discusses the different approaches that have been used for assessing total evaporation, highlighting their strengths and weaknesses. Research gaps in the estimation of total evaporation, using remote sensing, as well as possible future research, were also highlighted.

Key words: Total evaporation, remote sensing, energy balance models, water resources management,

2.1 Introduction

In this study, total evaporation is defined according to Savenije (2004) as a summation of evaporation from different surfaces, including interception (I), transpiration (T), surface evaporation (E_s) and open water bodies (E_o). Savenije (2004) argues that the widely-used term *evapotranspiration* should be avoided, as it is an outdated term for a combination of evaporation processes from different surfaces. McMahon *et al.* (2012) agree that the term is misleading, considering the significant contribution of evaporation from interception to actual evaporation from vegetated surfaces, especially in warm climatic regions. They further define evaporation as an aggregation of all processes through which water is transferred as vapor from different surfaces, such as soil moisture, vegetation and open water bodies (McMahon *et al.*, 2012). Total evaporation varies with space and time and for different land cover types, due to the spatial and temporal variations in climatic conditions and landscape characteristics (Mutiga *et al.*, 2010). Climatic conditions incorporate rainfall, solar radiation, temperature, wind speed and humidity, while the landscape encompasses vegetation, soil and topographic

characteristics (Zhang *et al.*, 2004). Therefore, different methods have been developed to estimate total evaporation at various spatial and temporal scales.

It is the aim of this chapter to briefly review various methods of estimating total evaporation and discuss their general strengths and weaknesses for improved and well-informed management of water resources. In addition, the remote sensing-based approaches for estimating total evaporation are discussed in detail. Various challenges associated with using remote sensing to map and monitor total evaporation, are highlighted and possible solutions are suggested.

2.2 Estimating Total Evaporation

Different methods have been developed and implemented to estimate total evaporation, including meteorological ground-based point data, field measurements and spatially explicit remotely sensed data. Total evaporation is estimated either directly, when it is quantified by an instrument, or indirectly, when it is derived by means of its relationship with other parameters, as well as using reference total evaporation (Rana and Katerji, 2000). Depending on data availability and the purpose of estimating total evaporation, different methods can be used. Nevertheless, some methods are more suitable than others in terms of accuracy, availability and cost, while others are suitable for a particular given space and time-scale. Direct measurements of total evaporation are rarely available and estimates are often derived from reference evaporation estimates (Chen *et al.*, 2005; Sumner and Jacobs, 2005).

2.2.1 Meteorological methods

Meteorological methods are based on a point measurement of meteorological conditions to estimate reference evaporation, which can be used to derive total evaporation (Sumner and Jacobs, 2005). Reference evaporation is described by Chen *et al.* (2005) as the atmospheric demand for water from vegetation and soil, without the influence of vegetation characteristics or soil management. McMahon *et al.* (2012) define reference evaporation as the loss of water from a prescribed reference surface, where water is abundantly available and soil factors have no effect. It includes evaporation from vegetated surfaces, such as grass or alfalfa, and measurements from free water, such as an evaporation pan or the British standard tank (S-

tank). Therefore, the potential evaporation from a grassed surface, pan or tank provides a reference for the estimation of total evaporation for other surfaces. A summary of some of the widely-used methods to estimate reference evaporation is shown in Table 2.1.

Table 2.1 Summary of the data requirements by different meteorological-based methods

Method	Meteorological variables required	Other Parameters
Blaney- Criddle (1962) (Fooladmand, 2011 ; Lee <i>et al.</i> , 2004; Xu and Singh, 2002)	Daily temperature, wind speed, relative humidity, sunshine hours	—
Hargreaves-Samani (1985) (Lu <i>et al.</i> , 2005)	Daily temperature, radiation	Latitude, day of the year
Kimberly-Penman (1982) (Praveen <i>et al.</i> , 2011; Weiß and Menzel, 2008)	Daily temperature, radiation, wind speed, atmospheric pressure	—
Makkink (1957) (Lu <i>et al.</i> , 2005)	Mean daily temperature, radiation	—
Penman-Monteith (Allen <i>et al.</i> , 1998; Monteith, 1965; Penman, 1948)	Daily temperature, radiation, wind speed, atmospheric pressure, relative humidity	Vegetation characteristics, Calibration constant
Priestley-Taylor (1972) (Alexandris <i>et al.</i> , 2008; Kalma <i>et al.</i> , 2008)	Mean daily temperature, radiation	Calibration constant
Thornthwaite (1948) (Maeda <i>et al.</i> , 2011; Pereira and Pruitt, 2004)	Mean daily temperature	Daytime length, latitude
Turc (1961) (Federer <i>et al.</i> , 1996; McMahan <i>et al.</i> , 2012)	Mean daily temperature, radiation, relative humidity	—

The Penman-Monteith method has been regarded as the most reliable method for precise reference evaporation estimates and is therefore used as a standard, for the verification of other meteorological-based methods (Chen *et al.*, 2005). The method is applicable globally across varying climatic regions (Alexandris *et al.*, 2008; Droogers and Allen, 2002; Lott and Hunt, 2001). The Penman-Monteith method has also been used successfully to validate remote sensing methods (Irmak *et al.*, 2011; Jun *et al.*, 2010). Although meteorological-based methods have been used, literature shows that they have limitations in mapping the spatial variations of total evaporation. It has been noted that these methods are based on meteorological stations, which are unevenly distributed spatially (Lee *et al.*, 2004; Maeda *et*

al., 2011) and reference evaporation is derived from the interpolation of point-based estimates. Interpolation introduces errors, especially in areas characterized by varying climatic conditions and land cover types (Gibson *et al.*, 2011; Lott and Hunt, 2001).

Total evaporation can also be estimated using micro-meteorological techniques (Table 2.2). All the methods are used to derive total evaporation, except for the A-pan or British Standard tank (S-tank), which estimate reference evaporation and use coefficients to derive total evaporation (Chen *et al.*, 2005). Brutsaert (2013) highlights that total evaporation from the surrounding area is proportional to the measured pan evaporation, using pan coefficients which vary, due to spatial variations of vegetation characteristics, as well as the environmental conditions (Brutsaert, 2013; Chen *et al.*, 2005). Micro-meteorological methods have been applied across the globe for various land cover types, including agricultural fields (Allen *et al.*, 2007b; Nagler *et al.*, 2005) and natural ecosystems (Drexler *et al.*, 2004; Lott and Hunt, 2001), with useful estimates.

In South Africa, micro-meteorological methods have also been applied across different land cover types under varying climatic conditions, including, grassland areas (Savage *et al.*, 2010), agricultural areas (Mengistu *et al.*, 2014), wattle (Clulow *et al.*, 2011) and eucalyptus forests (Jarmain and Everson, 2002). In addition, Jarmain *et al.* (2009b) highlighted that ground-based methods will always be in demand, as estimates based on these methods are required to validate remotely sensed estimates of total evaporation (Jarmain *et al.*, 2009a).

Table 2.2 Summary of micro-meteorological methods to estimate total evaporation

Method	Application	Reference
A-pan / S-tank	Estimates reference evaporation and then total evaporation is estimated using pan coefficients	Brutsaert (2013) McMahon <i>et al.</i> (2012)
Bowen ratio	Estimates total evaporation at a point	Drexler <i>et al.</i> (2004), Savage <i>et al.</i> (1997)
Eddy covariance	Estimates total evaporation at a point	Meyers and Baldocchi (2005), Scott (2010)
Scintillometer	Estimates total evaporation along a transect	McJannet <i>et al.</i> (2013) Odhiambo and Savage (2009),
Surface renewal	Estimates total evaporation at a point	Spano <i>et al.</i> (2000), Mengistu and Savage (2010)
Lysimeter	Estimates total evaporation at a point	Rana and Katerji (2000)

Micro-meteorological techniques have limitations in estimating total evaporation (Jarmain *et al.*, 2009b). With the exception of scintillometry, micro-meteorological methods are not representative of the spatial variability of total evaporation within the landscape, because their estimates are based on point measurements (Gibson *et al.*, 2013; Glenn *et al.*, 2007; Jarmain *et al.*, 2009b). On the other hand, scintillometry estimates total evaporation as the average of the fluxes along a defined transect (Meijninger and de Bruin, 2000), which allows the detection of ground-based areal total evaporation variations for a defined path, usually not more than ten kilometers (Hoedjes *et al.*, 2007). According to Meijninger and de Bruin (2000), scintillometry is a reliable method and an intermediate scale of measurement between ground-based point measurements and the spatial estimates from remotely-sensed data. It has a better spatial representation of total evaporation, when compared to point-based methods. Scintillometry has been successfully applied in agricultural fields (Anandakumar, 1999; McJannet *et al.*, 2013) and landscapes with mixed land cover types (Hemakumara *et al.*, 2003). The method has also been used to validate remote sensing-based total evaporation estimates (Bastiaanssen *et al.*, 2005; Bastiaanssen, 2000; Jia *et al.*, 2003; Jovanovic *et al.*, 2011). Scintillometry has also been used over different land cover types, in South Africa, with reasonable estimation accuracy (Clulow *et al.*, 2011; Kongo and Jewitt, 2006; Savage *et*

al., 2004; Savage *et al.*, 2010). Although scintillometry has been widely-used, Hoedjes *et al.* (2007) highlighted that it is more applicable in homogenous areas, such as agricultural fields.

In conclusion, the use of point-based and micro-meteorological methods in estimating the spatial variations of total evaporation remains a challenge. Remote sensing is gaining popularity in the spatial mapping and monitoring of natural resources at different spatial scales.

2.2.2 Remote sensing methods

The advent and advancement in remote sensing enables the spatial monitoring of total evaporation over large areas. The increased availability and advancement of satellite data products provides an opportunity to monitor variations of total evaporation at different spatial and temporal scales (Glenn *et al.*, 2007; Ruhoff *et al.*, 2012) and allows the monitoring of inaccessible areas (Li *et al.*, 2009). In addition, Gibson *et al.* (2013) highlight that remote sensing technology holds great promise for the long-term monitoring of water resources on a relatively large scale and in a cost effective manner. Methods based on the use of remote sensing data are therefore well-suited for the spatial variations of total evaporation over time. The methods include the use of vegetation indices and the energy balance models, such as the Surface Energy Balance Index (SEBI), the Simplified Surface Energy Balance Index (S-SEBI), the Surface Energy Balance System (SEBS), the Surface Energy Balance Algorithm for Land (SEBAL) and Mapping EvapoTranspiration at High Resolution with Internalized Calibration (METRIC). Energy balance models are based on the energy balance approach, since total evaporation requires energy in order to occur. Therefore, these models estimate total evaporation, using the following equation:

$$R_n = G_0 + H + \lambda E \quad (2.1)$$

where:

- R_n = net radiation at the surface [W/m^2],
- G_0 = soil heat flux [W/m^2],
- H = sensible heat flux to the air [W/m^2], and
- λE = latent heat flux [W/m^2].

Net radiation can be acquired from remote sensing or ground-based meteorological stations, whereas soil heat flux is indirectly derived, using empirical relationships between vegetation and land surface characteristics, or directly, using soil heat plates. However, sensible and latent heat fluxes are derived in various ways depending on the model. Some models rely on the characteristics of the input image (to derive dry and wet limits), while others are based on the bio-physical characteristics of the area under study (Li *et al.*, 2009).

2.2.3 Vegetation indices

Remotely sensed derived vegetation indices, combined with ground data, are useful in the estimation of total evaporation for crops and natural vegetation (Guerschman *et al.*, 2009). Commonly-used indices include the Normalized Difference Vegetation Index (NDVI), the Soil Adjusted Vegetation Index (SAVI) and the Enhanced Vegetation Index (EVI). Seevers and Ottmann (1994) estimated the total evaporation of irrigated fields, using NDVI derived from the Advanced Very High Resolution Radiometer (AVHRR). Their results indicated a high correlation between the Blaney-Criddle meteorological ground-based method and NDVI-based estimates. However, they noted that NDVI could only detect severe water deficiencies, rather than slight changes. Similarly, based on the results of their study, Glenn *et al.* (2010) indicated that vegetation indices have problems in detecting water stress from vegetation during early stages. Nagler *et al.* (2005) used the Moderate Resolution Imaging Spectroradiometer (MODIS) derived NDVI and EVI, together with the eddy covariance system, to estimate total evaporation from riparian vegetation. Their results showed a high correlation between EVI and the eddy covariance measurements.

Although remotely sensed vegetation indices enable the spatial estimation of total evaporation over large areas, they cannot provide accurate estimates in water-stressed vegetation. EVI and NDVI underestimate total evaporation from unhealthy vegetation and bare areas (Senay *et al.*, 2011; Szilagyi *et al.*, 1998). In addition, SAVI cannot accurately detect total evaporation in areas with sparse vegetation cover (Gilabert *et al.*, 2002; Qi *et al.*, 1994; Rondeaux *et al.*, 1996).

2.2.4 Surface Energy Balance Index

According to van den Hurk (2001), SEBI is a modified Crop Water Stress Index (CWSI) (Jackson *et al.*, 1981; Moran *et al.*, 1996). The SEBI model computes total evaporation by combining remotely sensed inputs and meteorological data. SEBI derives total evaporation and the evaporative fraction, based on land surface dry and wet limits, which are characterized by maximum surface temperature, with low or no evaporation, and minimum surface temperature, with high or maximum evaporation, respectively (Li *et al.*, 2009). In the SEBI model, the evaporative fraction is estimated from minimum and maximum surface temperatures and from the aerodynamic roughness length or roughness height of heat transfer, to derive latent heat flux (Li *et al.*, 2009). However, van den Hurk (2001) highlighted that the SEBI roughness height is poorly computed for estimating total evaporation, hence the SEBI model needs further testing and verification against ground-based estimates under various bio-physical and climatic regions.

Menenti *et al.* (2003) has demonstrated the applicability of the SEBI model in France, Spain, Italy, China and the United States of America. Their results agreed well with estimates derived from the ground-based scintillometer (Menenti *et al.*, 2003). Roerink *et al.* (2000) highlighted that total evaporation can be accurately estimated in wet or humid areas (*e.g.* England) and in extremely dry areas, such as the Sahara Desert, using the SEBI model, where the S-SEBI is unapplicable.

2.2.5 Simplified Surface Energy Balance Index

The S-SEBI model estimates instantaneous evaporation, using surface temperature, albedo and NDVI derived from remote sensing (Roerink *et al.*, 2000). The major strength of S-SEBI is that it is simple, does not need additional meteorological data, which is ideal in inaccessible areas, nor does it need the vegetation height for heat transfer, like SEBS (Gowda *et al.*, 2007). The model computes total evaporation and the evaporative fraction, by assuming a constant atmospheric forcing (*i.e.* constant global radiation and air temperature). Under constant atmospheric forcing, surface temperature is correlated with surface reflectance (Menenti *et al.*, 1989). The evaporative fraction estimated from the image feature

space (*i.e.* the relationship between surface reflectance and surface temperature) is useful for deriving latent and sensible heat fluxes, as shown in Figure 2.1 after Roerink *et al.* (2000).

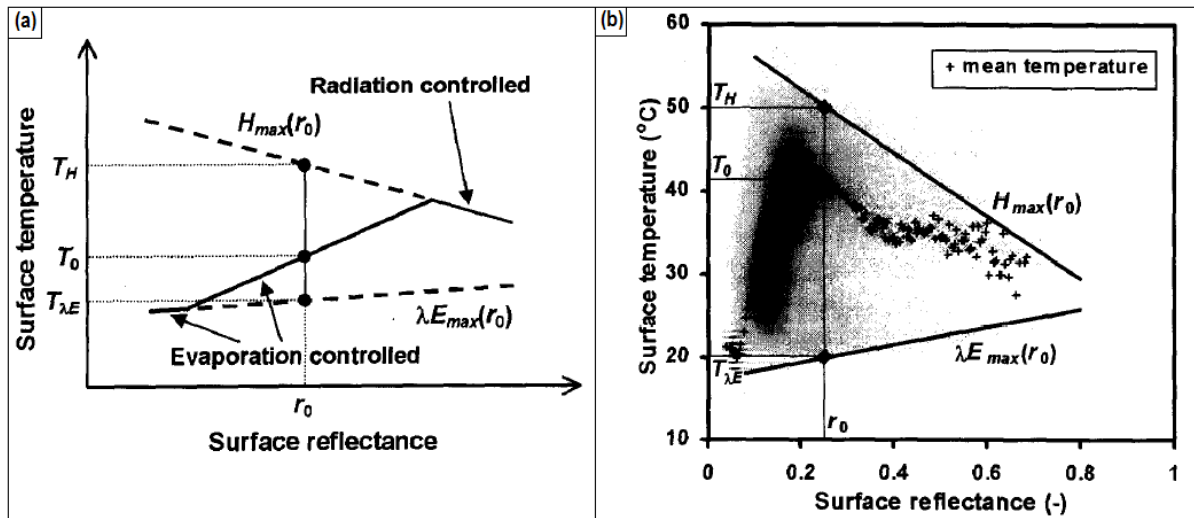


Figure 2.1 S-SEBI principle for deriving evaporative fraction and total evaporation

Evaporative fraction is computed, based on the image feature space in Figure 2.1 (b) as:

$$\Lambda = \frac{T_H - T_0}{T_H - T_{\lambda E}} \quad (2.2)$$

where

Λ = evaporative fraction [dimensionless],

T_0 = land surface temperature [°C],

T_H = temperature of dry condition for a given reflectance value [°C], and

$T_{\lambda E}$ = temperature of wet condition for a given reflectance value [°C].

To date, a number of international studies have estimated total evaporation, using the S-SEBI method (Boronina and Ramillien, 2008; Roerink *et al.*, 2000; Sobrino *et al.*, 2007). In the Alpilles Province of France, Gómez *et al.* (2005b) estimated the total evaporation from agricultural fields (*i.e.* corn, maize, wheat and alfalfa) and the results were validated, using ground-based Bowen ratio estimates. Their results show that the derived S-SEBI total evaporation estimates were in agreement with the crop development stages in the fields and also close to ground-based Bowen ratio estimates. In addition, Sobrino *et al.* (2007) estimated the total evaporation in the Iberian Peninsula, using S-SEBI (derived from AVHRR images) for different land cover types, namely, rice fields, olive trees, vineyard, forests and non-

irrigated agricultural area. From the results, estimated total evaporation coincided well with surface characteristics, where high estimates of total evaporation were obtained from vegetated areas. The effect of incoming radiation and seasonal variations on total evaporation was also indicated, where higher estimates were obtained during summer and spring, while low estimates were obtained during the winter and autumn seasons. Boronina and Ramillien (2008), using AVHRR-derived S-SEBI, observed similar seasonal patterns of total evaporation estimates over the Lake Chad Basin.

The major limitations of S-SEBI include its assumption of constant atmospheric forcing and its requirement of extreme surface temperature values, which are not always available on every remote sensing image (Roerink *et al.*, 2000; Sobrino *et al.*, 2007). Global radiation and air temperature are not always constant, especially in mountainous areas. Moreover, unlike SEBI, this model performs poorly in humid areas, as it prefers dry pixels, as well as in extremely dry conditions, such as the Sahara Desert, and over larger continental areas, where atmospheric conditions are not constant (Roerink *et al.*, 2000). S-SEBI yields low estimates, when using coarse resolution images, due to mixed land cover spectral features in a single pixel. Further, the selection of extreme temperatures, representing the dry and wet conditions of the area, are derived by means of the image feature space (relationship between reflectance and surface temperature), without the use of location specific conditions. This introduces errors and uncertainties in the estimation of total evaporation.

2.2.6 Surface Energy Balance System for Land

SEBAL is a model, which was developed by Bastiaanssen *et al.* (1998) for computing turbulent fluxes or energy exchanges between land and the atmosphere using remote sensing data and meteorological data. Remote sensing inputs include vegetation indices, albedo and surface temperature, whereas meteorological inputs include temperature, wind speed, humidity and solar radiation (Teixeira *et al.*, 2009). A detailed explanation of how all the energy balance components are derived to compute evaporation, using SEBAL is provided by Bastiaanssen *et al.* (1998). In brief, SEBAL uses the aerodynamic roughness length or roughness height of heat transfer (Li *et al.*, 2009) in estimating latent heat flux. SEBAL has been widely-used internationally under varying climatic conditions in agriculture and natural

forests (Bastiaanssen, 2000; Long *et al.*, 2011; Minacapilli *et al.*, 2009; Ruhoff *et al.*, 2012; Shilpakar *et al.*, 2011; Teixeira *et al.*, 2009).

In Africa, Mutiga *et al.* (2010) used SEBAL to estimate total evaporation for a catchment in Kenya and their results showed that the model is effective in estimating the spatial variation of total evaporation for water resources management. In South Africa, Kongo and Jewitt (2006) used SEBAL-derived total evaporation estimates to examine the hydrological effects of rain water harvesting within a catchment. Their results indicated that SEBAL underestimated sensible heat flux, when compared with measurements from eddy covariance. Hellegers *et al.* (2009) used SEBAL to estimate total evaporation for the Inkomati Catchment and their results showed the variation of total evaporation between different vegetation types. They concluded that SEBAL, when combined with biomass production and rainfall data, shows the spatial distribution of water availability, consumption and surplus, based on different land cover types. Furthermore, Jarman *et al.* (2009a) also used SEBAL in estimating total evaporation from Landsat images over different climatic regions and with varying land cover types, in the KwaZulu-Natal and Eastern Cape provinces. They concluded that the SEBAL model agrees well with ground-based measurements, especially with regard to net radiation. They further highlighted that SEBAL agrees well with the other energy balance models (SEBS, METRIC and VITT), which were used.

Even though SEBAL has been successfully applied, a further understanding of the model and the impact of surface heterogeneity on heat fluxes at watershed or regional scales is required (Long *et al.*, 2011). Despite its usefulness in understanding the spatial variations of total evaporation, SEBAL has some drawbacks. Gibson *et al.* (2013) state that the SEBAL model is protected by intellectual property in terms of availability, when compared to other models. SEBAL is also difficult to apply at large spatial scales (van den Hurk, 2001). In addition, if the SEBAL model is applied, its surface roughness parameter is poorly defined and its use of fixed temperature values for the dry and wet conditions of evaporation is problematic (Li *et al.*, 2009).

2.2.7 Mapping EvapoTranspiration at High Resolution with Internalized Calibration

The METRIC model (Allen *et al.*, 2007b) was developed based on the SEBAL model and it computes the spatial variations of total evaporation, based on remotely sensed data and reference evaporation (Li *et al.*, 2009). The model also requires solar radiation, air temperature dew point temperature and wind speed (Hankerson *et al.*, 2012). METRIC computes and shows the estimated total evaporation as a fraction of the reference evaporation (Hankerson *et al.*, 2012) independent of vegetation type. METRIC differs from SEBAL in its use of meteorological-based reference evaporation (Allen *et al.*, 2007b) and it also incorporates the soil moisture balance from meteorological-based data, to determine wet and dry limits for estimating evaporative fraction (Gowda *et al.*, 2007). The METRIC model has been widely-used in United States under varying climatic and land cover types for various applications (Allen *et al.*, 2007a). The model-based results also agreed well with ground-based lysimeter measurements.

The METRIC model was also used in South Africa (Jarman *et al.*, 2009a) to estimate total evaporation for different sites under varying climatic conditions. The results showed that METRIC agreed well with other energy balance models, as well as with ground-based measurements, especially with regard to the estimation of net radiation.

Although METRIC has been used extensively, much of its utility has been shown in the United States (where the model was developed), with Landsat images, or images with similar spatial resolution. Allen *et al.* (2011) also highlighted that the disadvantage of the METRIC model is that it requires trained experts or specialized personnel, high quality weather data and it relies highly on the ability of the operator to select the appropriate cold and hot pixels for the accurate estimation of total evaporation.

2.2.8 Surface Energy Balance System

The SEBS model, which was developed by, Su (2002), estimates heat fluxes, using remotely sensed data (*i.e.* land surface temperature, albedo, emissivity, fractional vegetation cover, leaf area index, NDVI) and meteorological data (*i.e.* temperature, humidity, wind speed and pressure) at a reference height. SEBS also requires solar radiation, which can be directly

measured on the ground or it can be modelled from remote sensing data (Su, 2002). Based on the energy balance equation, SEBS calculates the net radiation as:

$$Rn = [(1 - \alpha) \cdot R_{swd}] + [\varepsilon \cdot \varepsilon_a \sigma T^4 - \varepsilon \cdot \sigma \cdot T^4] \quad (2.3)$$

where

- Rn = net radiation [W/m^2],
- α = surface albedo [dimensionless],
- R_{swd} = downward shortwave solar radiation [W/m^2],
- ε = surface emissivity [dimensionless],
- ε_a = atmospheric emissivity [dimensionless],
- σ = Stefan-Boltzmann constant [$5.670\,373 \times 10^{-8} \text{ W m}^{-2} \text{ K}^{-4}$], and
- T = surface temperature [K] (Su, 2002).

Soil heat flux (G_0) is the amount of heat energy flowing into a cross-sectional area of soil per unit of time in response to the temperature gradient. It is computed as:

$$G_0 = R_n \cdot [\Gamma_c + (1 - f_c) \cdot (\Gamma_s - \Gamma_c)] \quad (2.4)$$

where

- G_0 = soil heat flux [W/m^2],
- Rn = net radiation [W/m^2],
- Γ_c = 0.05 [dimensionless,] ratio of soil heat flux to net radiation for full vegetation conditions
- Γ_s = 0.315 [dimensionless] ratio of soil heat flux to net radiation for bare soil, and
- f_c = fractional vegetation cover [dimensionless] (Su, 2002).

SEBS uses the Monin-Obukhov Similarity Theory (MOST) to estimate the sensible heat (H) and latent heat (λE) fluxes. MOST relates surface fluxes to surface variables and variables in the Atmospheric Surface Layer (ASL), a detailed explanation of which is given by Su (2002). Unlike other energy balance models, SEBS computes the aerodynamic resistance of heat transfer more explicitly, instead of using fixed values, like SEBI and SEBAL (Li *et al.*,

2009). Aerodynamic resistance varies with environmental conditions for different surface types, hence it has an effect on the estimation of heat fluxes, and subsequently, on total evaporation (Sugita and Kishii, 2002). Liu *et al.* (2006) highlight the importance of aerodynamic resistance when estimating total evaporation, using remotely sensed-based methods. SEBS is part of the open source freeware Integrated Land and Water Information System (ILWIS) package available free of charge (<http://www.52north.org>), unlike SEBAL, which is protected by intellectual property (Gibson *et al.*, 2013).

SEBS has been used internationally to estimate total evaporation for different land cover types, using different remote sensing sensors (Table 2.3) and yields reliable estimates. Su *et al.* (2007) evaluated the accuracy of total evaporation estimates from SEBS, using MODIS data, against ground-based measurements in the grasslands of Netherlands and Germany, the croplands of the United States, the rainforests of Brazil and the Canadian forests. Their results showed a close agreement between SEBS-based estimates and ground-based measurements, as well as the feasibility of using SEBS to estimate heat fluxes over inaccessible areas, where *in-situ* data are not readily available. However, there were uncertainties, due to satellite spatial resolution in capturing the spatial heterogeneity of the land cover types; hence, they recommended the use of medium resolution Landsat imagery. This is also supported by Vinukollu *et al.* (2011), who noted a disparity between total evaporation estimates derived using remote sensing data and ground-based measurements using eddy covariance system. They highlighted that the coarse spatial resolution MODIS data did not capture the heterogeneity of the surface (Vinukollu *et al.*, 2011).

Table 2.3 Summary of SEBS applications at different spatial scales

Remote Data	Sensing	Resolution (m)	Location and Scale of Application	Findings	Reference
MODIS		1000	Regional land cover types of northern China	SEBS concurs with previous results and the existing knowledge of total evaporation estimates in the area.	He <i>et al.</i> (2007)
MODIS		1000	River basin (Iran)	Mixed land cover types within a pixel make it difficult to derive land cover type based estimates accurately.	Muthuwatta <i>et al.</i> (2010)
MODIS		1000	Catchment (Zimbabwe)	Air temperature should be spatially represented, especially at heterogeneous areas.	Rwasoka <i>et al.</i> (2011)
AVHRR		1000	Tibetan Plateau (China)	Sub-pixel heterogeneity has been omitted due to coarse resolution imagery.	Ma <i>et al.</i> (2003)
AATSR		1000	Nile delta (Egypt)	High correlation of SEBS with ground data Applicability of SEBS over agricultural areas.	Elhag <i>et al.</i> (2011)
MODIS		1000	Catchment (South Africa)	SEBS is sensitive to temperature gradient and should not be used with coarse resolution images in mountainous areas as temperature changes will not be captured.	Gibson <i>et al.</i> (2011)
AATSR		1000	Landscape (Spain)	SEBS estimates were comparable with ground-based scintillometer results for the different agricultural fields.	Jia <i>et al.</i> (2003)
MODIS		1000	Global scale	SEBS estimates correlates well with the ground-based eddy covariance and the Penman-Monteith estimates.	Vinukollu <i>et al.</i> (2011)
MODIS		1000	National (Taiwan)	SEBS spatial trends correspond to seasonal variations and vegetation cover conditions.	Che-sheng <i>et al.</i> (2011)

ASTER	90	Agricultural region (Spain)	SEBS agrees well with ground-based estimates under one land cover type and errors are introduced when different land cover types occur	van der Kwast <i>et al.</i> (2009)
ASTER	90	Irrigation area (418000 ha) of Australia	SEBS correlates well with ground-based estimates and seasonal conditions.	Ma <i>et al.</i> (2013)
Landsat 5 TM	30	Agricultural crops of Texas, USA	Performed well for crop under irrigation and dry land conditions	Gowda <i>et al.</i> (2013)
MODIS Landsat ETM 7 Landsat 8	1000 30 30	Agricultural fields (South Africa)	Landsat images provide better estimates when compared to MODIS.	Mengistu <i>et al.</i> (2014)
ASTER	15	Tibetan Plateau (China)	SEBS results were reliable, but there is need to further assess the performance of other satellite sensors.	Ma <i>et al.</i> (2011)

In the African context, Elhag *et al.* (2011) used SEBS to estimate total evaporation for the Nile Delta agricultural production zone of Egypt from Advanced Along-Track Scanning Radiometer (AATSR) images. SEBS showed a very high correlation, with ground-based measurements and its applicability in estimating daily total evaporation over agricultural areas was demonstrated. Rwasoka *et al.* (2011) used SEBS to estimate the spatial variation of total evaporation of a catchment in Zimbabwe, using MODIS data. The results showed that SEBS is a valuable model for determining the spatial variations of total evaporation and for managing water resources. However, Rwasoka *et al.* (2011) concluded that there is also a need for further research to determine the best approach for arid and semi-arid areas characterized by various land cover types.

Gibson *et al.* (2011) highlight the applicability of SEBS in estimating total evaporation in the heterogeneous catchment of the Piketberg region, in South Africa, based on MODIS data. Their results show that SEBS is very sensitive to temperature gradient. Recently, Gibson *et al.* (2013) reviewed the estimation of total evaporation using SEBS and they concluded that the model did not yield accurate daily evaporation results at the MODIS spatial resolution. They recommended that any further research, using the SEBS model in South Africa, should be limited to fully vegetated areas or agricultural areas, and should also consider the potential of high resolution images.

The SEBS model was also applied by Mengistu *et al.* (2014) to provide accurate estimates of total evaporation from agricultural fields in KwaZulu-Natal, South Africa. These estimates were based on images from MODIS, Landsat 7 ETM+ and Landsat 8 satellites. The results showed that Landsat provided better total evaporation estimates, when compared to MODIS, possibly because of their spatial resolution (30 m, compared to 1000 m).

In addition, Jarman *et al.* (2009a) reported the potential of several energy balance models (SEBS, SEBAL, METRIC and the Vegetation Index Temperature Trapezoid (VITT)), to estimate total evaporation from Landsat images over different climatic regions and with varying land cover types, in the KwaZulu-Natal and Eastern Cape provinces. They concluded that these methods extend the point-based measurement of total evaporation to large spatial scales and are also reliable in areas where measured meteorological data may be scarce. They also highlighted the previous application of the different energy balance models and major

findings across the globe for different land cover types. They also concluded that these models are useful for estimating total evaporation and therefore hold great potential for water resources management and planning.

2.2.9 The influence of spatial heterogeneity on total evaporation estimates using remote sensing

Although remote sensing provides an invaluable alternative for a better estimation of total evaporation at various spatial and temporal scales, the influence of landscape heterogeneity (*i.e.*, the spatial variations of land cover types) within a study area on these estimates must be considered. Previous studies have established that spatial heterogeneity has a considerable influence on the estimation of total evaporation using remote sensing (Kustas *et al.*, 2004; Kustas and Norman, 2000; McCabe and Wood, 2006; Norman *et al.*, 2003; Saura, 2004). For instance, the study by Kustas and Norman (2000) noted that the variability in land cover characteristics (such as area and patchiness) across a landscape influences the ability of the sensor to explicitly represent variations of heat fluxes and total evaporation. Furthermore, Garrigues *et al.*, (2006) found that the effect of land cover area in relation to the remote sensing sensor spatial resolution in determining the biophysical variables (*e.g.* leaf area index) had a considerable effect on estimates of total evaporation. More specifically, McCabe and Wood, 2006 emphasized the importance of landscape heterogeneity and its influence on surface fluxes as detected by different satellite sensors with varying spatial resolutions. They further highlighted that the ability of the sensor to detect the specific land cover characteristics is limited when the scale of land cover is less than the spatial resolution. Thus the spatial arrangement including variations in area, patchiness and fragmentation of land cover types across a landscape is critical. It is, therefore important to explore not only the composition (land cover types) of the landscape, but also the spatial extent or scale and arrangement (patchiness) relative to the scale of remote sensing observation.

Spatial heterogeneity refers to the complex spatial distribution of surface patterns or patch mosaics across a landscape (McGarigal, 2006). This depends primarily on the variability of climate, topography and human activities (Turner, 2001). Therefore the quantification of spatial heterogeneity provides a means of selecting optimum remote sensing sensors to detect the spatial variations. To quantify landscape heterogeneity, various methods, which are

widely known as landscape or spatial metrics, have been developed (Fiener *et al.*, 2011; Kowe *et al.*, 2014; Seto and Fragkias, 2005; Turner, 1989; Turner, 2001). Landscape metrics are geospatial data analysis algorithms, which quantify specific spatial characteristics of landscape mosaics, including patches and classes of patches (McGarigal, 2006). Furthermore, Kowe *et al.* (2014) noted that landscape metrics have the capability to determine land cover patterns and their spatial configuration (*e.g.* size, shape, edge, patches,) within a given landscape. Configuration refers to the spatial distribution or structure of patches, or more simply, the spatial arrangement of different land cover types within a landscape (Turner, 2001). Although landscape metrics describe various properties of landscape heterogeneity, the choice of selecting these metrics depends on their relevance to the problem under investigation. Generally it is recognized that the spatial structure of elements (*i.e.* patches) in a land cover mosaic determines the biophysical processes which operate within it (Haines-Young and Chopping, 1996).

Recently, Uuemaa *et al.* (2009) have highlighted the applicability of various landscape metrics in understanding patterns and processes within the earth surface. In addition, it has been established that spatial heterogeneity, particularly composition and structure, influences various biophysical processes across the landscape (Turner, 2001; Zhou *et al.*, 2011). The studies by Uuemaa *et al.* (2013), Weng *et al.* (2007) and Zhou *et al.*, 2011 have emphasized the relevance of landscape composition and configuration in water and energy flows, in urban planning and in ecology. They also suggest that variability in composition and configuration of a landscape plays an important role in determining the spatial patterns of biophysical processes and variables (*e.g.*, land surface temperature). Even though many of the landscape metrics represent fundamental information, with regard to the estimation of total evaporation using remote sensing, particularly spatial resolution, configuration metrics are more likely to have a potential effect on the ability of the sensor to detect landcover spatial characteristics. Many of the landscape metrics are derived from the widely used primary metrics, and these are presented in Table 2.3.

Table 2.4 Primary landscape metrics used to determine spatial heterogeneity

Landscape Metric	Brief Definition	References
Number of patches (NP)	Determines the total number of patches of a specific land cover type within a landscape.	Turner (1989), Uuemaa <i>et al.</i> (2009)
Mean patch size (MPS)	Determines the mean area of patches of a specific land cover type within a landscape. The higher the value, the larger the area of the majority of patches.	Turner (2001) Weng <i>et al.</i> (2007)
Total edge (TE)	It is an absolute measure of total edge length of all edge segments involving the corresponding patch type across a landscape. TE is equal to zero when the entire landscape consists of a single patch and increases when the landscape consists of many patches. It is a measure of landscape fragmentation.	Riitters <i>et al.</i> (1995), Kowe <i>et al.</i> (2014)

2.3 Discussion and conclusion

Understanding the spatial variability of total evaporation remains a concern for water resources management at various spatial and temporal scales. A review of literature has demonstrated that there are various methods that have been developed to better understand variations of total evaporation estimates at different spatial scales and for a wide range of applications. Most notably, each of these methods has its own limitations and advantages. For instance, although meteorological-based methods have been widely-used, with acceptable estimates of total evaporation, it is evident that their point-based approach is inadequate for the accurate representation of the spatial variability of total evaporation. The interpolation approach, of point-based meteorological methods, overlooks the effect of spatial heterogeneity in land cover or climatic conditions and consequent total evaporation estimates, as it generalizes the characteristics of the land. Although the intermediate scintillometry method gives a better spatial representation of total evaporation, when compared to point-based methods, this approach is mainly suitable for applications in homogenous areas. Despite their weaknesses, it has been shown that ground-based estimates still play a fundamental role in the estimation of total evaporation. However, remote sensing techniques provide an opportunity to spatially characterize total evaporation at different spatial scales, with reliable accuracy, although it has limitations, such as cloud cover, poor temporal and

spatial resolution, which hampers the continuous availability of quality data required for accurate estimation of total evaporation.

Mindful of its shortcomings, remote sensing provides a cost-effective and reliable alternative for the accurate representation of the spatial variability of total evaporation at local, regional or international scale, when compared to point-based meteorological and micro-meteorological methods. Specifically, it has been noted that remote sensing-based energy balance methods provide better spatial variations of total evaporation at different spatial scales, for water resources management. The SEBS model has been the most extensively used, with different satellite products, under different climatic regions, compared to other energy balance models.

Although remote sensing methods provide a better way of estimating spatial variations of total evaporation at different spatial scales, the ability of different satellite products in the spatial representation of total evaporation remains a concern. Sensor spatial resolution in relation to land cover characteristics plays a critical role in determining total evaporation estimates. It is also apparent that the spatial heterogeneity (*i.e.*, spatial arrangement and scale of land cover types) of the study area land cover characteristics is an important factor, when estimating the spatial variations of total evaporation using remote sensing, especially with regard to the sensor spatial resolution. Previously, spatial variations of total evaporation estimates were mainly derived from specific land cover types (*e.g.* agricultural fields, vineyards or wetlands) for a particular application. Variation of total evaporation across a heterogeneous catchment still requires further investigation, especially with regard to the influence of scale of observation. Catchments are characterized by various land cover types with varying water consumption. There is a need to understand water consumption and the contributions of different land cover types to total evaporation for water accounting purposes. This will also provide a better understanding of spatial variations of total evaporation for management and allocation of water.

2.4 References

- Alexandris, S, Stricevic, R, Petkovic, S. 2008. Comparative analysis of reference evapotranspiration from the surface of rainfed grass in central Serbia, calculated by six empirical methods against the Penman-Monteith formula. *European Water* 21(22): 17-28.
- Allen, R, Irmak, A, Trezza, R, Hendrickx, JM, Bastiaanssen, W, Kjaersgaard, J. 2011. Satellite-based ET estimation in agriculture using SEBAL and METRIC. *Hydrological Processes* 25(26): 4011-4027.
- Allen, R, Tasumi, M, Morse, A, Trezza, R, Wright, J, Bastiaanssen, W, Kramber, W, Lorite, I, Robison, C. 2007a. Satellite-Based Energy Balance for Mapping Evapotranspiration with Internalized Calibration (METRIC)—Applications. *Journal of Irrigation and Drainage Engineering* 133(4): 395-406.
- Allen, R, Tasumi, M, Trezza, R. 2007b. Satellite-Based Energy Balance for Mapping Evapotranspiration with Internalized Calibration (METRIC)-Model. *Journal of Irrigation and Drainage Engineering* 133(4): 380-394.
- Allen, RG, Pereira, LS, Raes, D, Smith, M. 1998. *Crop evapotranspiration: Guidelines for computing crop water requirements- FAO Irrigation and Drainage Paper 56*. Food and Agriculture Organization of the United Nations, Rome, Italy, pp. 15-64.
- Anandakumar, K. 1999. Sensible heat flux over a wheat canopy: optical scintillometer measurements and surface renewal analysis estimations. *Agricultural and Forest Meteorology* 96(1): 145-156.
- Bastiaanssen, W, Noordman, E, Pelgrum, H, Davids, G, Thoreson, B, Allen, R. 2005. SEBAL model with remotely sensed data to improve water-resources management under actual field conditions. *Journal of Irrigation and Drainage Engineering* 131(1): 85-93.
- Bastiaanssen, WGM. 2000. SEBAL-based sensible and latent heat fluxes in the irrigated Gediz Basin, Turkey. *Journal of Hydrology* 229(1–2): 87-100.
- Bastiaanssen, WGM, Menentia, M, Feddesb, RA, Holtslagc, AAM. 1998. A remote sensing surface energy balance algorithm for land (SEBAL) 1. Formulation. *Journal of Hydrology* 212: 198–212.
- Blaney, HF, Criddle, WD. 1962. *Determining consumptive use and irrigation water requirements*. US Department of Agriculture.

- Boronina, A, Ramillien, G. 2008. Application of AVHRR imagery and GRACE measurements for calculation of actual evapotranspiration over the Quaternary aquifer (Lake Chad basin) and validation of groundwater models. *Journal of Hydrology* 348(1–2): 98-109.
- Brutsaert, W. 2013. Use of pan evaporation to estimate terrestrial evaporation trends: The case of the Tibetan Plateau. *Water Resources Research* 49: 3054–3058.
- Che-sheng, Z, Jie, Z, Hui-xiao, W, Jian, Y. 2011. Quantitative estimation of land surface evapotranspiration in Taiwan based on MODIS data. *Water Science and Engineering* 4(3): 237-245.
- Chen, D, Gao, G, Xu, C, Guo, J, Ren, G. 2005. Comparison of the Thornthwaite method and pan data with the standard Penman-Monteith estimates of reference evapotranspiration in China. *Climate Research* 28: 123–132.
- Clulow, A, Everson, C, Gush, M. 2011. *The long-term impact of Acacia mearnsii trees on evaporation, streamflow and ground water resources*. Report No. TT505/11 Water Research Commission, Pretoria, South Africa.
- Drexler, J, Snyder, R, Spano, D, Paw, KT. 2004. A review of models and micrometeorological methods used to estimate wetland evapotranspiration. *Hydrological Processes* 18(11): 2071-2101.
- Droogers, P, Allen, RG. 2002. Estimating reference evapotranspiration under inaccurate data conditions. *Irrigation and Drainage Systems* 16: 33–45.
- Elhag, M, Psilovikos, A, Manakos, I, Perakis, K. 2011. Application of the Sebs Water Balance Model in Estimating Daily Evapotranspiration and Evaporative Fraction from Remote Sensing Data Over the Nile Delta. *Water Resources Management* 25: 2731–2742.
- Federer, CA, Vorosmarty, C, Fekete, B. 1996. Intercomparison of methods for calculating potential evaporation in regional and global water balance models. *Water Resources Research* 32(7): 2315-2321.
- Fiener, P, Auerswald, K, Van Oost, K. 2011. Spatio-temporal patterns in land use and management affecting surface runoff response of agricultural catchments—A review. *Earth-Science Reviews* 106(1): 92-104.
- Fooladmand, HR. 2011 Evaluation of Blaney-Criddle equation for estimating evapotranspiration in south of Iran *African Journal of Agricultural Research* 6(13): 3103-3109.

- Garrigues, S, Allard D, Baret, F, Weiss, M. 2006. Influence of landscape spatial heterogeneity on the non-linear estimation of leaf area index from moderate spatial resolution remote sensing data. *Remote Sensing of Environment* 106: 286-298.
- Gibson, LA, C Jarman, C, Su, Z, Eckardt, FE. 2013. Estimating evapotranspiration using remote sensing and the Surface Energy Balance System – A South African perspective. *Water SA* 39(4): 477-484.
- Gibson, LA, Munch, Z, Engelbrecht, J. 2011. Particular uncertainties encountered in using a pre-packaged SEBS model to derive evapotranspiration in a heterogeneous study area in South Africa. *Hydrology and Earth System Sciences* 15: 295–310.
- Gilbert, M, González-Piqueras, J, Garcia-Haro, F, Meliá, J. 2002. A generalized soil-adjusted vegetation index. *Remote Sensing of Environment* 82(2): 303-310.
- Glenn, EP, Huete, AR, Nagler, PL, Hirschboeck, KK, Brown, P. 2007. Integrating Remote Sensing and Ground Methods to Estimate Evapotranspiration. *Critical Reviews in Plant Sciences* 26: 139–168.
- Glenn, EP, Nagler, PL, Huete, AR. 2010. Vegetation index methods for estimating evapotranspiration by remote sensing. *Surveys in Geophysics* 31(6): 531-555.
- Gómez, M, Olioso, A, Sobrino, JA, Jacob, F. 2005. Retrieval of evapotranspiration over the Alpillles/ReSeDA experimental site using airborne POLDER sensor and a thermal camera. *Remote Sensing of Environment* 96: 399–408.
- Gowda, PH, Chávez, JL, Colaizzi, PD, Evett, SR, Howell, TA, Tolk, JA. 2007. Remote sensing based energy balance algorithms for mapping ET: Current status and future challenges. *American Society of Agricultural and Biological Engineers* 50(5): 1639-1644.
- Gowda, PH, Howell, TA, Paul, G, Colaizzi, PD, Marek, TH, Su, B, Copeland, KS. 2013. Deriving Hourly Evapotranspiration Rates with SEBS: A Lysimetric Evaluation. *Vadose Zone Journal* 12(3): 1-40.
- Guerschman, JP, Van Dijk, AI, Mattersdorf, G, Beringer, J, Hutley, LB, Leuning, R, Pipunic, RC, Sherman, BS. 2009. Scaling of potential evapotranspiration with MODIS data reproduces flux observations and catchment water balance observations across Australia. *Journal of Hydrology* 369(1): 107-119.
- Haines-Young, R, Chopping, M. 1996. Quantifying landscape structure: a review of landscape indices and their application to forested landscapes. *Progress in Physical Geography* 20(4): 418-445.

- Hankerson, B, Kjaersgaard, J, Hay, C. 2012. Estimation of Evapotranspiration from fields with and without cover crops using remote sensing and in situ methods. *Remote Sensing* 4(12): 3796-3812.
- Hargreaves, GH, Samani, ZA. 1985. Reference crop evapotranspiration from ambient air temperature. *Applied Engineering in Agriculture* 1(2): 96-99.
- He, YB, Z, S, L, J, Wang, SL. 2007. Regional evapotranspiration of different land covers based on remote sensing. *Journal of Applied Ecology* 18(2): 288-296.
- Hellegers, PJGJ, Soppe, R, Perry, CJ, Bastiaanssen, WGM. 2009. Combining remote sensing and economic analysis to support decisions that affect water productivity. *Irrigation Science* 27(3): 243-251.
- Hemakumara, HM, Chandrapala, L, Moene, AF. 2003. Evaporation fluxes over mixed vegetation areas measured from large aperture scintillometer. *Agricultural Water Management* 58: 109-122.
- Hoedjes, JCB, Chehbouni, A, Ezzah, J, Escadafal, R, de Bruin, HAR. 2007. Comparison of Large Aperture Scintillometer and Eddy Covariance Measurements: Can Thermal Infrared Data Be Used to Capture Footprint-Induced Differences? *Journal of Hydrometeorology* 8: 144-159.
- Irmak, A, Ratcliffe, I, Ranade, P, Hubbard, K, Singh, KR. 2011. Estimation of Land Surface Evapotranspiration with a Satellite Remote Sensing Procedure. *Great Plains Research* 21: 73-88.
- Jackson, RD, Idso, S, Reginato, R, Pinter, P. 1981. Canopy temperature as a crop water stress indicator. *Water Resources Research* 17(4): 1133-1138.
- Jacobsen, A. 1999. Estimation of the soil heat flux/net radiation ratio based on spectral vegetation indexes in high-latitude Arctic areas. *International Journal of Remote Sensing* 20(2): 445-461.
- Jarmain, C, Bastiaanssen, W, Mengistu, M, Jewitt, G, Kongo, V. 2009a. *A Methodology for Near-Real Time Spatial Estimation of Evaporation*. Report No. 1751/1/09 Water Research Commission, Pretoria, South Africa.
- Jarmain, C, Everson, C. 2002. *Comparative evaporation measurements above commercial forestry and sugarcane canopies in the KwaZulu-Natal midlands*. Report No. ENV-CS CSIR, Pretoria, South Africa.

- Jarman, C, Everson, C, Savage, M, Mengistu, M, Clulow, A, Walker, S, Gush, M. 2009b. *Refining tools for evaporation monitoring in support of water resources management*. Report No. 1567/1/08 Water Research Commission, Pretoria, South Africa.
- Jia, L, Su, Z, van den Hurk, B, Menenti, M, Moene, A, De Bruin, HAR, Yrisarry, JJB, Ibanez, M, Cuesta, A. 2003. Estimation of sensible heat flux using the Surface Energy Balance System (SEBS) and ATSR measurements. *Physics and Chemistry of the Earth* 28(1–3): 75-88.
- Jovanovic, N, Jarman, C, De Clercq, W, Vermeulen, T, Fey, M. 2011. Total evaporation estimates from a Renosterveld and dryland wheat/fallow surface at the Voëlvlei Nature Reserve (South Africa). *Water SA* 37(4): 471-482.
- Jun, X, Bingfang, W, Nana, Y, Yuan, Z, Shufu, L. 2010. Estimation and Validation of Land Surface Evaporation Using Remote Sensing and Meteorological Data in North China. *IEEE Journal of Selected Topics in Applied Earth Observations and Remote Sensing* 3(3): 337-344.
- Kalma, JD, McVicar, TR, McCabe, MF. 2008. Estimating Land Surface Evaporation: A Review of methods using remotely sensed surface temperature data. *Survey Geophysics* 29: 421–469.
- Kongo, VM, Jewitt, GPW. 2006. Preliminary investigation of catchment hydrology in response to agricultural water use innovations: A case study of the Potshini catchment – South Africa. *Physics and Chemistry of the Earth* 31: 976–987.
- Kowe, P, Pedzisai, E, Gumindoga, W, Rwasoka, D. 2014. An analysis of changes in the urban landscape composition and configuration in the Sancaktepe District of Istanbul Metropolitan City, Turkey using landscape metrics and satellite data *Geocarto International*(just-accepted): 1-30.
- Kustas, WP, Li, F, Jackson, TJ, Prueger, JH, MacPherson, JI, Wolde, M. 2004. Effects of remote sensing pixel resolution on modeled energy flux variability of croplands in Iowa. *Remote Sensing of Environment* 92(4): 535-547.
- Kustas, WP, Norman, JM. 2000. Evaluating the effects of subpixel heterogeneity on pixel average fluxes. *Remote Sensing of Environment* 74(3): 327-342.
- Kustas, WP, Daughtry, CST. 1990. Estimating of the soil heat flux/net radiation ratio from spectral data. *Agricultural and Forest Meteorology* 49: 205-223.

- Lee, TS, Najim, MMM, Aminul, MH. 2004. Estimating evapotranspiration of irrigated rice at the West Coast of the Peninsular of Malaysia. *Journal of Applied Irrigation Science* 39(1): 103-111.
- Li, Z, Tang, R, Wan, Z, Bi, Y, Zhou, C, Tang, B, Yan, G, Zhang, X. 2009. A review of current methodologies for regional evapotranspiration estimation from remotely sensed data. *Sensors* 9: 3801-3853.
- Liu, S, Mao, D, Lu, L. 2006. Measurement and estimation of the aerodynamic resistance. . *Hydrology and Earth System Sciences Discussions* 3: 681–705.
- Long, D, Singh, VP, Li, Z-L. 2011. How sensitive is SEBAL to changes in input variables, domain size and satellite sensor? *Journal of Geophysical Research* 116(21): 1-20.
- Lott, RB, Hunt, RJ. 2001. Estimating evapotranspiration in natural and constructed wetlands. *Wetlands* 21(4): 614–628.
- Lu, J, Sun, G, McNulty, SG, Amatya, DM. 2005. A comparison of six potential evapotranspiration methods for regional use in the South Eastern United States. *Journal of American Water Resources Association* 41(3): 621-633.
- Ma, W, Hafeez, M, Ishikawa, H, Ma, Y. 2013. Evaluation of SEBS for estimation of actual evapotranspiration using ASTER satellite data for irrigation areas of Australia. *Theoretical and Applied Climatology* 112(3-4): 609-616.
- Ma, W, Ma, Y, Su, B. 2011. Feasibility of retrieving land surface heat fluxes from ASTER data using SEBS: a case study from the Namco area of the Tibetan plateau. *Arctic, Antarctic, and Alpine Research* 43(2): 239-245.
- Ma, Y, Ishikawa, H, Tsukamoto, O, Menenti, M, Su, Z, Yao, T, Koike, T, Yasunari, T. 2003. Regionalization of surface fluxes over heterogeneous landscape of the Tibetan Plateau by using satellite remote sensing data. *Journal of the Meteorological Society of Japan* 81(2): 277-293.
- Maeda, EE, Wiberg, DA, Pellikka, PKE. 2011. Estimating reference evapotranspiration using remote sensing and empirical models in a region with limited ground data availability in Kenya. *Applied Geography* 31: 251-258.
- Makkink, G. 1957. Testing the Penman formula by means of lysimeters. *Journal of the Institution of Water Engineers* 11(3): 277-288.
- McCabe, MF, Wood, EF. 2006. Scale influences on the remote estimation of evapotranspiration using multiple satellite sensors. *Remote Sensing of Environment* 105(4): 271-285.

- McGarigal, K. 2006. *Landscape Pattern Metrics*, Encyclopedia of environmetrics. John Wiley & Sons, Ltd.
- McJannet, D, Cook, F, McGloin, R, McGowan, H, Burn, S, Sherman, B. 2013. Long-term energy flux measurements over an irrigation water storage using scintillometry. *Agricultural and Forest Meteorology* 168: 93-107.
- McMahon, TA, Peel, MC, Lowe, L, Srikanthan, R, McVicar, T, R. 2012. Estimating actual, potential, reference crop and pan evaporation using standard meteorological data: a pragmatic synthesis. *Hydrology and Earth System Sciences Discussions* 9: 11829–11910.
- Meijninger, WML, de Bruin, HAR. 2000. The sensible heat fluxes over irrigated areas in western Turkey determined with a large aperture scintillometer. *Journal of Hydrology* 229(1–2): 42-49.
- Menenti, M, Bastiaanssen, W, van Eick, D, Abd el Karim, MA. 1989. Linear relationships between surface reflectance and temperature and their application to map actual evaporation of groundwater. *Advances in Space Research* 9(1): 165-176.
- Menenti, M, Jia, L, Su, H. 2003. On SEBI-SEBS validation in France, Italy, Spain, USA and China. *Proceedings of the workshop on use of remote sensing of crop evapotranspiration for large regions. International Commission on Irrigation and Drainage (ICID)*. Montpellier, France.
- Mengistu, M, Savage, M. 2010. Surface renewal method for estimating sensible heat flux. *Water SA* 36(1): 9-18.
- Mengistu, MG, Everson, CS, Moyo, NC, Savage, MJ. 2014. *The Validation of the Variables (Evaporation and Soil Moisture) in Hydrometeorological Models*. 2066/1/13 Pretoria, South Africa.
- Meyers, TP, Baldocchi, DD. 2005. *Current micrometeorological flux methodologies with applications in agriculture*, in: Hatfield, J., Baker, J. (Eds.), *Micrometeorology in Agricultural Systems*, pp. 381–396.
- Minacapilli, M, Agnese, C, Blanda, F, Cammalleri, C, Ciralo, G, D’Urso, G, Iovino, M, Pumo1, D, Provenzano, G, Rallo, G. 2009. Estimation of actual evapotranspiration of Mediterranean perennial crops by means of remote-sensing based surface energy balance models. *Hydrology and Erath System Sciences* 13: 1061–1074.
- Monteith, J. 1965. Evaporation and environment. *Symp. Soc. Exp. Biol.*

- Moran, M, Rahman, A, Washburne, J, Goodrich, D, Weltz, M, Kustas, W. 1996. Combining the Penman-Monteith equation with measurements of surface temperature and reflectance to estimate evaporation rates of semiarid grassland. *Agricultural and Forest Meteorology* 80(2): 87-109.
- Muthuwatta, L, Bos, M, Rientjes, T. 2010. Assessment of water availability and consumption in the Karkheh River basin, Iran using remote sensing and geo-statistics. *Water Resources Management* 24(3): 459-484.
- Mutiga, JK, Su, Z, Woldai, T. 2010. Using satellite remote sensing to assess evapotranspiration: Case study of the upper Ewaso Ng'iro North Basin, Kenya. *International Journal of Applied Earth Observation and Geoinformation* 12, Supplement 1(0): S100-S108.
- Nagler, PL, Cleverly, J, Glenn, E, Lampkin, D, Huete, A, Wan, Z. 2005. Predicting riparian evapotranspiration from MODIS vegetation indices and meteorological data. *Remote Sensing of Environment* 94(1): 17-30.
- Norman, J, Anderson, M, Kustas, W, French, A, Mecikalski, J, Torn, R, Diak, G, Schmugge, T, Tanner, B. 2003. Remote sensing of surface energy fluxes at 101-m pixel resolutions. *Water Resources Research* 39(8).
- Odhiambo, GO, Savage, MJ. 2009. Surface layer scintillometry for estimating the sensible heat flux component of the surface energy balance. *South African Journal of Science* 105: 208-216.
- Penman, HL. 1948. Natural Evaporation from Open Water, Bare Soil and Grass. *Proceedings of the Royal Society of London. Series A. Mathematical and Physical Sciences* 193(1032): 120-145.
- Pereira, AR, Pruitt, WO. 2004. Adaptation of the Thornthwaite scheme for estimating daily reference evapotranspiration. *Agricultural Water Management* 66(3): 251-257.
- Praveen, P, Kumar, MDS, Puttaswamy, H, Patil, PVM, Kumar, R. 2011. Estimation of evapotranspiration rate by different methods for paddy crop in South Kodagu, Central Western Ghats. *Plant Sciences Feed* 1(1): 1-5.
- Priestley, CHB, Taylor, RJ. 1972. On the Assessment of Surface Heat Flux and Evaporation Using Large-Scale Parameters. *Monthly Weather Review* 100(2): 81-92.
- Qi, J, Chehbouni, A, Huete, AR, Kerr, YH, Sorooshian, S. 1994. A modified soil adjusted vegetation index. *Remote Sensing of Environment* 48(2): 119-126.

- Rana, G, Katerji, N. 2000. Measurement and estimation of actual evapotranspiration in the field under Mediterranean climate: a review. *European Journal of Agronomy* 13(2–3): 125-153.
- Riitters, KH, O'Neill, R, Hunsaker, C, Wickham, JD, Yankee, D, Timmins, S, Jones, K, Jackson, B. 1995. A factor analysis of landscape pattern and structure metrics. *Landscape ecology* 10(1): 23-39.
- Roerink, GR, Su, Z, Menenti, M. 2000. S-SEBI: A Simple Remote Sensing Algorithm to Estimate the Surface Energy Balance. *Physics and Chemistry of the Earth* 25(2): 147-157.
- Rondeaux, G, Steven, M, Baret, F. 1996. Optimization of soil-adjusted vegetation indices. *Remote Sensing of Environment* 55(2): 95-107.
- Ruhoff, AL, Paz, AR, Collischonn, W, Aragao, LEOC, Rocha, HR, Malhi, YS. 2012. A MODIS-based energy balance to estimate evapotranspiration for clear-sky days in Brazilian Tropical Savannas. *Remote Sensing* 4: 703-725.
- Rwasoka, DT, Gumindoga, W, Gwenzi, J. 2011. Estimation of actual evapotranspiration using the Surface Energy Balance System (SEBS) algorithm in the Upper Manyame catchment in Zimbabwe. *Physics and Chemistry of the Earth* 36(14–15): 736-746.
- Saura, S. 2004. Effects of remote sensor spatial resolution and data aggregation on selected fragmentation indices. *Landscape ecology* 19(2): 197-209.
- Savage, M, Everson, C, Odhiambo, G, Mengistu, M, Jarman, C. 2004. *Theory and practice of evapotranspiration measurement, with special focus on surface layer scintillometer (SLS) as an operational tool for the estimation of spatially-averaged evaporation*. Water Research Commission, Pretoria, South Africa.
- Savage, M, Odhiambo, G, Mengistu, M, Everson, C, Jarman, C. 2010. Measurement of grassland evaporation using a surface-layer scintillometer. *Water SA* 36(1): 1-8.
- Savage, MJ, Everson, CS, Metelerkamp, BR. 1997. *Evaporation measurement above vegetated surfaces using micrometeorological techniques*. Water Research Commission, Pretoria South Africa.
- Savenije, HHG. 2004. The importance of interception and why we should delete the term evapotranspiration from our vocabulary. *Hydrological Processes* 18: 1507–1511.
- Scott, RL. 2010. Using watershed water balance to evaluate the accuracy of eddy covariance evaporation measurements for three semiarid ecosystems. *Agricultural and Forest Meteorology* 150: 219–225.

- Seevers, PM, Ottmann, RW. 1994. Evapotranspiration estimation using a normalized difference vegetation index transformation of satellite data. *Hydrological Sciences* 39(4).
- Senay, BG, Leake, S, Nagler, PL, Artan, G, Dickinson, J, Cordova, JT, Glenn, EP. 2011. Estimating basin scale evapotranspiration (ET) by water balance and remote sensing methods. *Hydrological Processes* 25: 4037–4049.
- Seto, KC, Fragkias, M. 2005. Quantifying spatiotemporal patterns of urban land-use change in four cities of China with time series landscape metrics. *Landscape ecology* 20(7): 871-888.
- Shilpakar, RL, Bastiaanssen, WGM, Molden, DJ. 2011. A remote sensing-based approach for water accounting in the East Rapti River Basin, Nepal. *Himalayan Journal of Sciences* 7(9): 15-30.
- Sobrino, JA, Gómez, M, Jiménez-Muñoz, JC, Olioso, A. 2007. Application of a simple algorithm to estimate daily evapotranspiration from NOAA–AVHRR images for the Iberian Peninsula. *Remote Sensing of Environment* 110: 139–148.
- Spano, D, Snyder, RL, Ducec, P, U.K.T., P. 2000. Estimating sensible and latent heat flux densities from grapevine canopies using surface renewal. *Agricultural and Forest Meteorology* 104: 171–183.
- Su, H, Wood, EF, McCabe, M, F., Su, Z. 2007. Evaluation of remotely sensed Evapotranspiration over the CEOP EOP-1 Reference Sites. *Journal of the Meteorological Society of Japan* 85A: 439-459.
- Su, Z. 2002. The Surface Energy Balance System (SEBS) for estimation of turbulent heat fluxes. *Hydrology and Earth System Sciences* 6(1): 85-99.
- Sugita, F, Kishii, T. 2002. Effect of roughness distribution on evaporation processes over non-homogeneous sand surfaces: a wind tunnel investigation. *Hydrological Processes* 16: 2141–2153.
- Sumner, DM, Jacobs, JM. 2005. Utility of Penman–Monteith, Priestley–Taylor, reference evapotranspiration, and pan evaporation methods to estimate pasture evapotranspiration. *Journal of Hydrology* 308: 81-104.
- Szilagy, J, Rundquist, DC, Gosselin, D, C., Parlange, MB. 1998. NDVI relationship to monthly evaporation. *Geophysical Research Letters*. 25(10): 1753-1756.
- Teixeira, AHC, Bastiaanssen, WGM, Ahmad, MD, Bos, MG. 2009. Reviewing SEBAL input parameters for assessing evapotranspiration and water productivity for the Low-Middle

- Saõ Francisco River basin, Brazil Part A: Calibration and validation. *Agricultural and Forest Meteorology* 149: 462-476.
- Thornthwaite, CW. 1948. An Approach toward a Rational Classification of Climate. *Geographical Review* 38(1): 55-94.
- Turc, L. 1961. Estimation of irrigation water requirements, potential evapotranspiration: A simple climatic formula evolved up to date. *Annual Agronomy* 12: 13-49.
- Turner, MG. 1989. Landscape ecology: the effect of pattern on process. *Annual review of ecology and systematics*: 171-197.
- Turner, MG. 2001. *Landscape ecology in theory and practice: pattern and process*. Springer.
- Uuemaa, E, Antrop, M, Roosaare, J, Marja, R, Mander, Ü. 2009. Landscape metrics and indices: an overview of their use in landscape research. *Living Reviews in Landscape Research* 3(1): 1-28.
- Uuemaa, E, Mander, Ü, Marja, R. 2013. Trends in the use of landscape spatial metrics as landscape indicators: A review. *Ecological Indicators* 28(0): 100-106.
- van den Hurk, B. 2001. Energy balance based surface flux estimation from satellite data and its application for surface moisture assimilation. *Meteorology and Atmospheric Physics* 76: 43-52.
- van der Kwast, J, Timmermans, W, Gieske, A, Su, Z, Olioso, A, Jia, L, Elbers, J, D. Karssenbergh, D, S. de Jong, S. 2009. Evaluation of the Surface Energy Balance System (SEBS) applied to ASTER imagery with flux-measurements at the SPARC 2004 site (Barrax, Spain). *Hydrology and Earth System Sciences* 13: 1337–1347.
- Vinukollu, RK, Wood, EF, Ferguson, RC, Fisher, JB. 2011. Global estimates of evapotranspiration for climate studies using multi-sensor remote sensing data: Evaluation of three process-based approaches. *Remote Sensing of Environment* 115: 801–823.
- Weiß, M, Menzel, L. 2008. A global comparison of four potential evapotranspiration equations and their relevance to stream flow modelling in semi-arid environments. *Advances in Geosciences* 18: 15–23.
- Weng, Q, Liu, H, Lu, D. 2007. Assessing the effects of land use and land cover patterns on thermal conditions using landscape metrics in city of Indianapolis, United States. *Urban Ecosystems* 10(2): 203-219.
- Wright, JL. 1982. Crop coefficient for estimates of daily crop evapotranspiration. *Irrigation and Drainage Division of the American Society of Civil Engineering* 108(2): 58-74.

- Xu, CY, Singh, VP. 2002. Cross comparison of empirical equations for calculating potential evapotranspiration with data from Switzerland. *Water Resources Management* 16: 197–219.
- Zhang, L, Hickel, K, Dawes, WR, Chiew, FHS, Western, AW, Briggs, PR. 2004. A rational function approach for estimating mean annual evapotranspiration. *Water Resources Research* 40: 1-14.
- Zhou, W, Huang, G, Cadenasso, ML. 2011. Does spatial configuration matter? Understanding the effects of land cover pattern on land surface temperature in urban landscapes. *Landscape and Urban Planning* 102(1): 54-63.

3. OVERVIEW OF METHODOLOGY

3.1 Introduction

Total evaporation was estimated for the uMngeni catchment in KwaZulu-Natal Province, South Africa, using the SEBS model. The SEBS model requires three sets of information or data. The first set of data consists of land surface albedo, emissivity, temperature, Normalized Difference Vegetation Index (NDVI) fractional vegetation coverage (FVC) leaf area index (LAI), and the height of the vegetation. If vegetation information is not available, the NDVI is used as a surrogate. These input data can be derived from remote sensing data in conjunction with other information about the surface of interest. The second set includes meteorological data, such as air pressure, temperature, humidity, and wind speed at a reference height. These meteorological variables can be estimated by large scale meteorological models. The third set includes downward solar radiation, which can either be measured or estimated as model output or parameterization (Su, 2002).

The study further estimates the spatial variations of total evaporation over a year (May 2013 to April 2014), which include the dry (May to October 2013) and wet (November to April) seasons. This was done using daily reference evaporation (ET_o) estimated for the uMngeni catchment from May 2013 to April 2014. In addition, the spatial heterogeneity across the uMngeni catchment was determined in relation to the scale of observation (spatial resolutions) of the two different sensors.

3.2 SEBS Remote Sensing Inputs

Remotely sensed SEBS inputs were derived from the 30 m resolution Landsat 8 and 1000 m resolution MODIS datasets, where these datasets include albedo, emissivity, NDVI, FVC, surface temperature (LST) and LAI. These parameters were derived from the two remotely sensed datasets using equations outlined in Appendices A and B. A sample of the derived remote sensing inputs from the two sensors is shown in Figures 3.1 for 24 June 2013 (representing the dry season) and in Figure 3.2 for 23 March 2014 (representing the wet season). These figures show the spatial variations of the SEBS inputs for the two selected days.

It can be observed that the remote sensing inputs from the Landsat 8 and MODIS datasets show the same spatial variations for the two days. For instance, higher LST estimates were obtained in the eastern and southern areas than in the western and northern areas of the catchment. The eastern and southern areas of the catchment are dominated by built up areas (urban areas), whereas the western and northern areas are occupied by plantations, natural forests, commercial irrigated agriculture, water bodies and wetlands. However, Landsat 8 showed higher LST values, with more variability across the catchment when compared to the 1000 m MODIS data (Figures 3.1 and 3.2).

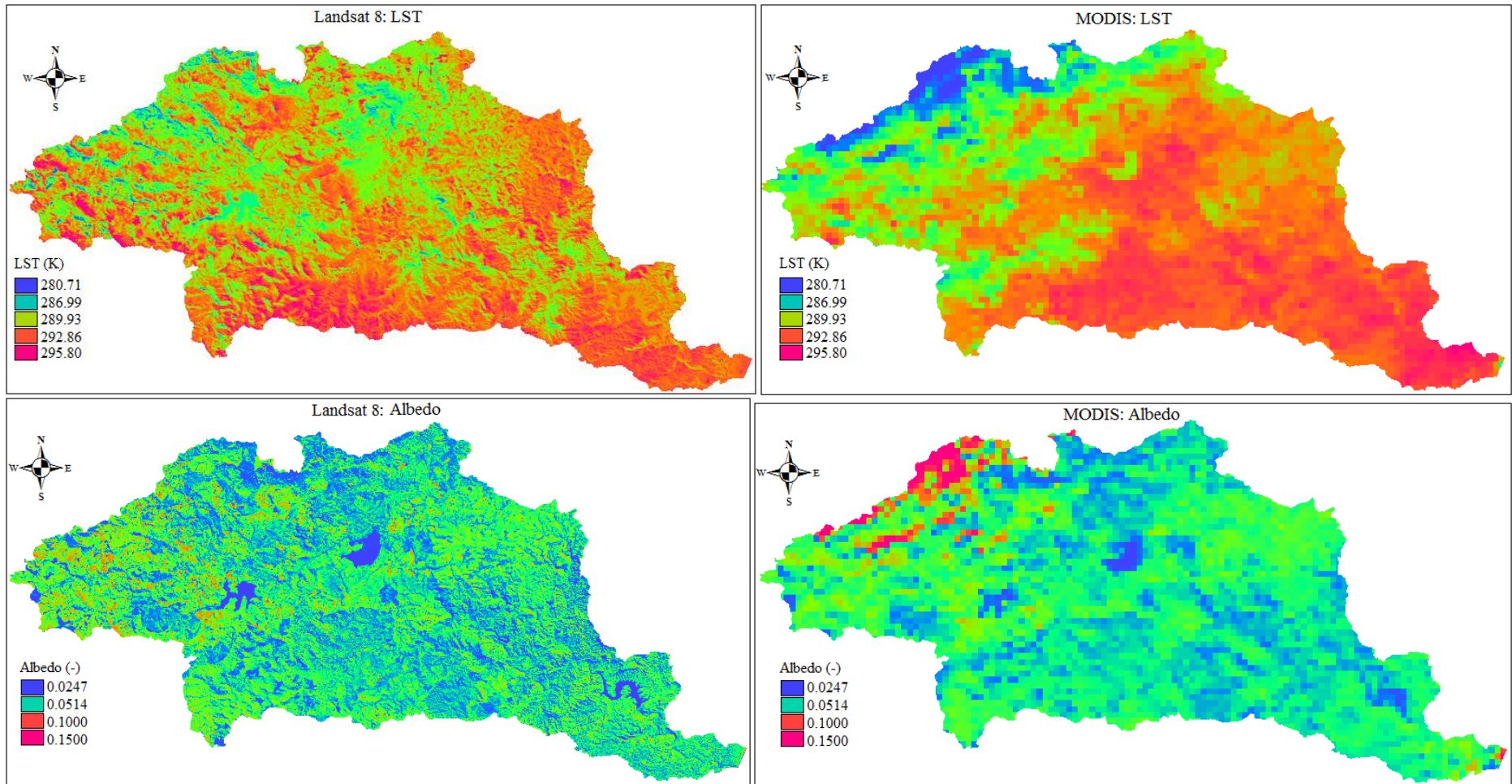


Figure 3.1 SEBS remote sensing inputs for 24 June 2013 (dry season)

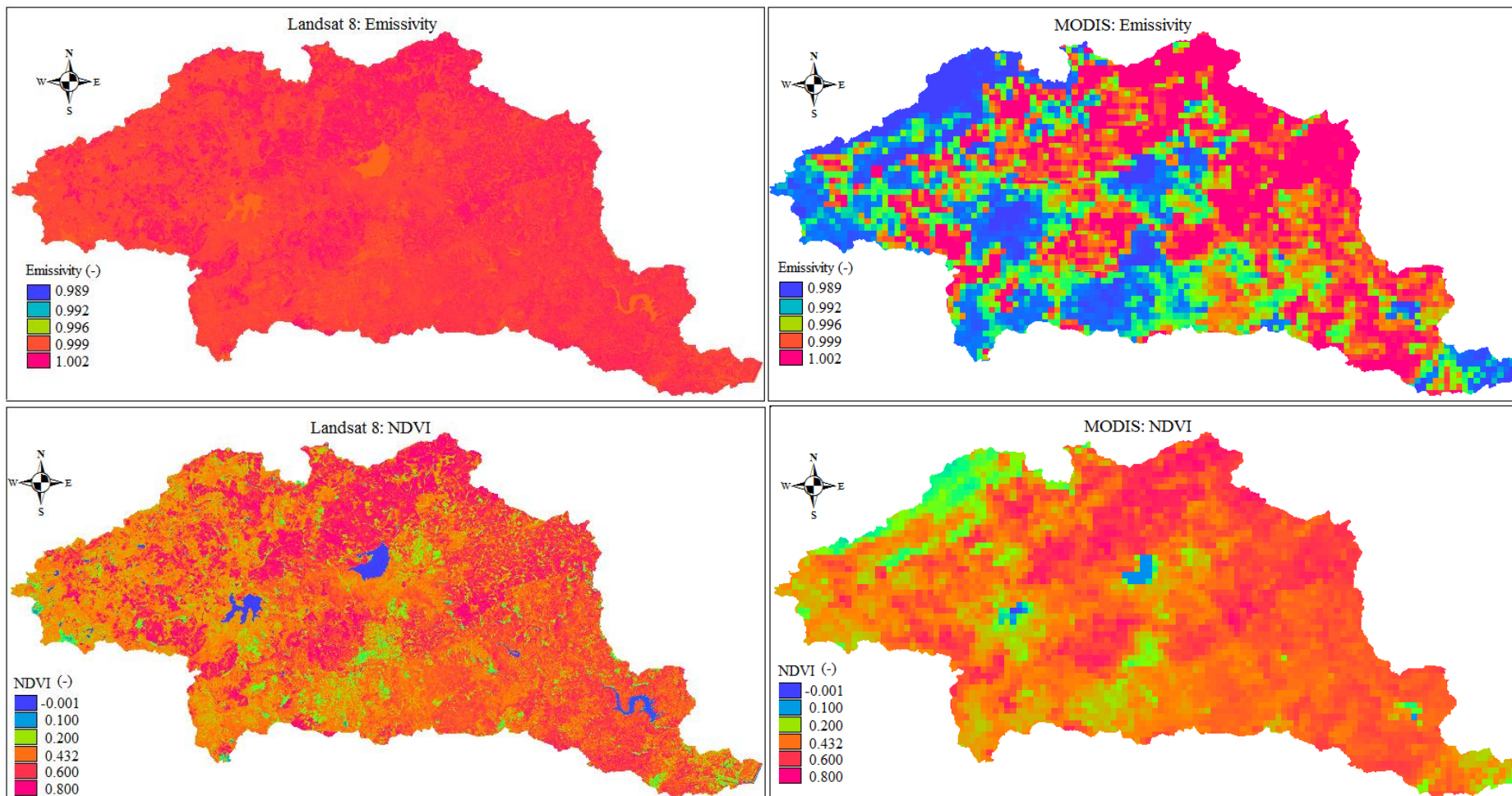


Figure 3.1 cont...

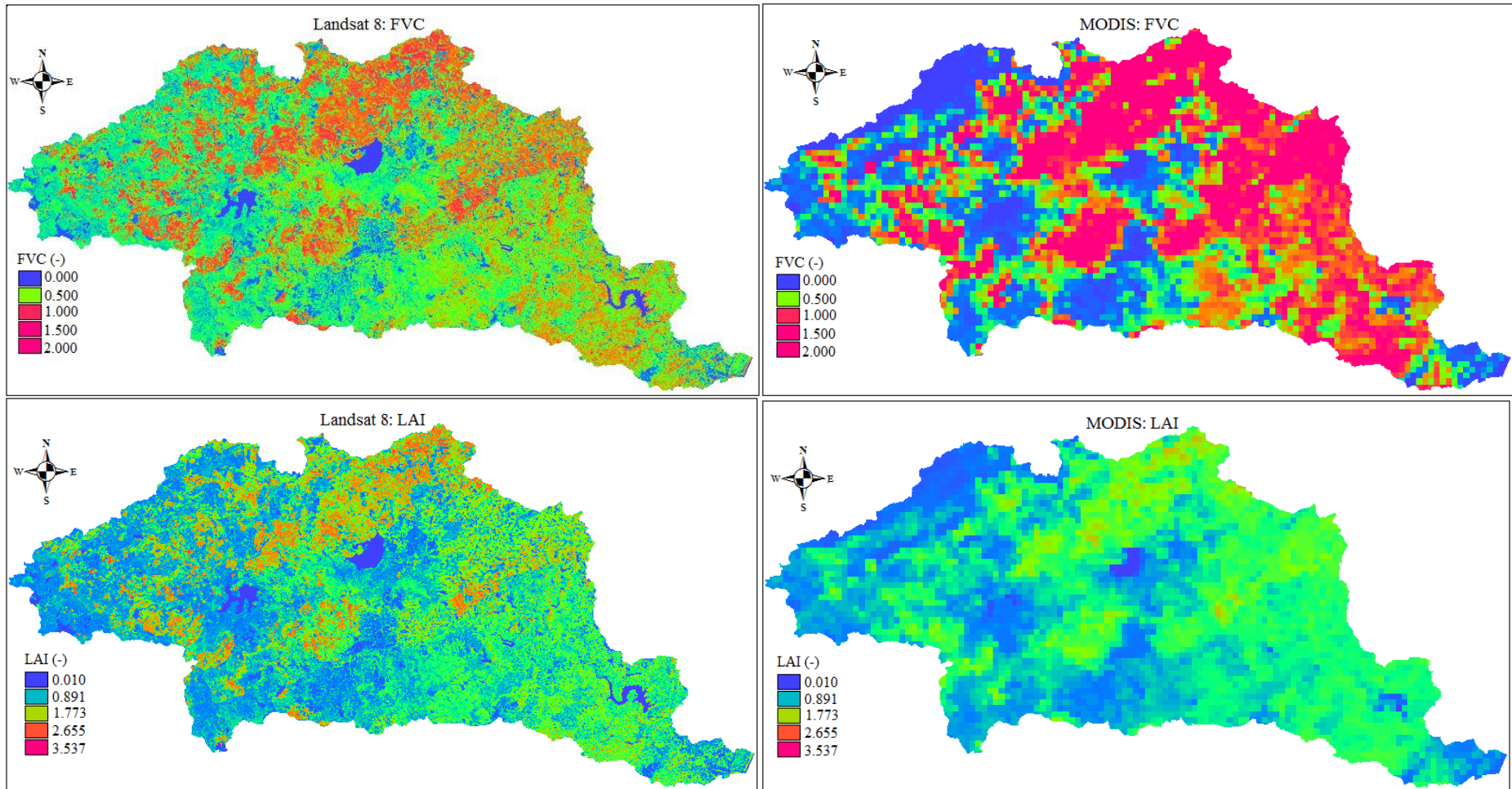


Figure 3.1 *cont...*

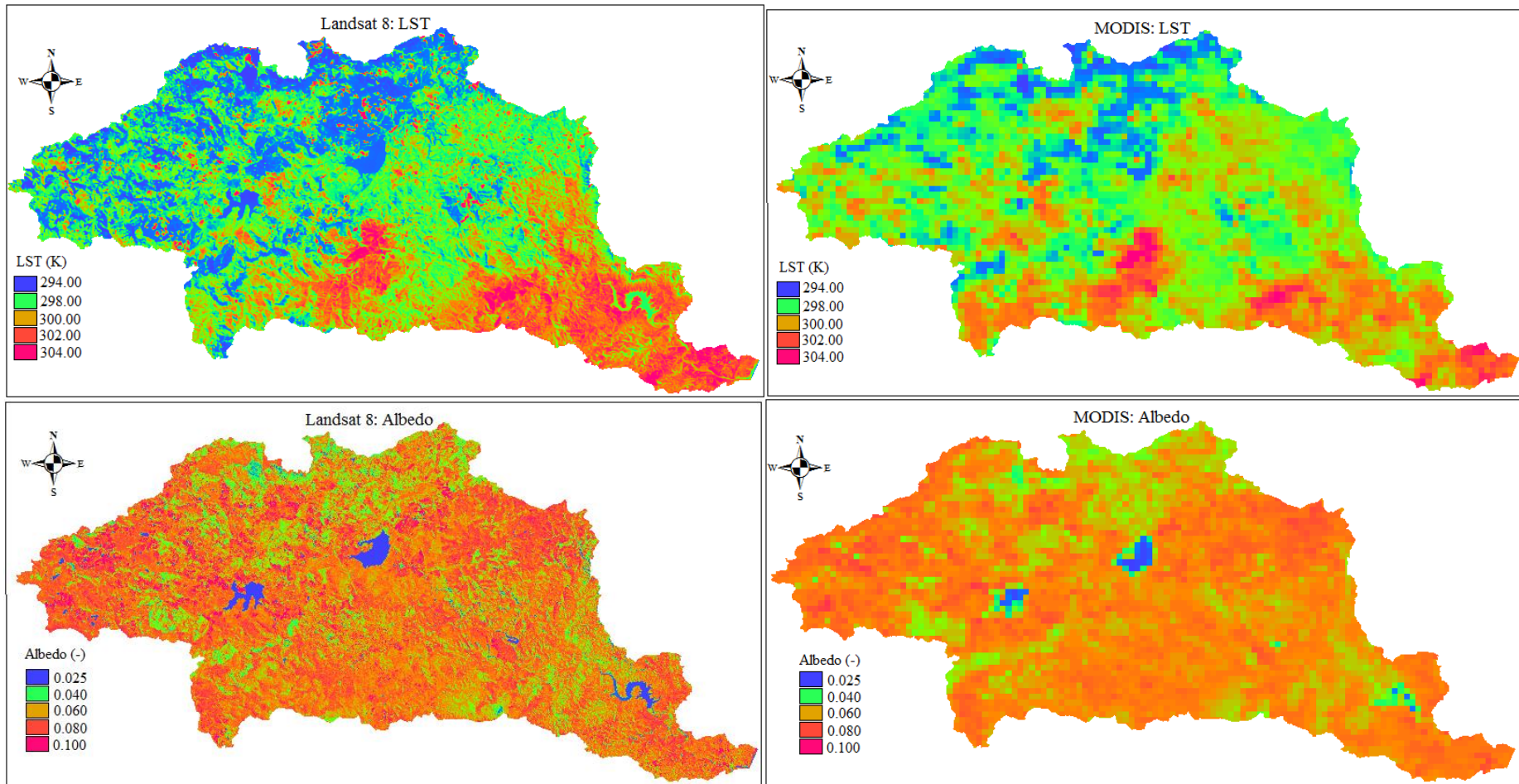


Figure 3.2 SEBS remote sensing inputs for 23 March 2014 (wet season)

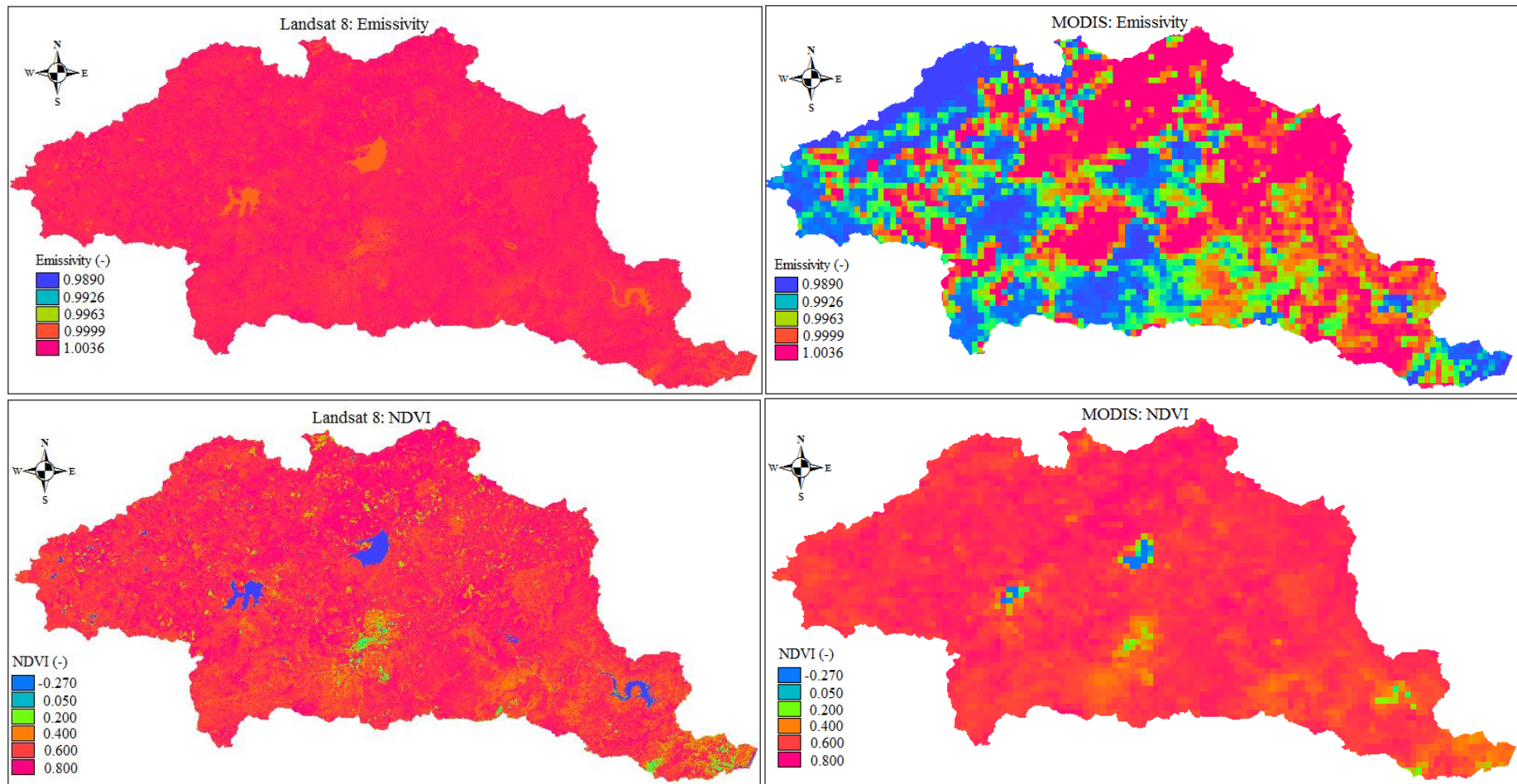


Figure 3.2 cont...

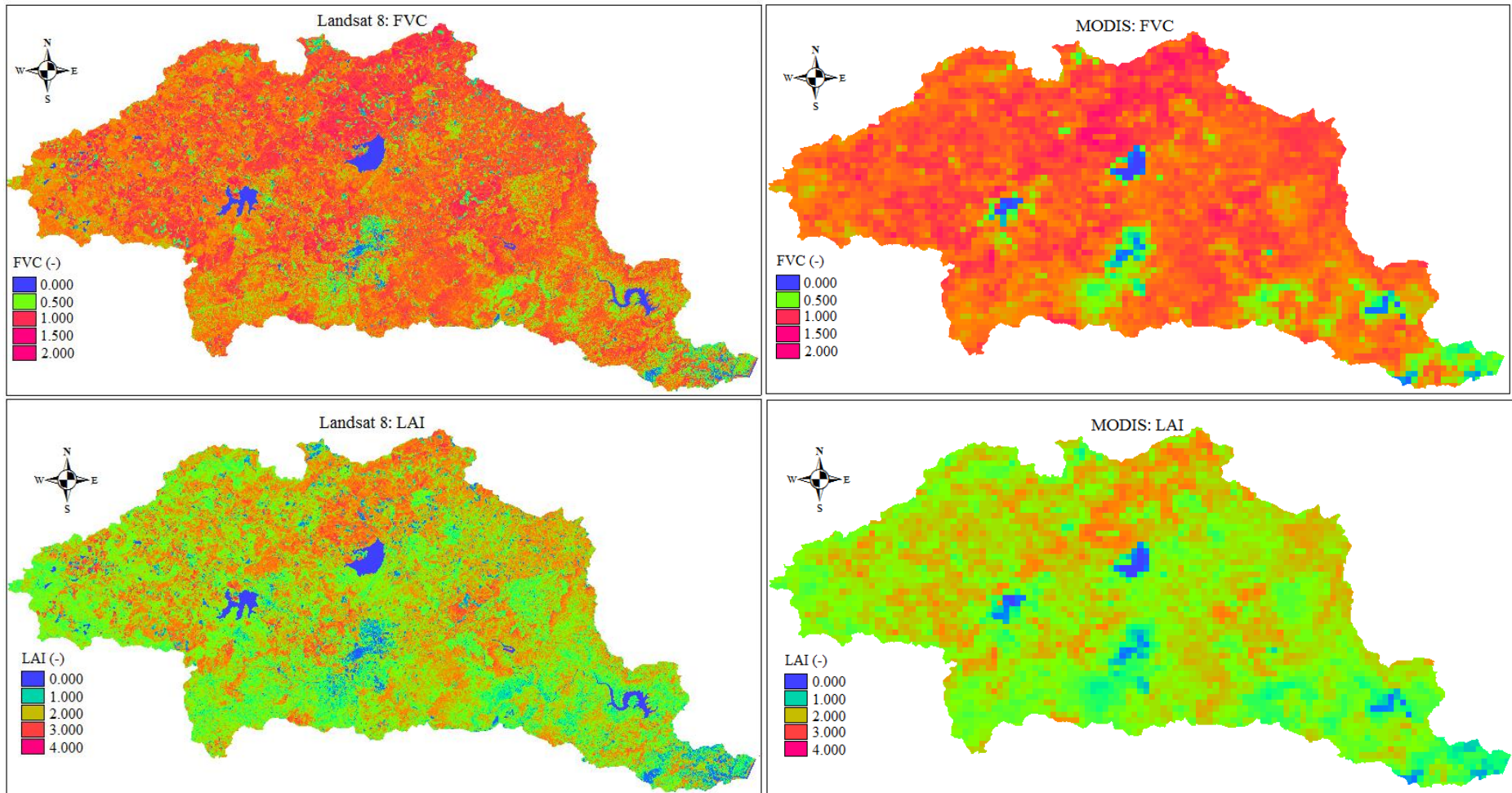


Figure 3.2 cont...

It was also found that the SEBS remote sensing inputs derived from the two sensors show variations between the two days representing dry and wet seasons. On the 24th of June 2013 (dry), LST estimates were low, ranging from 280.71 K in the western and northern escarpments to 295.80 K in the coastal areas (Figure 3.1). The western and northern areas are largely dominated by plantations, natural forests, commercial irrigated agriculture, water bodies and wetlands. In contrast, on the 23rd of March (wet), LST was higher, ranging from 294 K in the western and northern escarpments to 304 K in the southern and eastern coastal areas (Figure 3.2). The majority of the land cover types within the southern and eastern coastal areas are built-up areas. This highlights the spatial and temporal variability of surface temperature across the uMngeni catchment.

The MODIS dataset showed lower emissivity values, when compared to the Landsat 8 dataset. Emissivity refers to the ability of the surface to radiate incoming radiation and normally ranges between 0.9 and 1. Emissivity depends on surface-cover type, soil moisture content, soil organic content and vegetation density (Mallick *et al.*, 2012). Generally, vegetated areas show slightly higher emissivity, as compared to water or bare surfaces. Low emissivity values indicate high reflection. This implies that the surface has low absorption ability of incoming radiation, hence less energy available for evaporation (Mallick *et al.*, 2012). With regard to the estimation of albedo, although its values are normally very low (less than 0.5) for most surfaces, the MODIS sensor estimated slightly higher estimates, especially in the north-western part of the catchment. This implies less absorption of incoming radiation (less energy available) and consequently reduced evaporation.

A similar pattern was also observed for the other three SEBS input parameters namely: NDVI, LAI and FVC. The increase in NDVI, LAI and FVC may be attributed to the fact that the 23rd of March, represents wet period, which is characterized by higher rainfall, temperature and vegetation development, among other factors, which all contribute to an increase in total evaporation. However, it should be noted that high LST does not result in higher total evaporation estimates, since total evaporation is determined by the available energy ($R_n - G_0$) on the surface and various bio-physical characteristics (*e.g.*, land cover characteristics, moisture availability).

Overall, with regard to the derived SEBS inputs, it has been noted that the 1000 m MODIS datasets show lower and less variability of these parameters across the catchment, compared to the 30 m Landsat 8 data. This has a potential effect on the derived total evaporation estimates and energy fluxes. Total evaporation estimates derived from MODIS and Landsat 8 datasets are more likely to exhibit the same spatial variations as portrayed by the SEBS input parameters (*i.e.*, lower and less variability). Generally, areas with high NDVI, FVC and LAI (western and northern parts of the uMngeni catchment) are more likely to have higher total evaporation estimates, compared to the eastern and southern parts. The western and northern areas of the uMngeni catchment are predominantly natural forests, water bodies, plantations, commercial irrigated agriculture and wetlands, whereas the eastern and southern areas of the catchment are largely dominated by built up areas (urban areas).

3.3 SEBS Meteorological Inputs

Meteorological data used in the SEBS model included daily mean temperature, wind speed, humidity, pressure, sunshine duration and solar radiation. These datasets were recorded from meteorological stations within and adjacent to the uMngeni catchment, which are shown in Figure 3.3. The data from these stations were acquired from the South Africa Weather Services (SAWS) and the South African Sugarcane Research Institute (SASRI). The meteorological data acquired and used is summarised in Table 3.1. The data presented is only for the selected few days in which the SEBS model was run for the corresponding remote sensing images (Landsat 8 and MODIS). The meteorological data was also used to compute daily reference evaporation (from May 2013 to April 2014). The data used in the estimation of daily reference evaporation included wind speed, humidity and temperature. In addition, Table 3.2 shows the meteorological data corresponding to satellite overpass times, which were used in the SEBS model.

Additional inputs used in the SEBS model included a Digital Elevation Model (DEM), (shown in Figure 3.4), average shortwave transmissivity (derived from DEM) (shown in Figure 3.5) of the study area, as well as the Julian day.

Table 3.1 Meteorological data acquired and used in the study

23 May 2013	Meteorological station	T_{mean} (°C)	T_{max} (°C)	T_{min} (°C)	Mean wind speed (m/s)	Pressure (Pa)	Sunshine (hours)	Humidity (%)
	Mount Edgecombe	19.8	27.2	14.5	0.45	100750.0	7.1	80
	PMB-Faulklands	16.3	31.3	7.7	0.44	92468.3	7.7	68
	PMB - Ukulinga	18.8	28.2	11.3	0.50	94140.0	7.8	56
	Wartburg - Bruyns Hill	17.9	26.5	9.9	0.80	90132.1	7.4	45
	Cedara	16.5	26.7	6.3	1.20	89970.0	7.6	58
08 June 2013	Meteorological station	T_{mean} (°C)	T_{max} (°C)	T_{min} (°C)	Mean wind speed (m/s)	Pressure (Pa)	Sunshine (hours)	Humidity (%)
	Mount Edgecombe	21.5	34.7	11.1	0.50	99780.0	7.3	61
	PMB-Faulklands	20.4	31.3	8.0	1.00	93300.0	7.5	53
	PMB - Ukulinga	16.3	28.9	13.0	1.00	92468.3	7.9	37
	Wartburg - Bruyns Hill	17.9	25.9	11.7	1.70	90132.1	7.4	42
	Cedara	16.9	26.8	7.1	1.90	89170.0	7.1	46
24 June 2013	Meteorological station	T_{mean} (°C)	T_{max} (°C)	T_{min} (°C)	Mean wind speed (m/s)	Pressure (Pa)	Sunshine (hours)	Humidity (%)
	Mount Edgecombe	16.2	25.9	9.4	0.38	100540.0	7.3	73
	PMB-Faulklands	14.9	30.1	6.9	0.70	93960.0	8.0	50
	PMB - Ukulinga	18.5	26.5	11.6	1.04	92468.3	8.3	27
	Wartburg - Bruyns Hill	16.0	24.8	7.9	1.52	90132.1	8.2	35
	Cedara	14.1	24.7	3.5	2.50	89800.0	7.8	46

26 July 2013	Meteorological station	T_{mean} (°C)	T_{max} (°C)	T_{min} (°C)	Mean wind speed (m/s)	Pressure (Pa)	Sunshine (hours)	Humidity (%)
	Mount Edgecombe	17.3	24.3	12	0.52	100410.00	7.0	80
	PMB-Faulklands	16.1	29.4	8.1	0.55	93960.00	7.7	67
	PMB - Ukulinga	17.7	27.7	9.9	0.35	92468.28	8.1	56
	Wartburg - Bruyns Hill	16.5	26.1	9.1	1.29	90132.10	7.8	50
	Cedara	15.4	26.1	4.8	1.50	89730.00	7.4	60
11 August 2013	Meteorological station	T_{mean} (°C)	T_{max} (°C)	T_{min} (°C)	Mean wind speed (m/s)	Pressure (Pa)	Sunshine (hours)	Humidity (%)
	Mount Edgecombe	15.9	22.1	7.2	0.99	100500.00	7.5	80
	PMB-Faulklands	13.1	22.7	4.6	0.90	93960.00	8.1	78
	PMB - Ukulinga	13.4	21.0	7.4	0.94	92468.28	8.2	75
	Wartburg - Bruyns Hill	12.1	20.2	5.5	1.93	90132.10	7.9	73
	Cedara	11.8	21.0	2.6	1.98	89580.00	8.1	81
24 March 2014	Meteorological station	T_{mean} (°C)	T_{max} (°C)	T_{min} (°C)	Mean wind speed (m/s)	Pressure (Pa)	Sunshine (hours)	Humidity (%)
	Mount Edgecombe	25.5	31.8	18.9	1.09	100170.40	9.2	80
	PMB-Faulklands	24.7	35.2	17.3	0.73	94140.00	8.6	71
	PMB - Ukulinga	25.2	33.0	18.9	0.75	94111.40	9.6	69
	Wartburg - Bruyns Hill	23.9	32.6	16.7	0.83	91733.60	9.2	61
	Cedara	22.8	34.1	17.1	1.23	92114.00	8.9	70

Table 3.2 Meteorological data corresponding to satellite overpass used in SEBS model

Date	Meteorological station	T_{air} (°C)	Radiation (W/m ²)	Wind speed (m/s)
23 May 2013	Mount Edgecombe	24.2	430.8	1.20
	PMB-Faulklands	18.5	437.8	0.40
	PMB - Ukulinga	20.8	452.3	0.60
	Wartburg - Bruyns Hill	21.6	435.4	0.90
	Cedara	20.2	421.3	1.80
08 June 2013	Meteorological station	T_{air} (°C)	Radiation (W/m ²)	Wind speed (m/s)
	Mount Edgecombe	27.6	404.2	1.20
	PMB-Faulklands	24.2	399.6	1.20
	PMB - Ukulinga	25.2	412.3	2.40
	Wartburg - Bruyns Hill	23.4	426.2	2.00
24 June 2013	Meteorological station	T_{air} (°C)	Radiation (W/m ²)	Wind speed (m/s)
	Mount Edgecombe	22.0	421.6	1.80
	PMB-Faulklands	19.1	410.0	0.55
	PMB - Ukulinga	20.9	429.5	1.60
	Wartburg - Bruyns Hill	18.0	433.1	1.80
26 July 2013	Meteorological station	T_{air} (°C)	Radiation (W/m ²)	Wind speed (m/s)
	Mount Edgecombe	23.3	532.0	0.50
	PMB-Faulklands	18.1	501.3	0.75
	PMB - Ukulinga	20.3	540.6	0.40
	Wartburg - Bruyns Hill	17.4	513.5	1.30
11 August 2013	Meteorological station	T_{air} (°C)	Radiation (W/m ²)	Wind speed (m/s)
	Mount Edgecombe	19.5	454.0	1.70
	PMB-Faulklands	16.4	435.4	1.30
	PMB - Ukulinga	16.6	463.2	1.50
	Wartburg - Bruyns Hill	15.3	459.7	1.80
23 March 2014	Meteorological station	T_{air} (°C)	Radiation (W/m ²)	Wind speed (m/s)
	Mount Edgecombe	28.2	617.7	0.10
	PMB-Faulklands	26.9	653.4	1.60
	PMB - Ukulinga	29.8	673.8	2.00
	Wartburg - Bruyns Hill	25.7	643.8	1.30
	Cedara	24.3	636.1	1.80

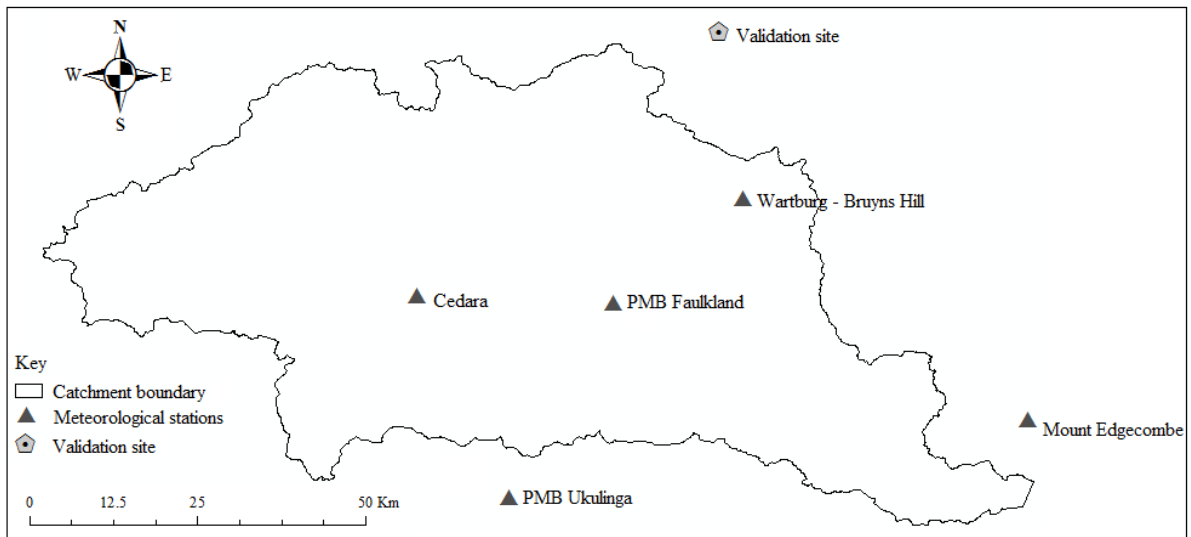


Figure 3.3 Location of meteorological stations and the validation site

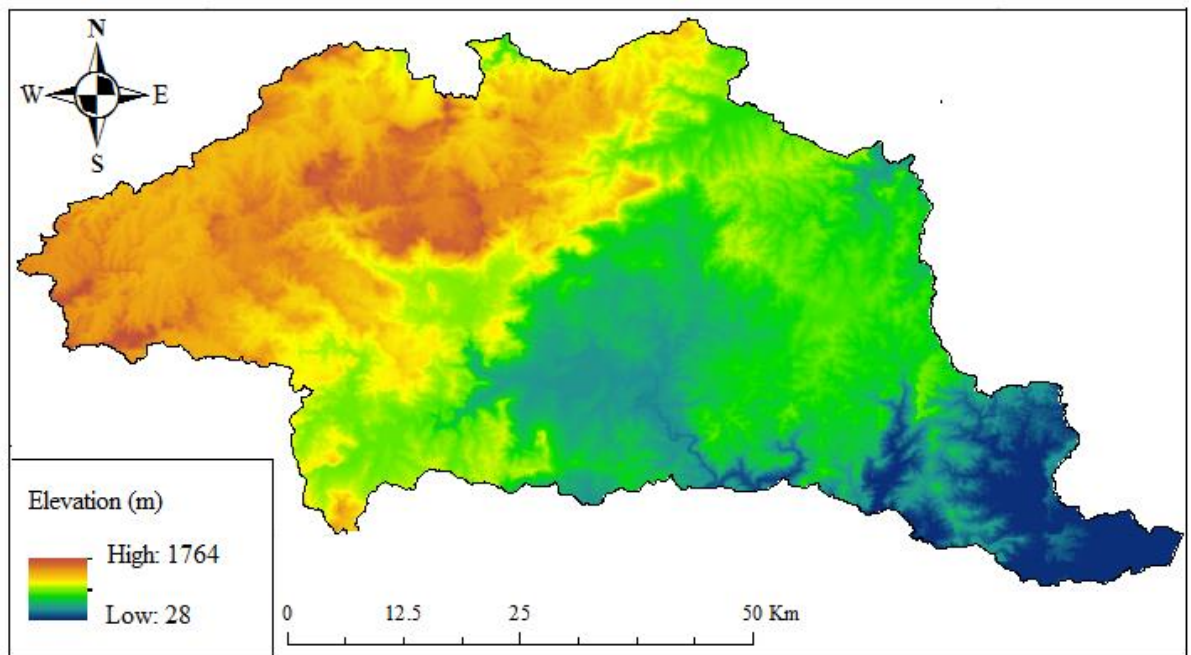


Figure 3.4 DEM for the uMngeni catchment

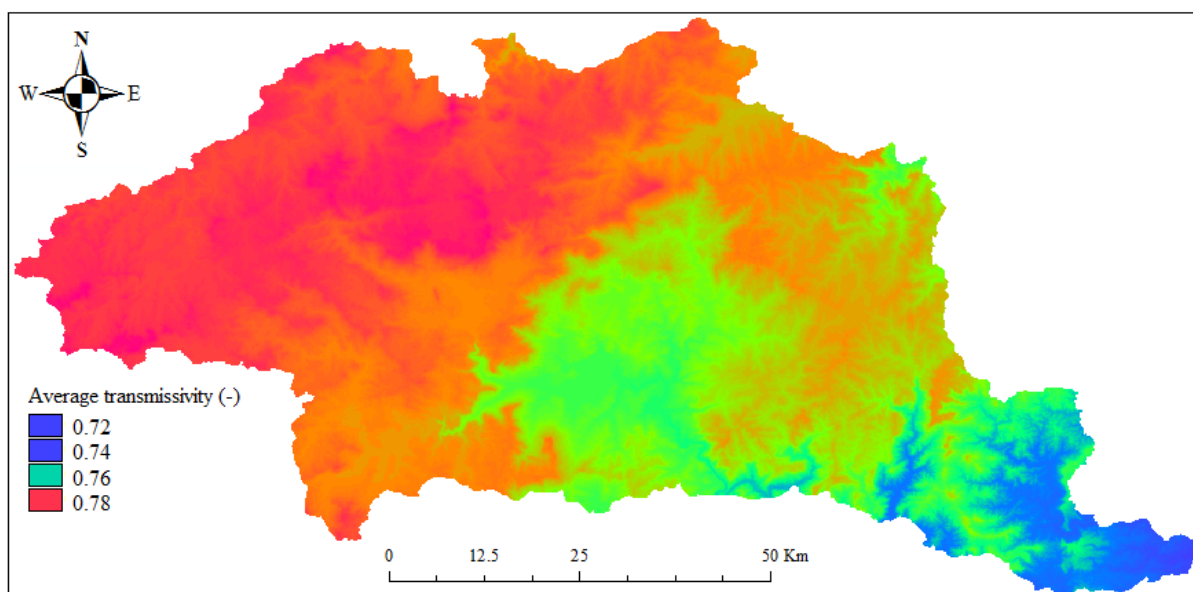


Figure 3.5 Average transmissivity of the uMngeni catchment

3.4 SEBS Outputs

As part of the process of estimating total evaporation the SEBS model also produces estimates of the other energy balance components or energy fluxes, which include net radiation (R_n), soil heat (G_o), sensible heat (H) and latent heat (LE) fluxes. Given the large number of the SEBS outputs, a sample of the outputs fluxes for two selected days, 24 June 2013 (representing dry season) and 23 March 2014 (representing wet season) are shown in Figure 3.6 and 3.7. These figures show the spatial variations of the SEBS output fluxes, as derived by the two different sensors. Generally, it can be observed that both Landsat 8 and MODIS datasets show the same spatial variations of energy fluxes across the uMngeni catchment. For instance, the western and northern parts of the catchment have higher estimates of R_n , compared to the eastern and southern parts of the catchment. The same pattern was observed for LE . Although both sensors show the same spatial variations of energy fluxes, the MODIS data shows lower fluxes, with less variability, when compared to the Landsat 8 data.

The spatial variations of H flux (Figure 3.6 and 3.7) show that the western and northern parts of the catchment have lower estimates, compared to the southern and eastern parts of the catchment. Generally, H refers to the heat energy that can be sensed or simply measured with a thermometer and results in temperature changes. Lower estimates of H flux in the western

and northern areas (mainly dominated by plantations, natural forests, commercial irrigated agriculture, water bodies and wetlands) may be attributed to the fact that heat energy is being drawn from the surface to evaporate water. This results in cooling of the surfaces and lower temperatures across those areas. In contrast, in the eastern and southern parts of the catchment (dominated by built-up areas), slightly higher estimates were derived by both sensors. This is because the dominant landcover types (*i.e.*, built-up areas) warm the lower levels of the atmosphere as they release heat energy. In addition, it has been observed that built-up areas are characterized with high H flux from the surface, due to lower vegetation cover and low evaporation (Nadeau *et al.*, 2009). With regard to G_0 , it can also be observed that the lowest amount of incoming solar radiation was absorbed by the soil surface. This mainly applies to vegetated areas, due to interception of radiation, whereas in slightly covered areas (with vegetation) or bare soils, less radiation is intercepted, thus it penetrates the soil, resulting in a slight increase in G_0 flux.

It is evident that energy fluxes exhibit seasonal dynamics, they vary between the two days used to represent the dry and wet periods. For instance, on the 24th of June 2013 (representative of dry), the estimated Rn values were lower (Figure 3.6), whereas on the 23rd of March (representative of wet) they increased (Figure 3.7).

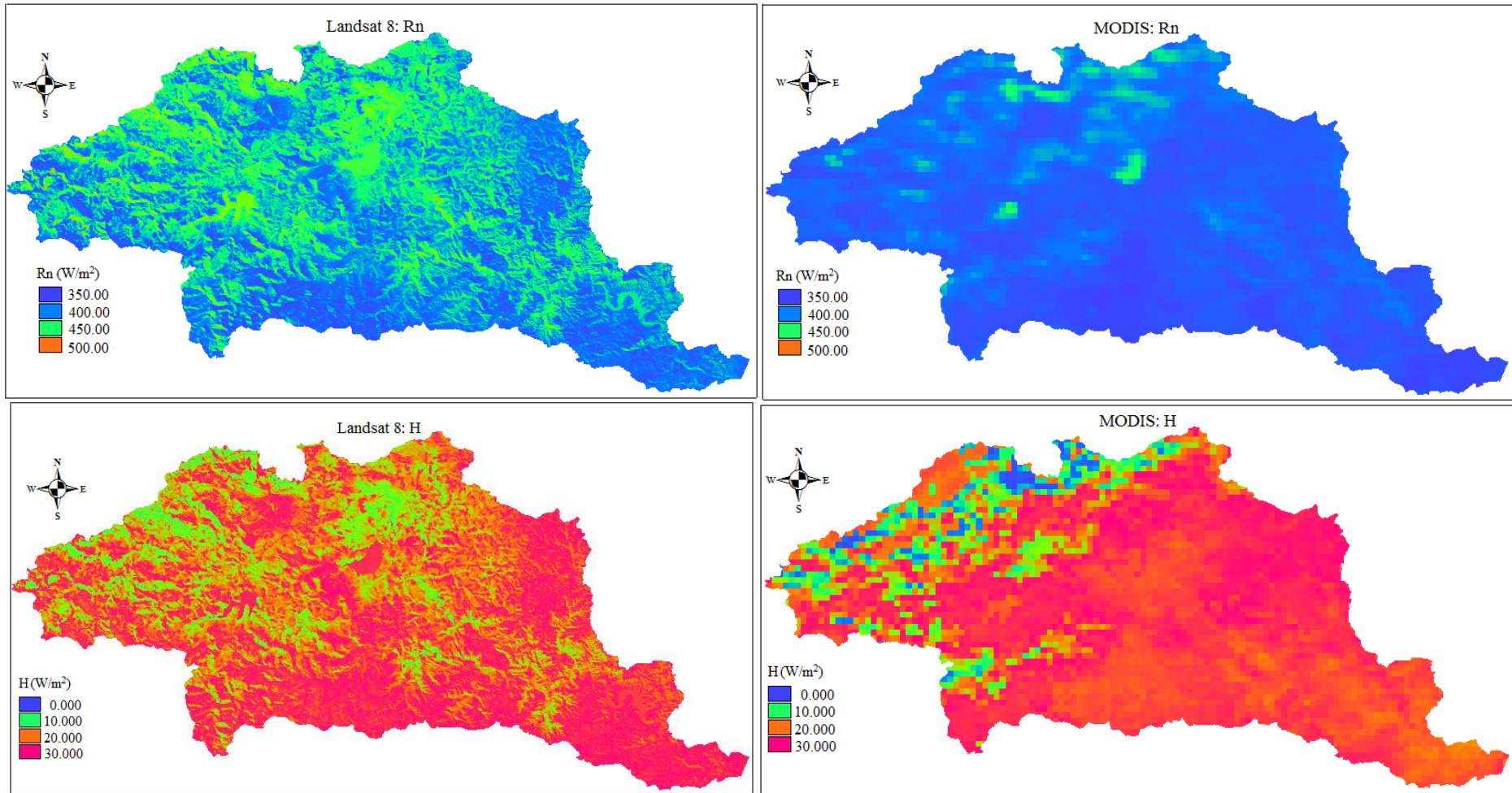


Figure 3.6 SEBS outputs for the 24th of June 2013

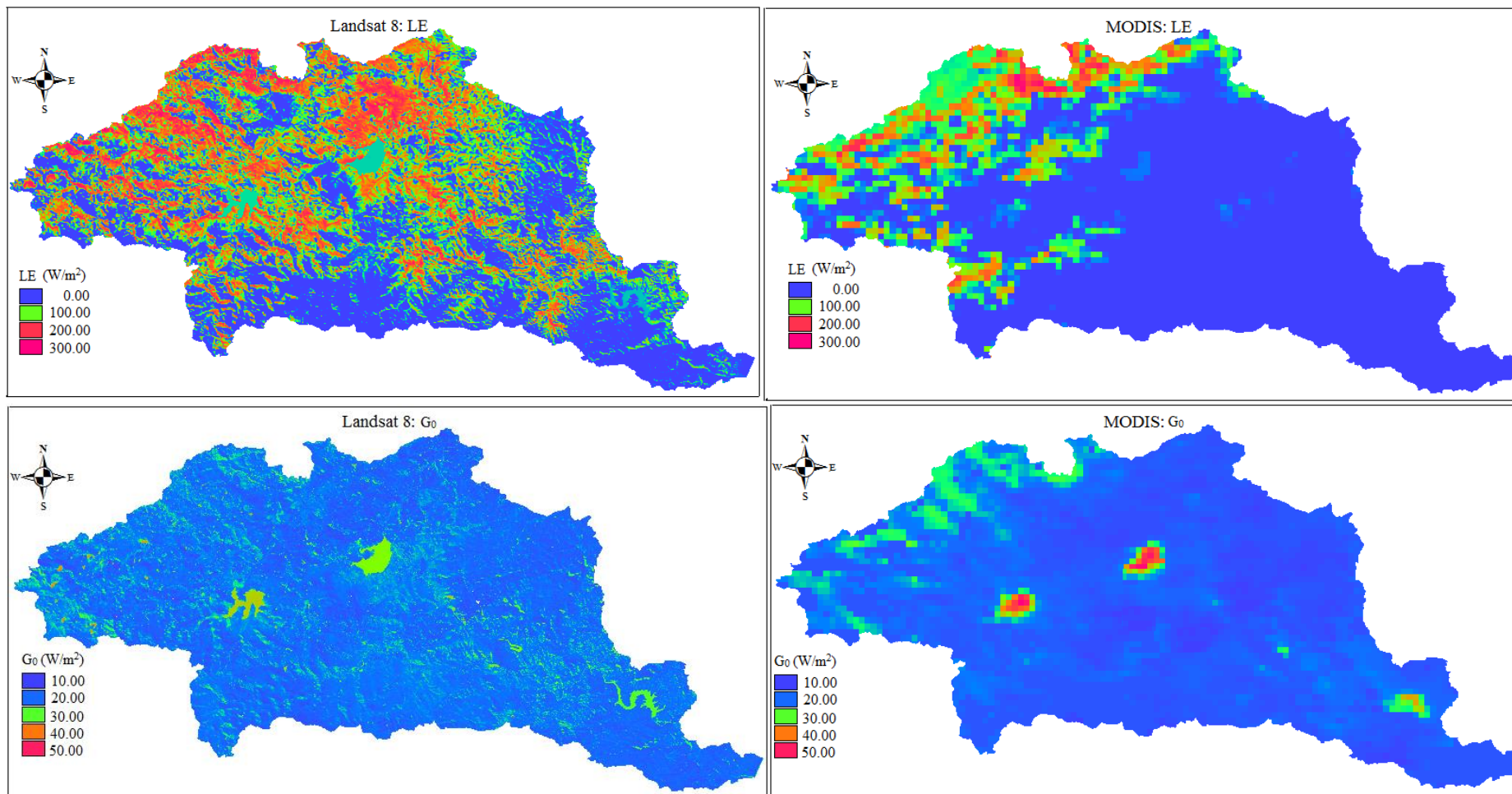


Figure 3.6 cont...

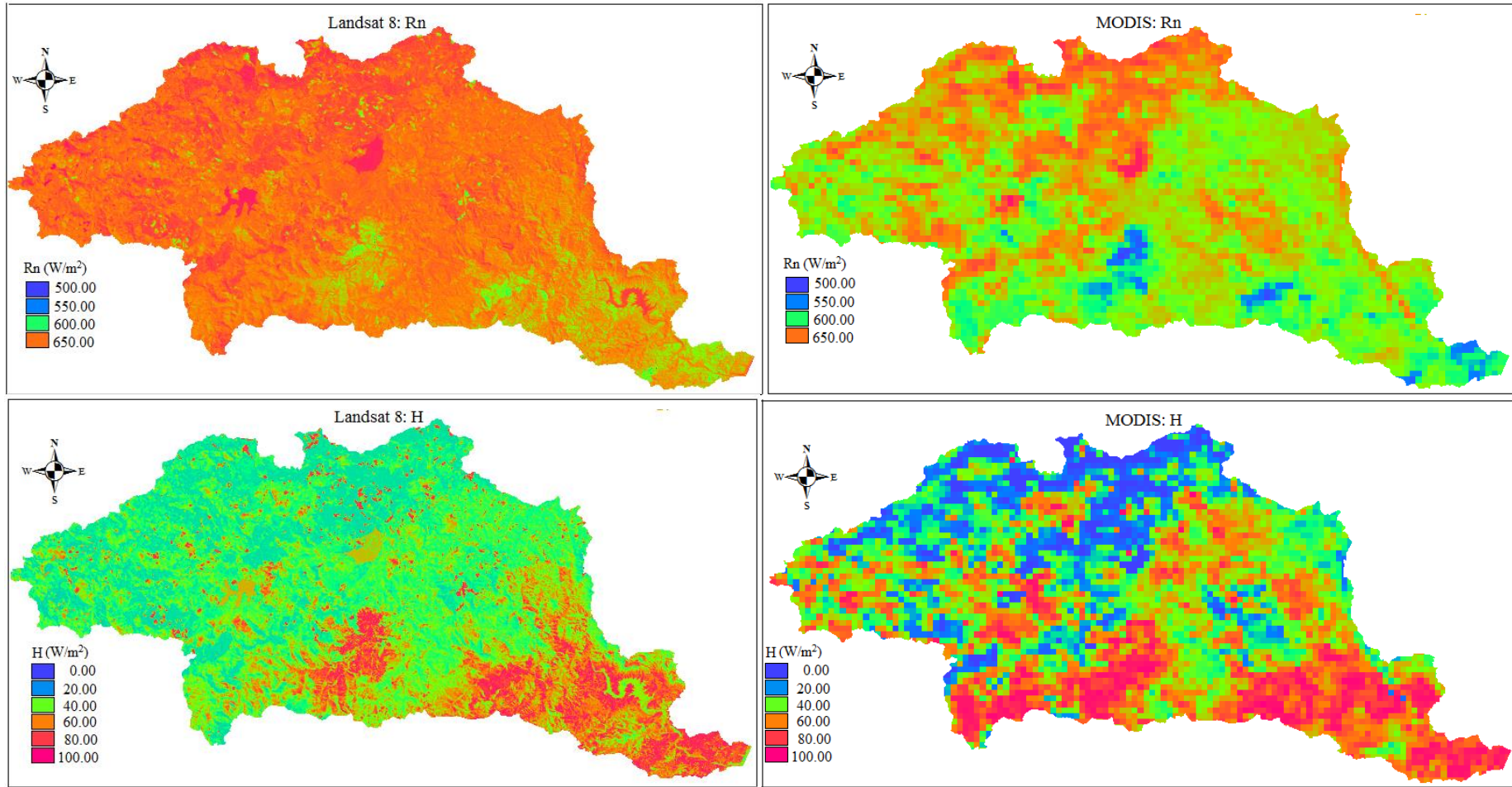


Figure 3.7 SEBS outputs for the 23rd of March 2014

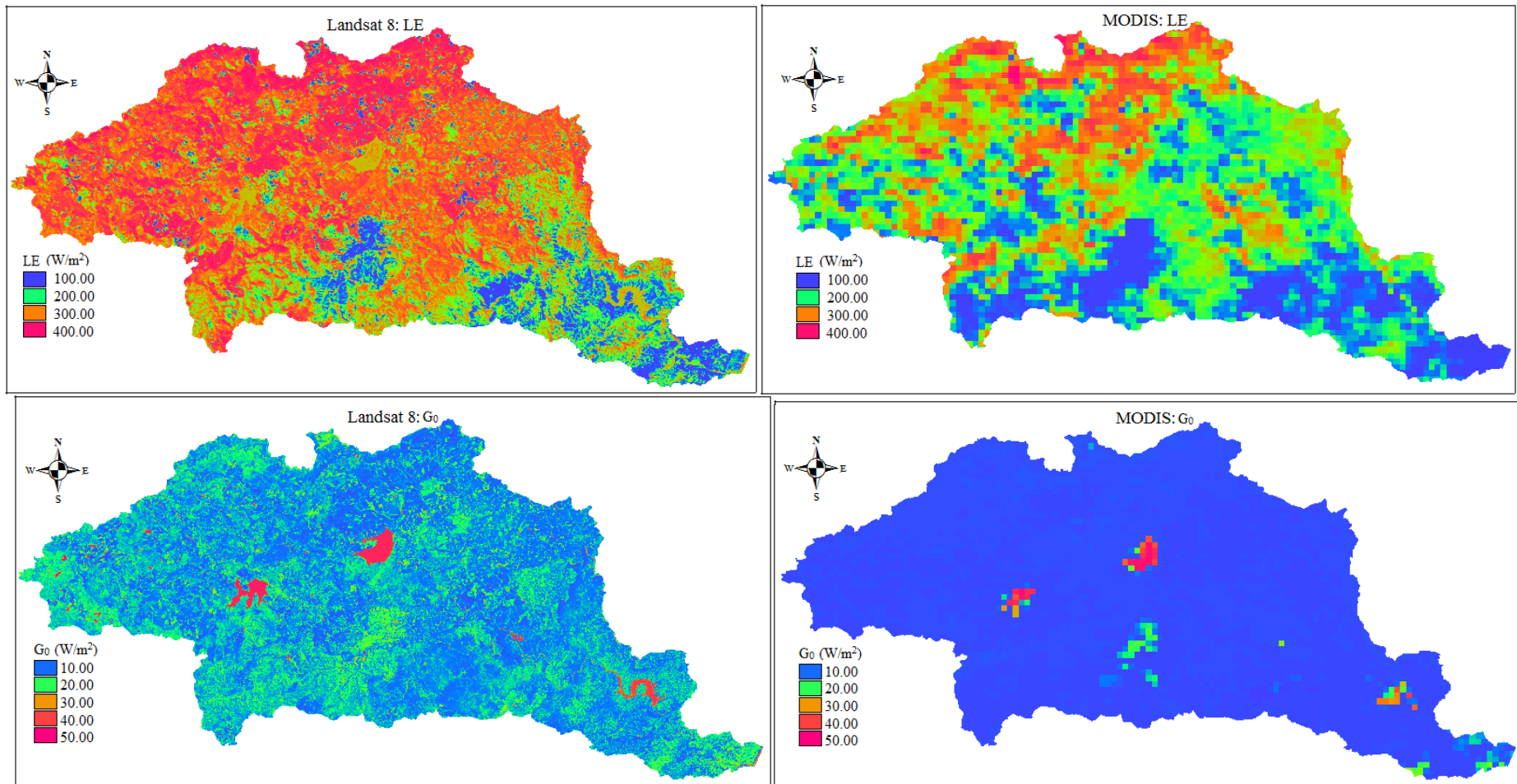


Figure 3.7 *cont...*

3.5 Reference Evaporation Estimates

Since the estimation of reference evaporation using ground-based meteorological data was done on a daily basis from May 2013 to April 2014, estimates for two selected days, 24 June 2013 (representing dry) and 23 March 2014 (representing wet) are shown in Figure 3.8 and 3.9. Reference evaporation varied spatially across the uMngeni catchment, with high values exhibited in the western and northern parts of the catchment, whereas the eastern and southern parts experienced lower values. This is may be attributed to variations in climatic conditions (radiation, temperature, humidity, wind speed), which are the primary factors which influence reference evaporation. For instance, the western and northern parts of the uMngeni catchment receive more radiation than the eastern and southern parts. On the other hand, reference evaporation for the 23rd of March shows less variability, when compared to that of 24 June. This is because reference evaporation is influenced by climatic conditions, such as temperature and rainfall. The observed variability in June can be attributed to the high spatial variations in climatic conditions across the catchment, whereas in March, within the catchment, there was a smaller spatial variation in climatic conditions resulting in less variability in reference evaporation.

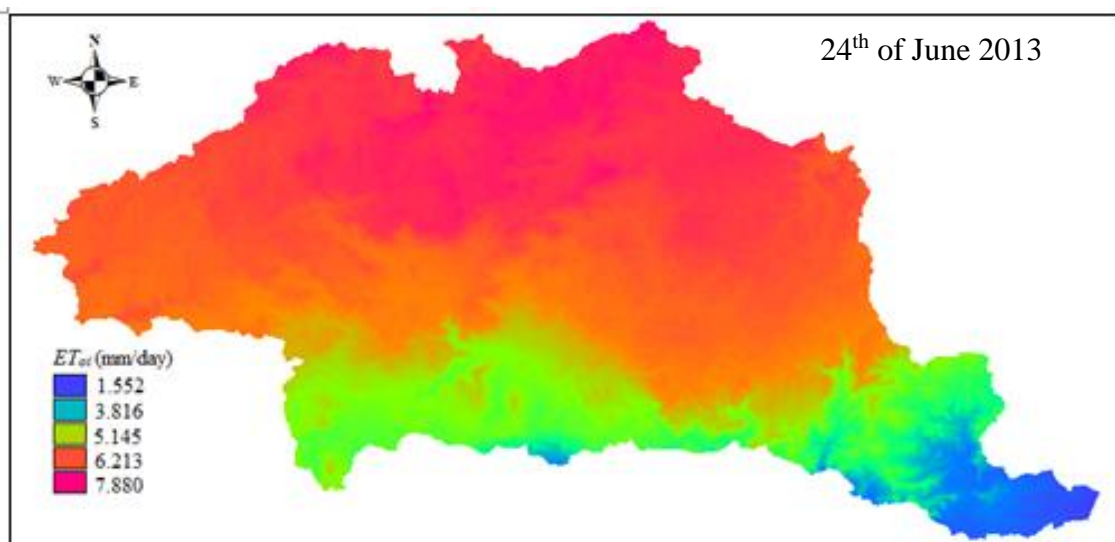


Figure 3.8 Spatial variation of reference evaporation across the catchment

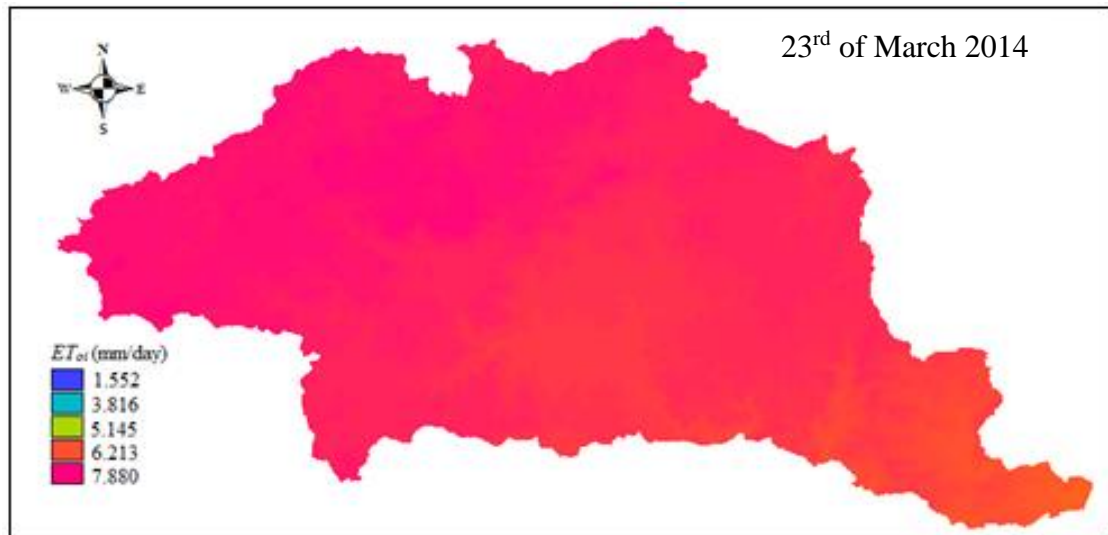


Figure 3.9 Spatial variation of reference evaporation across the catchment

3.6 Spatial Heterogeneity

To determine the spatial heterogeneity of the uMngeni catchment, the following landscape configuration metrics were used: (i) the number of patches (NP), (ii) mean patch size (MPS) and (iii) total edge (TE). These metrics measure the spatial arrangement of land cover types at class level across a landscape, which is likely to have a potential effect on the estimation of total evaporation using remote sensing, especially in relation to the sensor spatial resolution.

In addition, land cover roughness length (Z_{0m}) for momentum transfer was determined for the different land cover types within the catchment. The values used for the Z_{0m} were derived based on published values in the literature (Brutsaert, 2005; Pardalos *et al.*, 2014; Ramli *et al.*, 2009; Su, 2006; WMO, 2008), for land cover types which coincided or were close to the different land cover types in the uMngeni catchment. The roughness lengths derived and used are shown in Table 3.1. The land cover map for the uMngeni catchment was derived from the KwaZulu-Natal Landcover dataset which was generated from SPOT5 satellite images at 20 m spatial resolution.

Table 3.3 Values used to determine land cover Z_{om} for uMngeni Catchment (after Brutsaert, 2005; Pardalos *et al.*, 2014; Ramli *et al.*, 2009; Su, 2006; WMO, 2008)

Land Cover Type	Z_{om} (m)
Built-up areas	1
Com. Irrigation	0.0639
Natural Forest	1.2214
Grassland	0.0340
Nat. Bush	0.5
Orchards	0.6065
Plantation	1.0
Sub. Agric	0.496
Sugarcane	0.1
Waterbodies	0.001
Wetland	0.02

3.7 Validation of Remote Sensing Estimates

Validation data for the period under study was not available at any sites within the uMngeni Catchment. Therefore, to validate remote sensing estimates of total evaporation from Landsat 8 and MODIS datasets, ground-based measurements derived using eddy covariance system from a station adjacent to the catchment (shown in Figure 3.3) were used. Although the data used were derived from a station outside the catchment under study (shown Figure 3.3), it was covered by the same remote sensing scenes which were used to derive total evaporation estimates for the catchment. Furthermore the station is only approximately 8 km from the boundary of the catchment under study. It is important to note that only one site and land cover type was used for validation. The ground measurements from this station were used to validate the corresponding remote sensing estimates from the site. Although extensive validation using ground-based measurements was not possible, this small validation was intended to provide some insight to the performance of remote sensing in estimating total evaporation within the catchment.

3.8 Discussion and Conclusion

The use of remote sensing data with varying spatial resolution influences the ability of the sensor to detect spatial variations of biophysical input parameters (LAI, FVC, NDVI, and LST). This results in the poor representation of the derived energy fluxes and total

evaporation estimates. For instance, at 1000 m spatial resolution, MODIS input parameters, such as LST and NDVI show less variability, as compared to Landsat 8 at 30 m spatial resolution. At coarse spatial resolution, the sensor detects variations in biophysical parameters (*e.g.* LST, NDVI and LAI) within a single pixel as an aggregation, without distinguishing mixed coverage from different landcover types. This result in an aggregation of energy fluxes with less variability. Kustas and Norman (2000) found that coarse spatial resolution sensors invariably result in pixel-averaged heat flux estimation for different surfaces with varying land cover. They concluded that the lack of discrimination of sub-pixel variability can cause a significant departure of energy fluxes.

Energy fluxes corresponded with surface characteristics and seasonal variations in the input meteorological data. Highly vegetated areas (as indicated by high NDVI, FVC and LAI parameters) resulted in higher estimates of LE , as compared to less vegetated areas. According to Irmak *et al.* (2011), vegetation acts as a barrier to the conduction of solar radiation to the soil surface, such that, less R_n is consumed in heating of the soil, instead, it is available for evaporation to occur. For instance, the majority of the western, central and northern parts of the catchment have land cover which is predominantly plantations, natural forests and commercial irrigated agriculture. In addition, in relation to seasonal variations, vegetation cover tends to be lower in density and productivity during the dry season (except for irrigated areas), whereas in the wet season, which is characterized by higher temperatures, incoming radiation and rainfall, there is increased vegetation density. This results in lower radiation being absorbed by soil surface, whereas in wet season, much of the radiation is available for evaporation to occur, as much of the soil surfaces are covered by dense vegetation.

Spatial variations in H flux also corresponded with surface characteristics, with higher estimates in the southern and eastern parts, compared to the western and northern parts of the catchment. The southern and eastern parts are dominated by built-up areas which warm the lower levels of the atmosphere as they release heat energy. In addition, it has been observed that built-up areas are characterized with high H flux from the surface, due to reduced vegetation cover and low evaporation (Nadeau *et al.*, 2009), when compared to more densely vegetated areas in the western and northern parts of the catchment.

The spatial variations in reference evaporation indicated the importance of ground-based meteorological data. As highlighted by Gong *et al.* (2006), reference evaporation is determined primarily by variations in meteorological conditions. For instance, in the dry season (24 June 2013), mean temperatures recorded from all stations used were lower (ranging from 14.1 to 18.5°C), whereas in the wet season (23 March 2014), they increased (ranging from 22.8 to 25.5). This is also supported by the findings of Zhang *et al.* (2007) and Xu *et al.* (2006), who demonstrated that the spatial variations in climatic variables influence the temporal spatial trends of reference evaporation.

In conclusion, the differences in spatial resolution of remote sensing sensors influence the ability of the sensor to derive biophysical parameters and therefore total evaporation estimates. Coarse spatial resolution sensors aggregate variations of biophysical parameters within a single pixel, without discrimination. This results in the aggregation of energy fluxes, with less variability. In contrast, fine resolution sensors have the ability to discriminate variations in biophysical parameters for different landcover types. This underscores the importance of fine resolution remote sensors in discriminating land surface biophysical parameters of different landcover types for well-informed water consumption and management at catchment scale.

3.9 References

- Brutsaert, W. 2005. Hydrology: An introduction. Pg 45. Cambridge University Press, UK.
- Boronina, A, Ramillien, G. 2008. Application of AVHRR imagery and GRACE measurements for calculation of actual evapotranspiration over the Quaternary aquifer (Lake Chad basin) and validation of groundwater models. *Journal of Hydrology* 348(1–2): 98-109.
- Gibson, L, Münch, Z. 2011. The importance of selecting accurate vegetation parameters when estimating evapotranspiration using the SEBS model-an example from a sparsely vegetated catchment, Eastern Cape, South Africa.
- Irmak, A, Ratcliffe, I, Ranade, P, Hubbard, K, Singh, KR. 2011. Estimation of Land Surface Evapotranspiration with a Satellite Remote Sensing Procedure. *Great Plains Research* 21: 73-88.

- Kustas, WP, Norman, JM. 2000. Evaluating the effects of subpixel heterogeneity on pixel average fluxes. *Remote Sensing of Environment* 74(3): 327-342
- Nadeau, DF, Brutsaert, W, Parlange, M, Bou-Zeid, E, Barrenetxea, G, Couach, O, Boldi, M-O, Selker, J, Vetterli, M. 2009. Estimation of urban sensible heat flux using a dense wireless network of observations. *Environmental fluid mechanics* 9(6): 635-653.
- Pardalos, P, Rebennack, S, Pereira, MV, Iliadis, NA, Pappu, V. 2014. *Handbook of Wind Power Systems*. Springer.
- Ramli, NI, Ali, MI, Saad, MSH, Majid, T. 2009. Estimation of the Roughness Length (zo) in Malaysia using Satellite Image. *The Seventh Asia-Pacific Conference on Wind Engineering, November 8-12, 2009, Taipei, Taiwan*.
- Su, Z. 2002. The Surface Energy Balance System (SEBS) for estimation of turbulent heat fluxes. *Hydrology and Earth System Sciences* 6(1): 85-99.
- Su Z 2006. ‘An introduction to the surface energy balance system (SEBS)’, Lecture notes, ESA TIGER Capacity Building Facility 1st Training Course on “Advanced optical remote sensing”, Cape Town, 22-25 November 2006.
- WMO. 2008. Guide to Meteorological Instruments and Methods of Observation. World Meteorological Organization, Switzerland.
- Xu, C-y, Gong, L, Jiang, T, Chen, D, Singh, VP. 2006. Analysis of spatial distribution and temporal trend of reference evapotranspiration and pan evaporation in Changjiang (Yangtze River) catchment. *Journal of Hydrology* 327(1–2): 81-93.
- Zhang, Y, Liu, C, Tang, Y, Yang, Y. 2007. Trends in pan evaporation and reference and actual evapotranspiration across the Tibetan Plateau. *Journal of Geophysical Research: Atmospheres* 112(D12): n/a-n/a.

4. THE EFFECT OF SPATIAL RESOLUTION ON REMOTE SENSING ESTIMATES OF TOTAL EVAPORATION IN THE UMNGENI CATCHMENT, SOUTH AFRICA

Shoko C*, Clark DJ, Bulcock H and Mengistu MG

Centre for Water Resources Research, University of KwaZulu-Natal, Private Bag X01, Scottsville, Pietermaritzburg 3209, South Africa

Abstract

Total evaporation is one of the key components of the hydrological cycle and its reliable and accurate quantification is crucial for water accounting and management. Nevertheless, the scarcity of ground-based meteorological datasets remains one of the challenges of accurate estimation of total evaporation. The advent of remote sensing provides an invaluable opportunity for the accurate spatial characterization of total evaporation on a large scale. This study therefore aimed to determine if the accurate estimation of total evaporation depends on the sensor spatial-resolution and its ability to detect variations of total evaporation at catchment scale. Specifically, this study investigates the effect of 30 m Landsat 8 and 1000 m MODIS datasets in estimating total evaporation in the heterogeneous uMngeni Catchment, South Africa, using the Surface Energy Balance System (SEBS) model. The results show that Landsat 8 has greater potential for estimating total evaporation for different land cover types, when compared to MODIS, which has a coarser spatial resolution. For example, MODIS-based daily total evaporation estimates did not show any significant differences across different land cover types (One way ANOVA; $F_{1,924} = 1.412$, $p = 0.186$), when compared to Landsat 8, which yielded significantly different estimates between different land cover types (One way ANOVA; $F_{1,993} = 5.185$, $p < 0.001$). This therefore underscores the importance of sensor spatial resolution in estimating total evaporation at catchment scale.

Keywords: *total evaporation, Landsat 8, MODIS, land cover types, SEBS,*

4.1 Introduction

The estimation of total evaporation plays a vital role in understanding water accounting for monitoring and management of water resources. Total evaporation is the sum of evaporation from different surfaces, including interception, transpiration, soil moisture and open water bodies (Savenije, 2004). Total evaporation is the second largest quantity in a catchment water balance after precipitation (Maeda *et al.*, 2011) and is one of the processes by which water is depleted from a catchment (Molden and Sakthivadivel, 1999), hence it has a bearing on water availability. Knowledge of the spatial variation of total evaporation will assist in the conservation of water resources at both local and regional scales, especially in the light of increased consumption, changing climate and the decreasing water availability and quality (Gibson *et al.*, 2013; Jarmain *et al.*, 2009). This therefore underscores the importance of estimating total evaporation for water use allocation and management.

Total evaporation remains one of the most important components of the hydrological cycle and, as such, numerous methods have been developed to estimate it (Jin *et al.*, 2013; Jovanovic and Israel, 2012; Mutiga *et al.*, 2010). Most total evaporation estimation approaches focus on deriving point-based estimates, for example, the Penman–Monteith (Allen *et al.*, 1998; Monteith, 1965; Penman, 1948), Hargreaves (Hargreaves and Samani, 1985), Makkink (Makkink, 1957), Thornthwaite (Thornthwaite, 1948) and the Priestley and Taylor (Priestley and Taylor, 1972) equations. Although these methods have a proven record of yielding accurate total evaporation estimates, their point-based approach is not applicable to map spatial variations of total evaporation at large scales and in heterogeneous environments, especially in areas with limited field datasets (Gibson *et al.*, 2011; Lee *et al.*, 2004; Lott and Hunt, 2001; Maeda *et al.*, 2011). Remote sensing technologies enable the accurate and reliable quantification of total evaporation in complex environments and across large areas (Glenn *et al.*, 2007; Ruhoff *et al.*, 2012). Moreover, increased availability and advancement in remote sensing products enables the estimation of total evaporation at various temporal and spatial scales (Glenn *et al.*, 2007; Ruhoff *et al.*, 2012), including inaccessible and remote areas (Li *et al.*, 2009). Gibson *et al.* (2013) state that remote sensing technologies have a great potential for long-term and large-scale water resource monitoring in a cost-effective manner. Remote sensing-based methods are well-suited for estimating spatial variations of total evaporation trends over time.

The use of remote sensing technologies to estimate spatial variations of total evaporation provides more information on water consumption by different land cover types. This will aid water resources management within the heterogeneous uMngeni Catchment, in KwaZulu-Natal in South Africa, which is characterized by diverse climatic and land cover characteristics. In the uMngeni Catchment, the use of traditional point-based approaches in estimating and mapping total evaporation is challenging, given the scarcity and limited number of field-based meteorological stations across the catchment. The limited number of meteorological stations is unable to provide adequate input datasets required for total evaporation estimation across heterogeneous land cover types and climate regions within the catchment. This prevents the consistent and accurate estimation of total evaporation from the catchment, which is a pre-requisite for water accounting and sustainable water resources monitoring, management and planning.

Better estimates of hydrologic loss fluxes, especially total evaporation across the uMngeni Catchment characterized by different land cover types, is required for water use accounting across the catchment. This study therefore seeks to investigate the spatial variability of total evaporation across different land cover types existing within uMngeni Catchment, using images from the multispectral Landsat 8 Operational Land Imager (OLI) and the long-serving Moderate Imaging Spectroradiometer (MODIS).

The newly-launched multispectral Landsat 8 sensor, unlike the earlier Landsat data series (*i.e.* Landsat Multispectral Scanner (MSS), thematic mapper (TM) 5, Enhanced Thematic Mapper plus: ETM+), provides a new and critical data source needed for the accurate monitoring and understanding of water resources. For instance, the Landsat 8 sensor is characterised by a refined spectral range for the most important near infra-red (NIR) band, thus enhancing its sensitivity in characterizing different earth surface properties (El-Askary *et al.*, 2014). Moreover, the enhanced radiometric resolution (from 8 bits to 12 bits) and, most importantly, the unique sensor design has led to substantial improvements in signal to noise ratios, approximately twice that of Landsat ETM+ (Pahlevan and Schott, 2013). It has also been noted that the narrowing of the NIR band avoids the effect of water vapour, similar to MODIS, and helps acquire accurate surface reflectance (Jia *et al.*, 2014). The enhanced

radiometric resolution improves the spectral record precision and avoids spectral saturation, compared to previous Landsat images. (El-Askary *et al.*, 2014).

It is hypothesized that accurate total evaporation estimates from satellite remote sensing datasets depend mainly on sensor spatial resolution and its ability to detect and differentiate between spatial variations in land cover types across the catchment. Given this background, it is expected that Landsat 8 datasets will yield better total evaporation estimates at catchment scale, when compared to MODIS datasets. Therefore the aim of this study was to determine the effect of sensor spatial resolution on the spatial variations of total evaporation across the uMngeni Catchment, using datasets from the Landsat 8 and MODIS sensors, based on the SEBS model. The choice of the SEBS model was based on its availability and strength in estimating total evaporation, compared to other energy balance models. For example, unlike other energy balance models, SEBS calculates aerodynamic resistance of heat transfer more explicitly (Li *et al.*, 2009) and this has an effect on the estimation of heat fluxes, and consequently, on total evaporation (Sugita and Kishii, 2002).

4.2 Materials and Methods

The effect of sensor spatial resolution on estimating the spatial variation of total evaporation was assessed in uMngeni Catchment characterized by different landcover types, using the SEBS model, based on two different multispectral sensors (*i.e.* Landsat 8 and MODIS data).

4.2.1 Study area description

The uMngeni Catchment is located in the KwaZulu-Natal Province of South Africa (Figure 4.1) with an areal coverage of approximately 4349 km² (Warburton *et al.*, 2010). The uMngeni Catchment experiences a warm subtropical climate and it receives rainfall during the summer months (November to January), varying from 700 mm in the drier interior to 1550 mm on the western side, with a 12°C mean annual temperature range in the escarpment areas and 20°C towards the coastal areas (Warburton *et al.*, 2010). The catchment supports 15% of the country's total population, supplying water to the Durban and Pietermaritzburg economic corridor, which produces approximately 20% of the country's Gross Domestic Product (Summerton *et al.*, 2010; Warburton *et al.*, 2010), hence it promotes economic

development. The catchment has heterogeneous land cover, consisting predominantly of urban, natural forest, plantations, commercial and small-scale agriculture, among others (Ghile and Schulze, 2010; Mauck and Warburton, 2013).

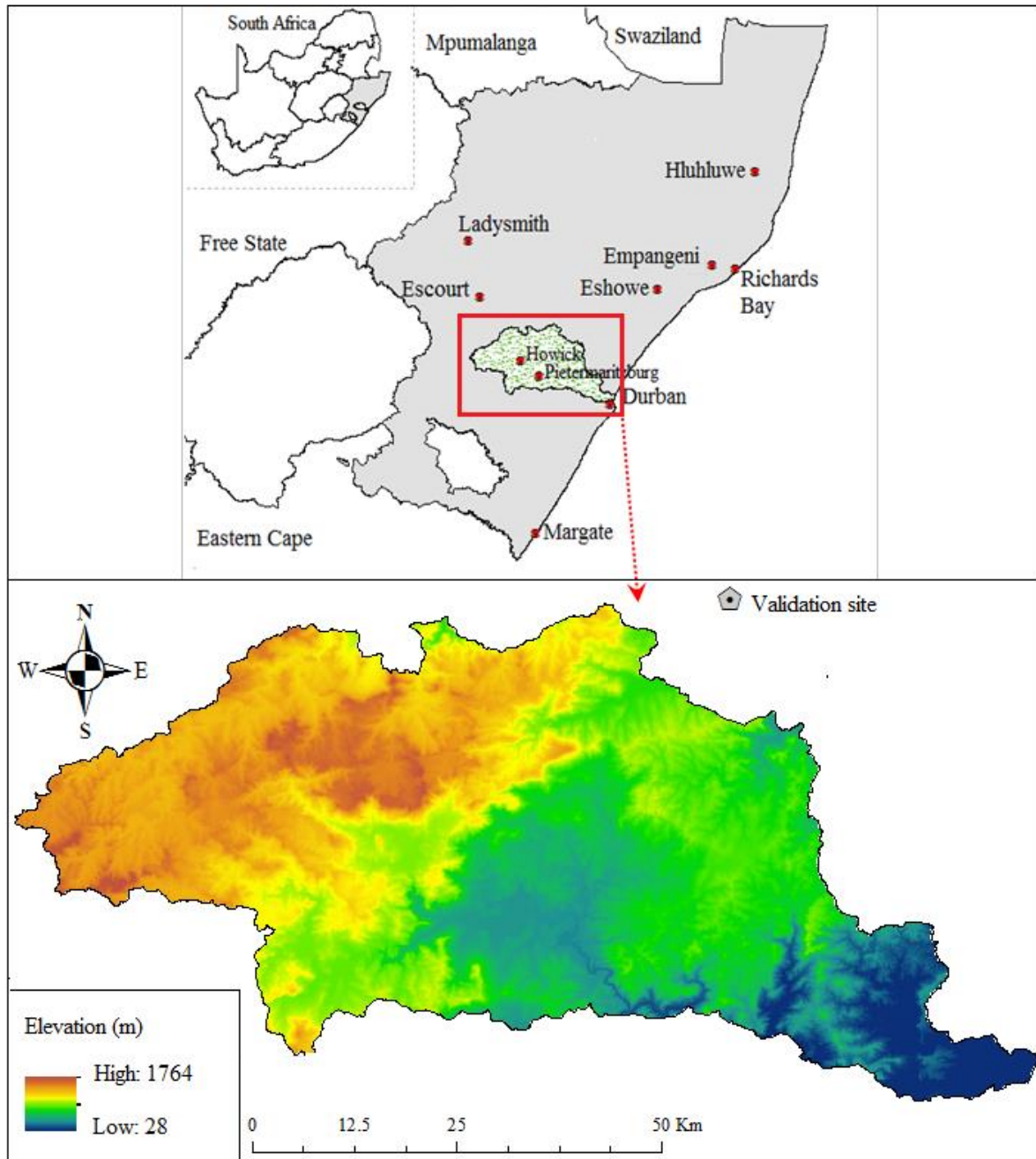


Figure 4.1 Location of the study area

4.2.2 Surface Energy Balance System model

The SEBS model, which was developed by Su (2002), was applied for the estimation of total evaporation across the uMngeni Catchment. SEBS estimates heat fluxes, using remotely sensed and meteorological datasets. Land surface physical properties derived from remotely sensed spectral reflectance and radiance bands include surface temperature, albedo, emissivity, Fractional Vegetation Cover (FVC), Normalized Difference Vegetation Index (NDVI) and Leaf Area Index (LAI) (Su, 2002). The meteorological data required include temperature, humidity, wind speed and pressure at a reference height. SEBS also requires downward solar radiation, which can be directly measured on the ground or modelled from remote sensing data. A digital elevation model and a sun zenith angle map are also required. For this research, the MODIS TERRA and Landsat 8 images were used for the estimation of total evaporation across the uMngeni Catchment. Detailed procedures for the data acquisition, pre-processing and SEBS computation using MODIS and Landsat 8 are outlined in APPENDIX A and APPENDIX B.

4.2.3 Landsat 8 and MODIS data acquisition and calibration

The remotely sensed images that were used for this study were acquired for the period 2013 to 2014. The period was chosen, based on the availability of Landsat 8 images. The Landsat 8 sensor was launched on the 11th of February 2013 by the National Aeronautics Space Administration and the United States Geological Survey (NASA-USGS) (<http://landsat.usgs.gov/>) and images for the study area were available from May 2013 to present. The study was also intended to cover one year (*i.e.*, May 2013 until April 2014), in order to include the wet and dry seasons. The comparison of sensor spatial resolution on total evaporation estimates was done for specific dates only. The exact dates include 23/05/2013, 08/06/2013, 24/06/2013, 23/07/2013, 11/08/2013 and 23/03/2014. These days were chosen based on Landsat 8 availability and the fact that cloud-free images were available from both sensors for comparison purposes. Landsat 8 images are available at the USGS data centre at a 16-day temporal resolution and these images were acquired using the bounding coordinates of the study area. All Landsat 8 scenes which covered the uMngeni Catchment were obtained, using path/row number 168/80 and 168/81 (*i.e.*, the catchment requires two Landsat scenes). Moreover, all raw Landsat 8 images acquired were calibrated to Top-Of-Atmosphere (TOA)

reflectance, following the approach summarized at the Landsat 8 website (<http://landsat.usgs.gov/>).

Clear sky calibrated MODIS Level 1B images (MOD021KM), including their respective geo-location files (MOD03), corresponding with the selected Landsat 8 images, were used for this study. These images are available at a daily temporal resolution and can be downloaded at the MODIS website (<http://ladsweb.nascom.nasa.gov/>). Images were pre-processed, using the MODIS swath reprojection tool (MRTSwath). Band-related reflectance scales and offset constants were obtained from MODIS image files, using the HDFview software. MODIS bands one and two have a 250 m spatial resolution and bands three to seven have a resolution of 500 m hence, they were resampled to match the 1km spatial resolution of the other bands. Resampling was done, using the nearest neighbour resampling technique embedded in the MRTSwath tool.

4.2.4 Atmospheric correction

All spectral reflectance bands were corrected for atmospheric effects using the inbuilt Simplified Method for Atmospheric Correction (SMAC) algorithm (Rahman and Dedieu, 1994). The SMAC algorithm is part of the open source Integrated Land and Water Information System (ILWIS 3.7) software (<http://52north.org>) and it requires water vapour content, aerosol optical thickness (AOT), ozone content, sun/sensor angle and the sensor coefficient file. AOT was derived from the NASA website (<http://earthobservatory.nasa.gov>), whereas ozone content data was extracted from the Aerosol Robotic Network (AERONET) (<http://macuv.gsfc.nasa.gov>). Air pressure was derived from meteorological stations available within and adjacent to the uMngeni Catchment. All the input parameters coincided with the day of image acquisition.

4.2.5 SEBS meteorological and ancillary data

Meteorological field-data were obtained from the South Africa Weather Services (SAWS) and the South African Sugarcane Research Institute (SASRI). Meteorological stations, within and adjacent to the uMngeni Catchment, were considered for the estimation of total evaporation. The meteorological data that were used include temperature, wind speed,

humidity, pressure, sunshine duration and solar radiation. To produce a spatial representation of the point-based meteorological observations, interpolation was done, using a simple Krigging technique in ArcGIS 10.2 software.

Additional data that were acquired include land cover types and elevation of the study area. The land cover data for the uMngeni Catchment were obtained from Ezemvelo KwaZulu-Natal Wildlife (EKZNW) (2013). The digital elevation model for the catchment was downloaded from the Shuttle Radar Topography Mission (SRTM), USGS Earth Resources Observation Systems (EROS) data centre (<http://srtm.csi.cgiar.org>).

4.2.6 Validation of remote sensing total evaporation estimates

To evaluate the reliability and accuracy of total evaporation estimates from the 30 m Landsat and 1000 m MODIS datasets, ground-based measurements were used. The validation was done for specific days (*i.e.* mean daily total evaporation) corresponding with Landsat 8 and MODIS datasets. However, within the uMngeni Catchment, ground-based data for the period under study was not available; therefore, estimates from the adjacent Two Streams Catchment were utilized. These measurements were derived, using an Eddy Covariance (EC) system, which was stationed within a wattle (*Acacia mearnsii*) plantation (Everson *et al.*, 2014), and they coincided with the selected image acquisition period. These measurements although they were outside the catchment under study, they were covered by the same remote sensing scenes, which were used to estimate total evaporation for uMngeni catchment. Hence may provide an insight on the performance of remote sensing in estimates of total evaporation within the catchment.

4.2.7 Statistical analysis

In order to derive total evaporation estimates for each land cover type, the Zonal Statistics function in ArcGIS 10.2 was used. Landsat 8 and MODIS sensor-derived mean total evaporation estimates were statistically compared, using a paired T-test, to determine whether they were significantly different. In addition, total evaporation estimates for each land cover type were compared statistically amongst land cover types, per sensor and between sensors, using the Analysis of Variance (ANOVA).

4.3 Results

To determine the effect of sensor spatial resolution on estimating spatial variations of total evaporation, different land cover types within the catchment were identified. In addition, the spatial and temporal variations of total evaporation estimates across the catchment from the two sensors were also determined and tested for significant differences.

4.3.1 Land cover types within the uMngeni Catchment

The different land cover types existing within the uMngeni Catchment, based on EKZWNW (2013) are shown in Figure 4.2. Natural bush, plantations, sugarcane, natural forest, water, built-up areas, grassland, wetlands, bush land and water-bodies are the predominant land cover types within the uMngeni Catchment.

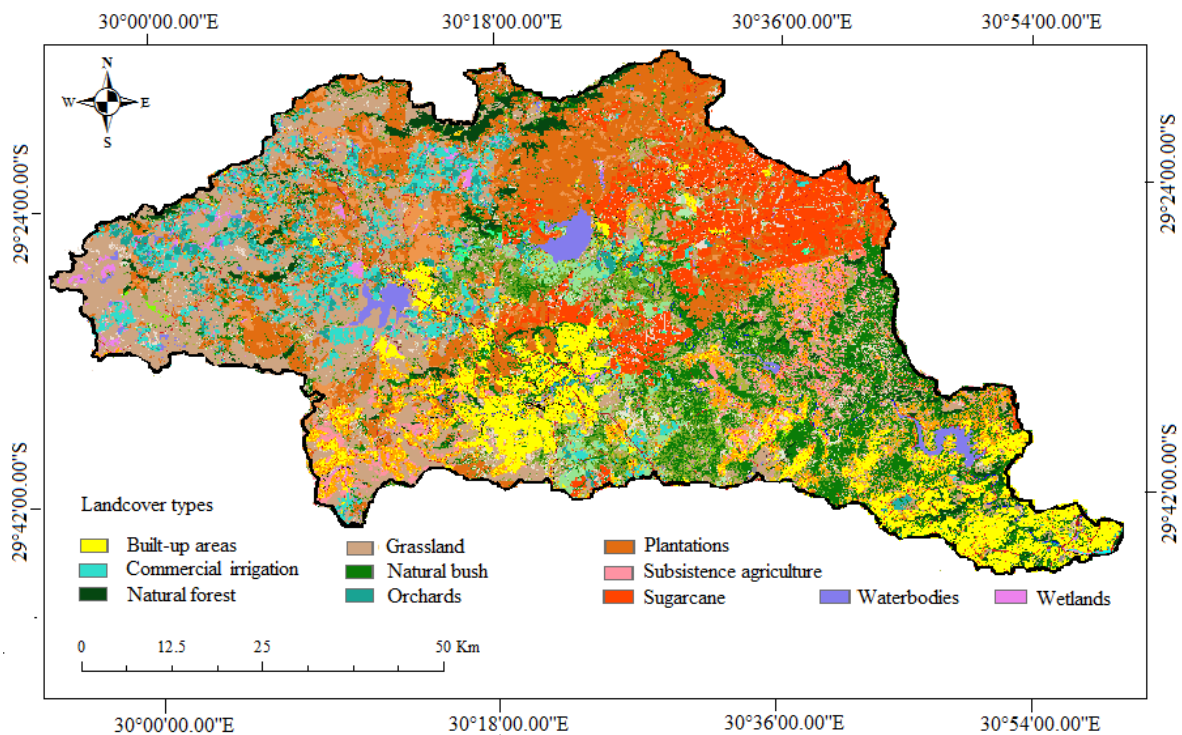


Figure 4.2 Main land cover types within the uMngeni Catchment, EKZWNW (2013)

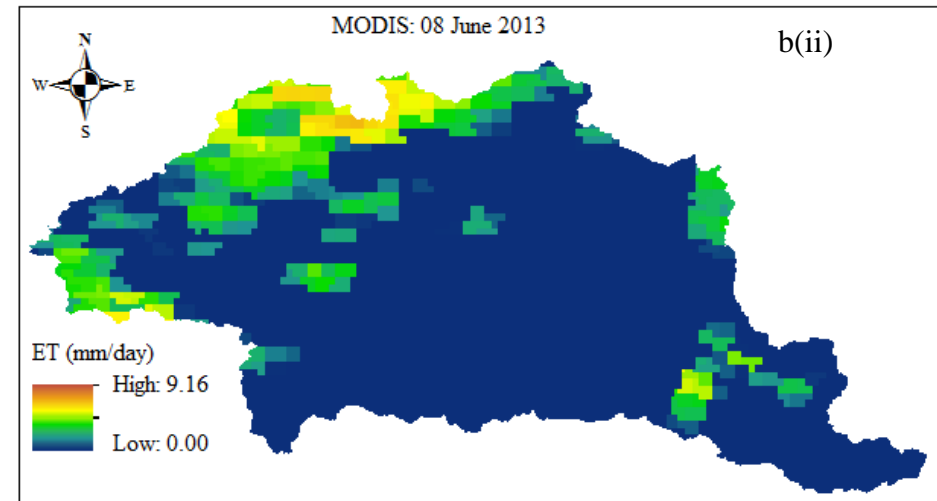
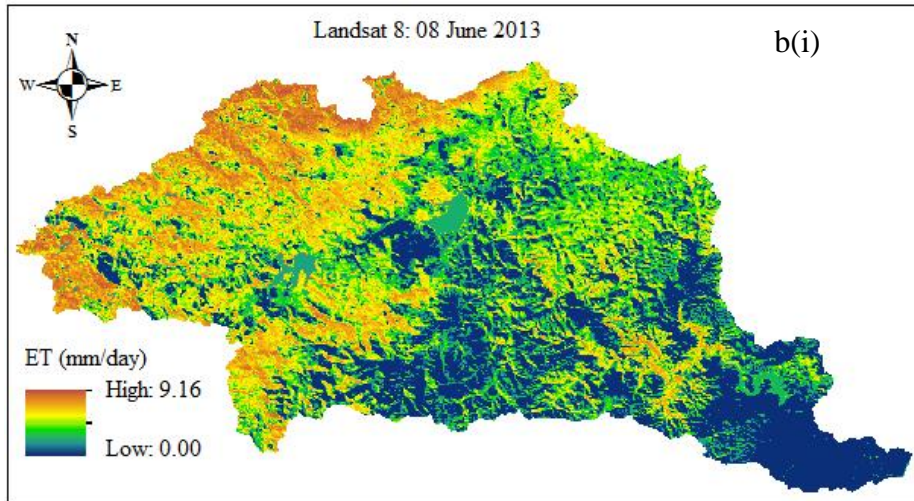
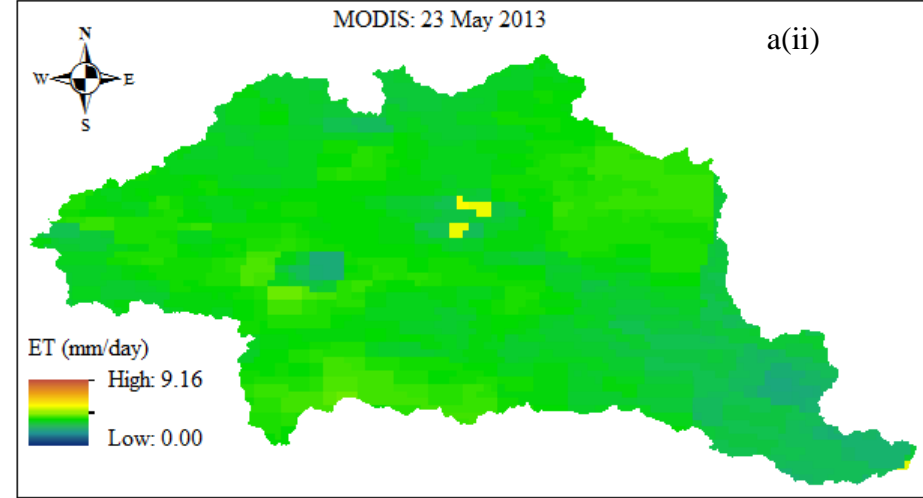
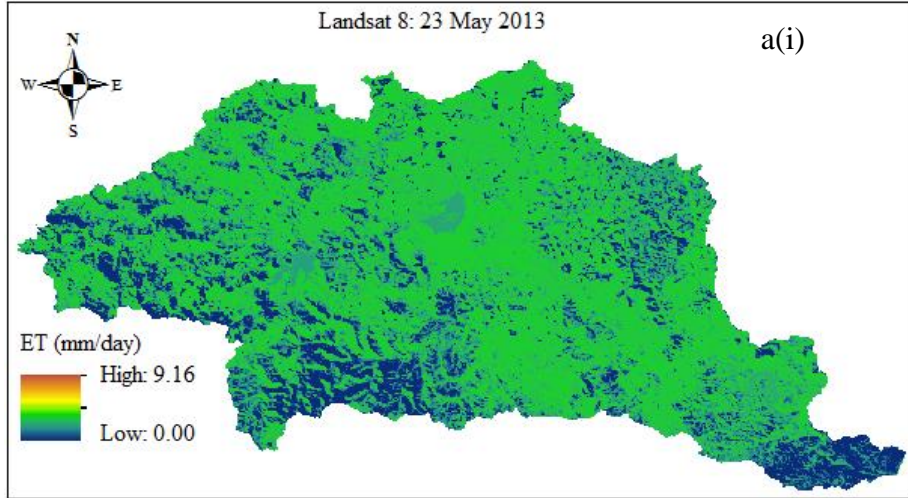
4.3.2 Spatial and temporal variability of total evaporation

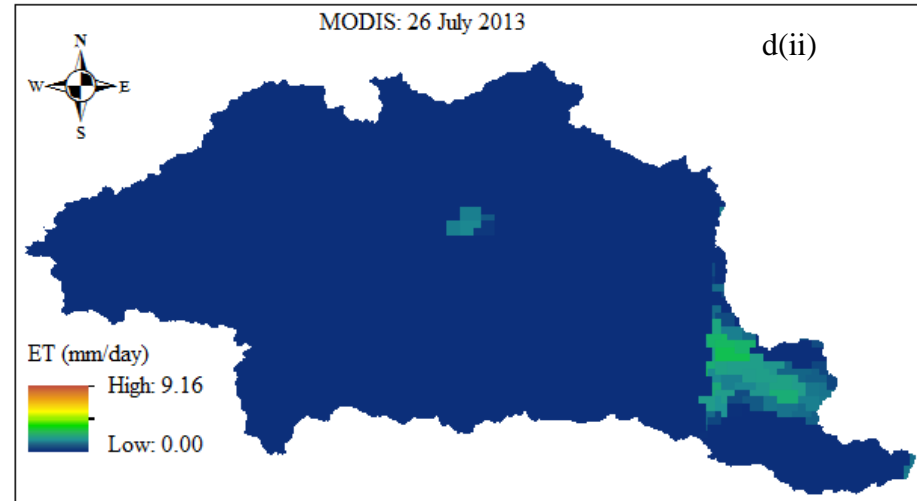
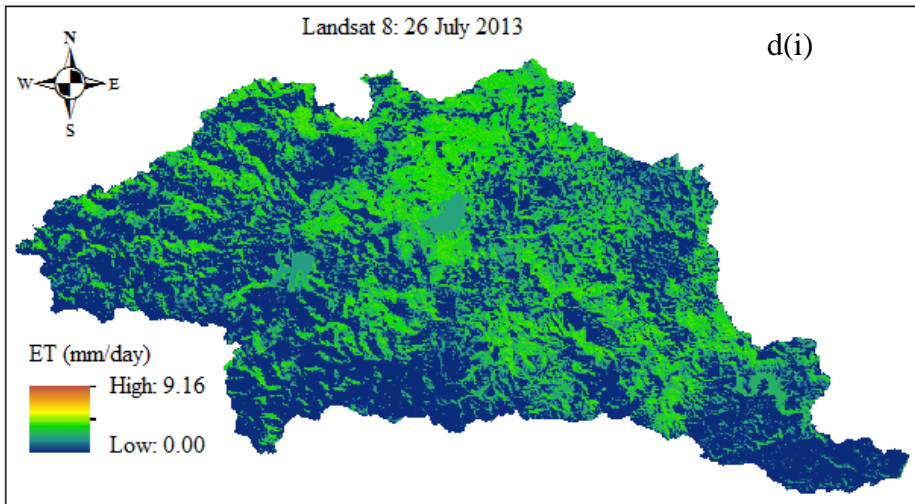
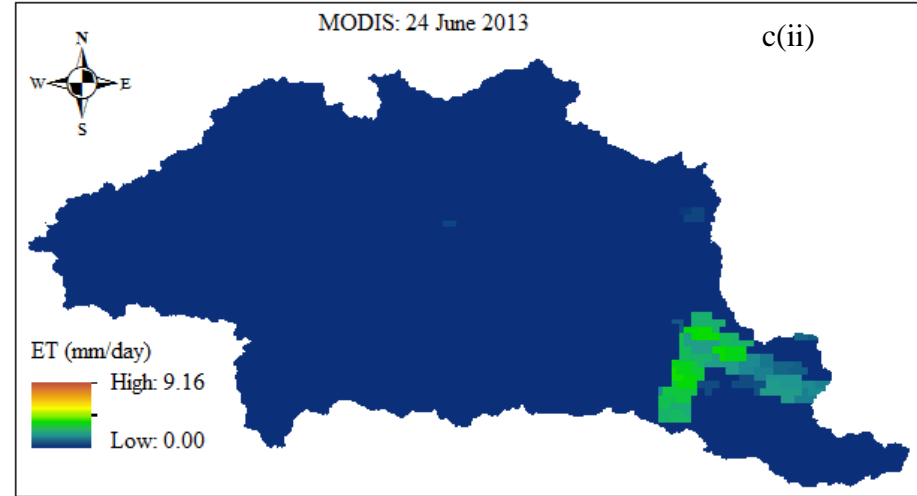
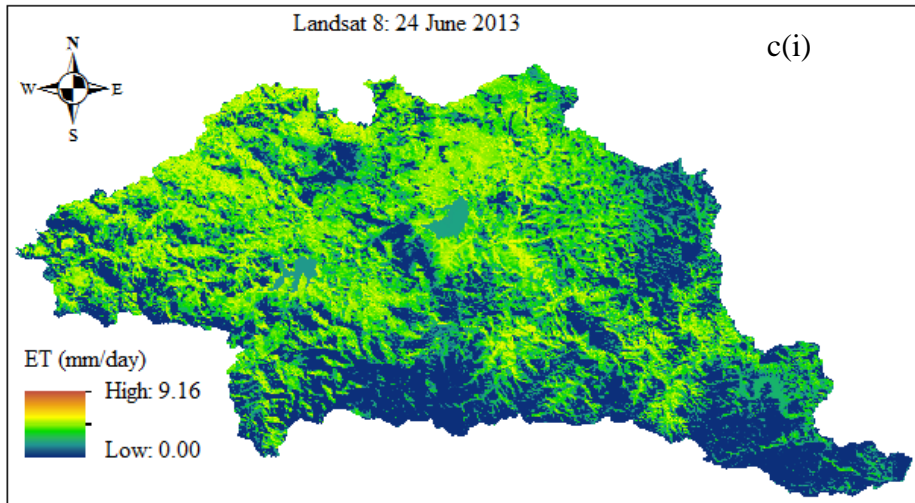
The spatio-temporal variation of total evaporation estimates across the uMngeni Catchment for the period under study is shown in Figure 4.3 (a-f). The results show that the highest total evaporation estimates occur in the northern, western and north-western parts of the catchment. This is in agreement with the spatial variations of the derived energy fluxes, such as R_n (Figure 3.6 and 3.7). These areas are largely dominated by plantations, natural forests, commercial irrigated agriculture, water bodies and wetlands, which all contributes to total evaporation. Although the two sensors depict similar trends of total evaporation, especially when considering Figure 4.3 (f), the paired T-test has shown that they are significantly different ($p < 0.05$).

It can be observed that over the period of study, the highest mean total evaporation estimates were observed on the 23rd of March 2014, whereas the lowest were on the 23rd of May and the 26th of July 2013. The results in Figure 4.3 a (ii) – f (ii) show that MODIS estimates of total evaporation were lower, especially in the dry season, when compared to Landsat 8. This was also the case with reference evaporation, where lower estimates were observed in dry season and higher in wet season (Figure 3.5). The results in Table 4.1 show the derived total evaporation statistics across the uMngeni Catchment for the selected period. Results from the paired T-test show that the derived mean daily total evaporation estimates from Landsat 8 and MODIS datasets differed significantly ($p = 0.028841$).

Table 4.1 Estimated total evaporation statistics for the uMngeni Catchment (mm)

Date	Landsat 8				MODIS			
	Min.	Max.	Mean	Stdev	Min.	Max.	Mean	Stdev
23/05/2013	0.00	3.67	2.45	1.09	0.00	6.90	0.65	0.98
08/06/2013	0.00	7.33	3.52	2.58	0.00	6.70	0.62	1.32
24/06/2013	0.00	5.58	2.53	1.91	0.00	3.80	0.09	0.50
26/07/2013	0.00	4.16	1.50	1.50	0.00	2.90	0.08	0.41
11/08/2013	0.00	7.07	1.98	1.91	0.00	2.70	0.06	0.27
23/03/2014	0.00	7.15	5.00	1.53	0.00	6.30	4.03	1.05





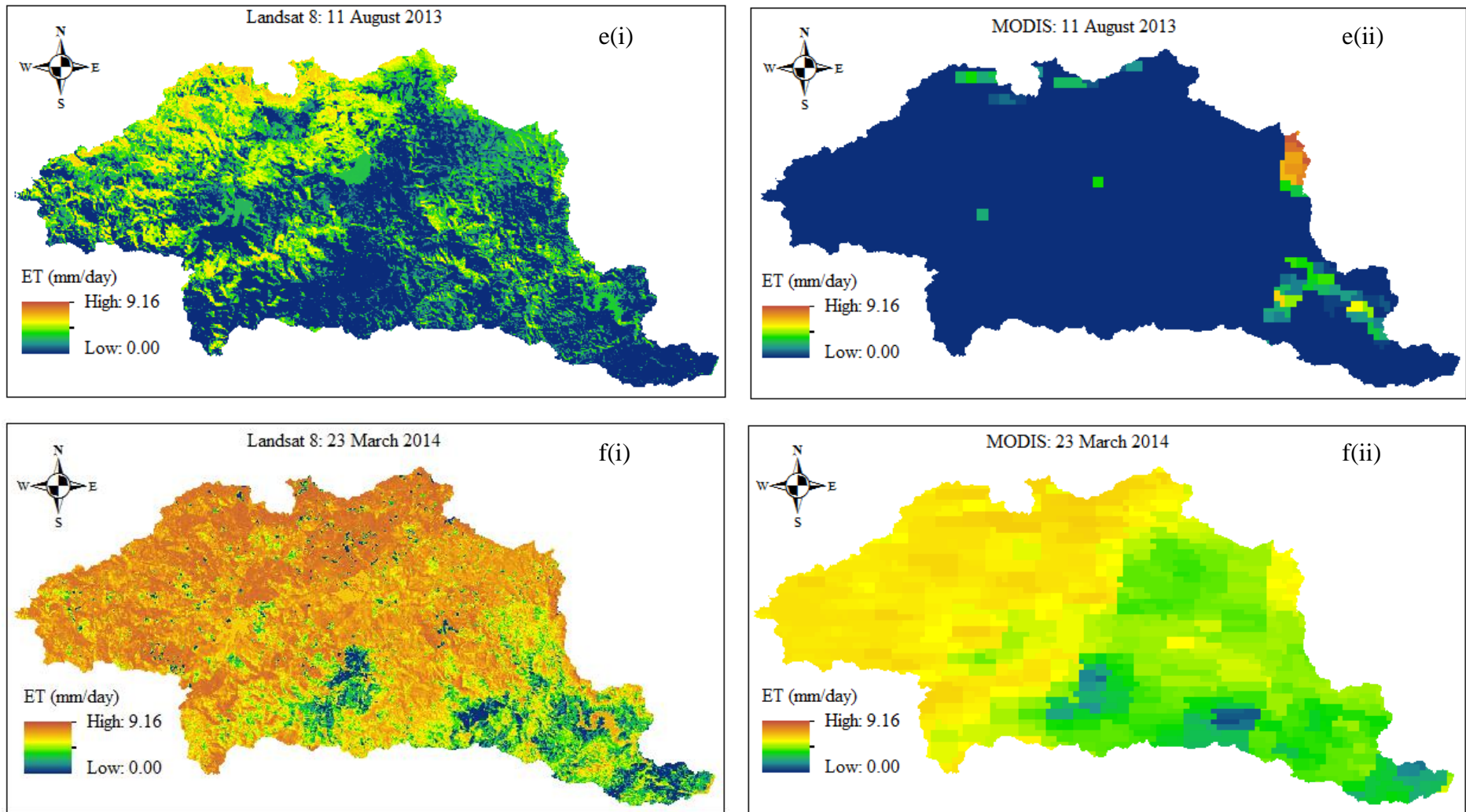
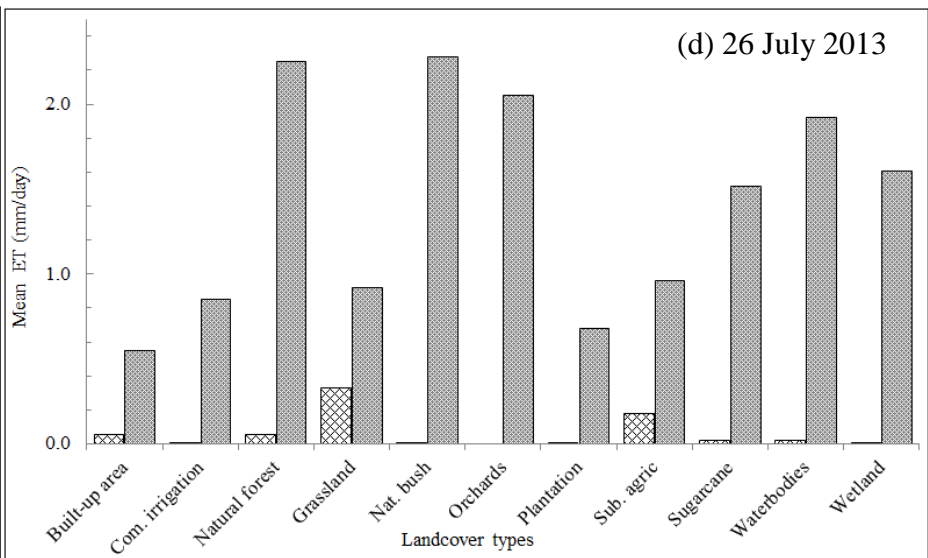
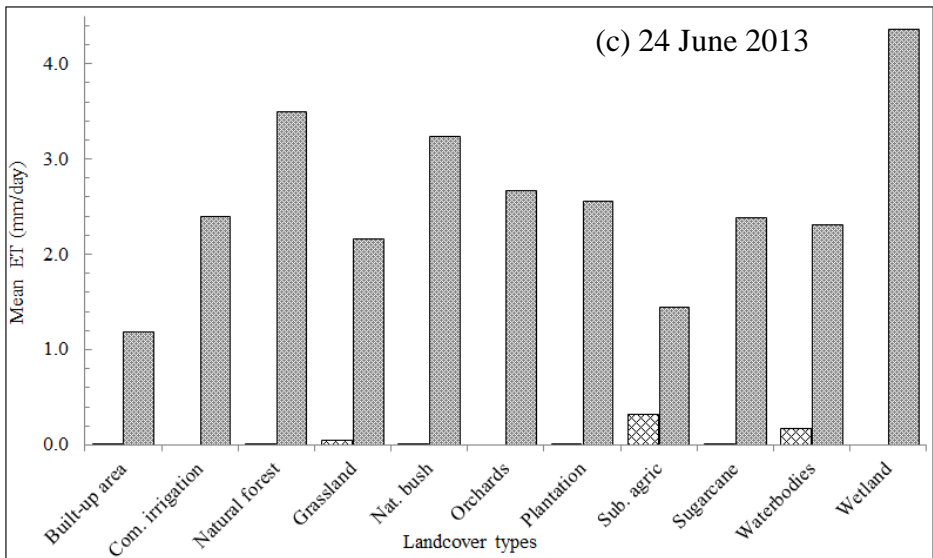
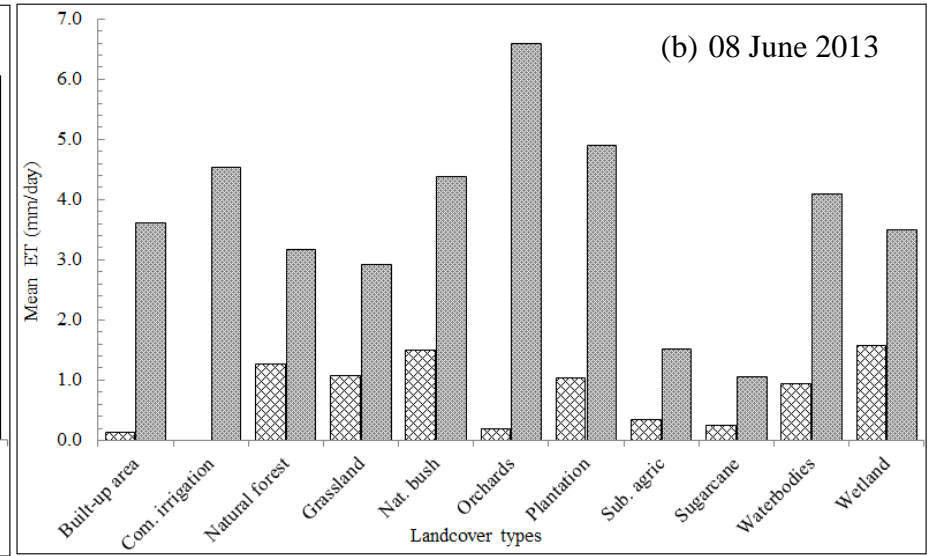
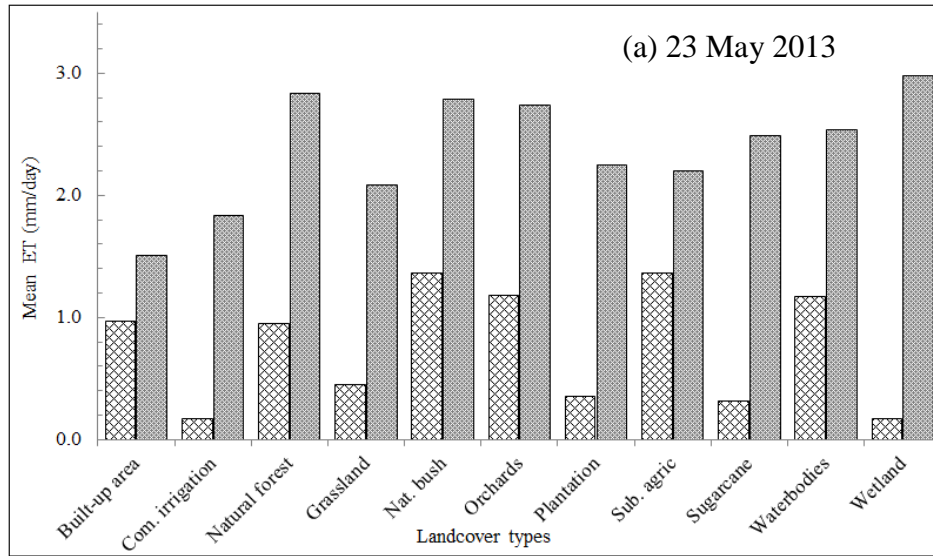


Figure 4.3 Spatial and temporal variability of total evaporation from the two sensors

4.3.3 Total evaporation variation between different land cover types

The mean total evaporation estimates for different land cover types within the uMngeni Catchment for the period under study are shown in Figure 4.4 (a – f). It can be observed that Landsat 8 produced higher total evaporation estimates across the entire period of study, when compared to MODIS dataset. As can be seen in Figure 4.4 (c-e), MODIS show lower total evaporation estimates across different land cover types, when compared to Landsat 8. However, it can be observed that MODIS produced higher estimates of total evaporation on the 23th of March, almost showing a similar trend to those of the Landsat 8 sensor. A paired t-Test was also performed to determine if there was any significant difference in mean total evaporation estimates obtained from the two sensors. Overall, the paired T-test results show that land cover-based total evaporation estimates from Landsat 8 and MODIS datasets exhibit significant differences ($p < 0.05$) for the period under study. Moreover, the ANOVA was performed to test any significant differences in total evaporation estimates between different land cover types. MODIS-based mean daily total evaporation estimates did not show any significant difference across different land cover types (One way ANOVA; $F_{1,924} = 1.412$, $p = 0.186$). The 30 m Landsat 8 sensor yielded significantly different ($p < 0.05$) total evaporation estimates between different land cover types (One way ANOVA; $F_{1,993} = 5.185$, $p < 0.001$).



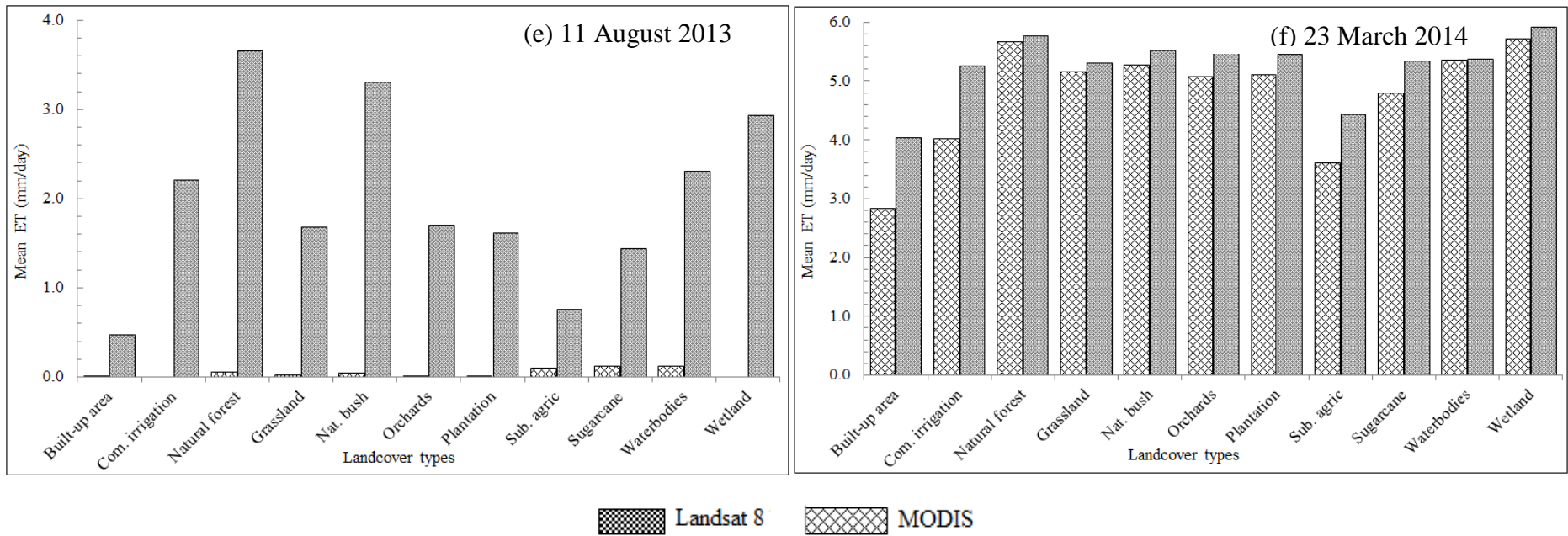


Figure 4.4 Mean total evaporation between different land cover types

4.3.4 Validation results

A comparison of Landsat 8 and MODIS-based mean daily total evaporation estimates and corresponding ground-based EC measurements are shown in Figure 4.5. In general, it can be observed that Landsat 8 total evaporation estimates and EC measurements show a close agreement. This observation was further confirmed by a paired T-test, which shows that there is no significant difference ($p = 0.426$) between Landsat 8 estimates and EC ground-based measurements. However, a comparison between MODIS and EC total evaporation, shows that there was a significant difference ($p < 0.001$), indicating that MODIS underestimated total evaporation.

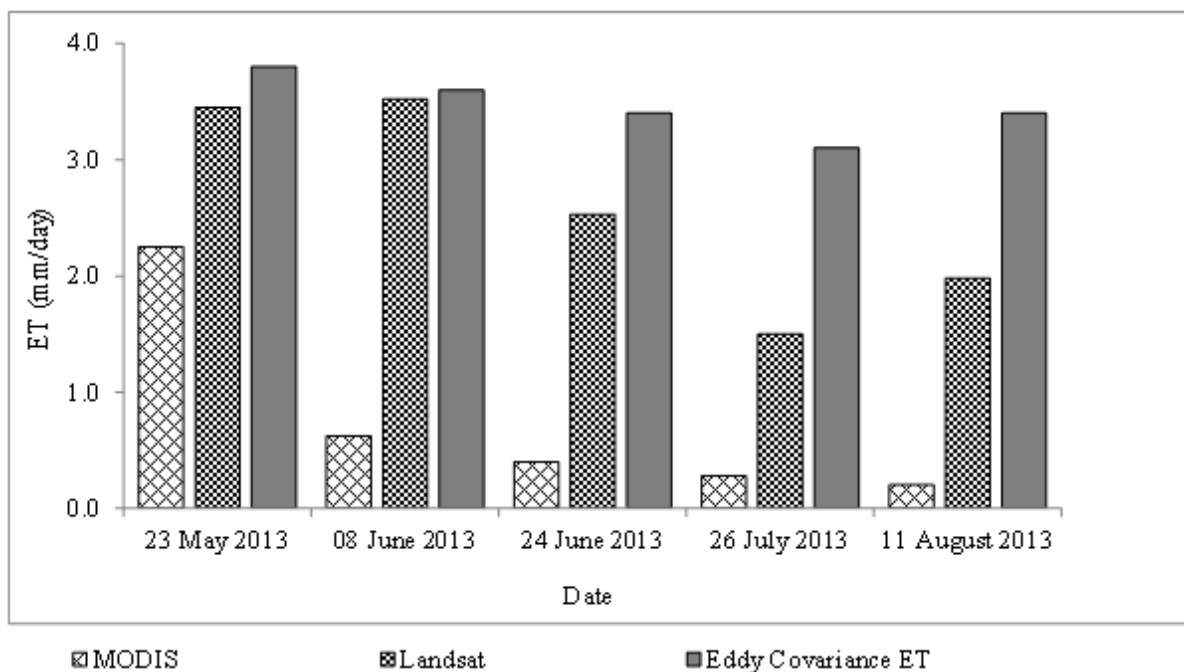


Figure 4.5 Comparison between remotely-sensed estimates and ground-based measurements

4.4 Discussion

Catchments with heterogeneous land cover types provide a challenge for deriving accurate total evaporation estimates from remote sensing datasets, due to the difficulties in detecting the existing variations (McCabe and Wood, 2006; Vinukollu *et al.*, 2011). While the application of multispectral sensors, with various radiometric, spectral and spatial resolutions,

have accomplished different estimation accuracies, there has been little reported research on the effect of sensor spatial-resolution on the accurate retrieval of total evaporation estimates, particularly at catchment scale. This study, therefore, explores the effect of varying sensor spatial resolution of the Landsat 8 and MODIS remote sensing products in estimating total evaporation in the uMngeni Catchment with heterogeneous land cover.

4.4.1 Spatio-temporal variability of total evaporation

The findings from the two multispectral sensors presented in this study have demonstrated that the variations in sensor spatial resolution have a significant effect on the accurate estimation of total evaporation at a catchment scale. As indicated by the spatial variations in remote sensing inputs (LST, NDVI, FVC *etc*) and derived energy fluxes (R_n , LE), MODIS showed lower estimates with less variability across the catchment. The poor spatio-temporal estimation of biophysical parameters and total evaporation estimates from MODIS datasets is a clear reflection of the effect of sensor spatial resolution in deriving biophysical parameters and total evaporation estimates across heterogeneous environments. At a localised scale, the coarse 1000 m MODIS sensor fails to detect and map the spatial variations of total evaporation. This may be explained by the fact that various land cover types are captured within a large single pixel and their biophysical characteristics (LST, NDVI, FVC, *etc*) are assigned to the land cover class with the highest percentage cover. The input parameters within a single pixel are derived as an aggregation, without variations. This limitation therefore results in the poor spatial retrieval of total evaporation estimates for land cover types within catchments. This was also highlighted by Roerink *et al.* (2000) who states that the MODIS pixel size fails to differentiate the existence of mixed land cover types within a particular pixel. On the other hand, it has been shown (Figure 4.3 (a-f)) that the 30 m Landsat 8 dataset provided better spatial variations in biophysical inputs and total evaporation estimates at catchment scale. Furthermore, a close agreement between EC ground-based measurements and Landsat 8, when compared to MODIS, may be attributed to the presence of the refined near infra-red band spectral range, improving its sensitivity in detecting fine variations of total evaporation between different land cover types. This study therefore demonstrates that the Landsat 8 multispectral dataset at 30 m spatial resolution has a better ability to detect small variations between land cover types and subsequently map the spatial variations of total evaporation at catchment scale.

Although MODIS data failed to adequately characterize total evaporation within the uMngeni Catchment, when compared to Landsat 8 and EC ground-based measurements, previous studies indicate the sensor as having greater potential at regional scales (McCabe and Wood, 2006; Ruhoff *et al.*, 2012).

4.4.2 Total evaporation variations between different land cover types

The variation of total evaporation between different land cover types is a clear indication that existing land cover types exhibit different evaporative signatures within a defined catchment. The results obtained using the Landsat 8 dataset, show that the sensor has managed to capture the variations of total evaporation estimates between the different land cover types within the uMngeni Catchment, when compared to the MODIS dataset. Some possible explanations for the better performance of the Landsat 8 dataset is that the improved sensor design (*i.e.* from 8 bit to 12 bit) has made it more sensitive to the bio-physical properties of individual land cover types, which are critical for total evaporation retrieval. The failure of the MODIS sensor to detect the differences in bio-physical properties within the catchment results in poor total evaporation estimates per land cover type and may be due to the large sensor spatial resolution, amongst other factors. Findings from this work are consistent with those by McCabe and Wood (2006), who estimated total evaporation, using SEBS model derived from MODIS, Landsat ETM+ and ASTER. High and reliable estimates were obtained from ASTER and Landsat, whereas MODIS failed to discriminate the effect of spatial heterogeneity at the field scale. These results also agree with Mengistu *et al.* (2014), who highlighted that Landsat images provided better total evaporation estimates, when compared to MODIS images, possibly because of their higher spatial resolution. In addition, results from this study are also supported by Allen *et al.* (2008), who compared the performance of MODIS and Landsat-based total evaporation estimates from an irrigated agricultural area, based on the METRIC model. They concluded that spatial variations of total evaporation using MODIS sensor are highly degraded.

4.5 Conclusion

The potential of two different multispectral sensors with different spatial resolutions, Landsat 8 (30 m) and MODIS (1000 m) to estimate total evaporation was tested, using the SEBS model for the uMngeni Catchment. The findings of this study demonstrated that spatial resolution has a considerable effect in determining variations of biophysical inputs and subsequent total evaporation estimates. It was shown that better estimates of total evaporation were obtained from the 30 m spatial resolution Landsat 8 dataset, when compared to the 1000 m MODIS dataset. The Landsat 8 sensor has also managed to detect and map variations of total evaporation between different land cover types, whereas the MODIS dataset failed to adequately capture these variations. The Landsat 8 estimates were in closer agreement with EC ground-based measurements. The promising 30 m Landsat 8 sensor results illustrated in this study show the sensor's effectiveness in determining total evaporation estimates per land cover type at catchment scale, when compared to remote sensing sensors with a coarse spatial resolution, such as MODIS. Although the Landsat 8 dataset proved effective in a catchment characterised by diverse land cover types, there is need for this dataset to be tested under different environments, with various bio-physical characteristics.

4.6 References

- Allen, RG, Pereira, LS, Raes, D, Smith, M. 1998. *Crop evapotranspiration - Guidelines for computing crop water requirements- FAO Irrigation and Drainage Paper 56*. Food and Agriculture Organization of the United Nations, Rome, Italy, pp. 15-64.
- Allen, RG, Robison, CW, Trezza, R, Garcia, M, Kjaersgaard, J. 2008. Comparison of Evapotranspiration Images from MODIS and Landsat along the Middle Rio Grande of New Mexico. *The 17th William T. Pecora Memorial Remote Sensing Symposium Proceedings, Denver, Colorado*.
- El-Askary, H, Abd El-Mawlad, SH, Li, J, El-Hattab, MM, El-Raey, M. 2014. Change detection of coral reef habitat using Landsat-5 TM, Landsat 7 ETM+ and Landsat 8 OLI data in the Red Sea (Hurghada, Egypt). *International Journal of Remote Sensing* 35(6): 2327-2346.
- Everson, C, Clulow AD, Becker, M, Watson, A, Ngubo, C, Bulcock, H, Mengistu, M, Lorentz S, Demlie M. 2014. *The long term impact of Acacia mearnsii trees on evaporation, streamflow, low flows and ground water resources. Phase II: Understanding the controlling environmental variables and soil water processes over a full crop rotation*. Water Research Commission, Project: K5/2022, Pretoria, South Africa.
- Ghile, YB, Schulze, RE. 2010. Evaluation of Three Numerical Weather Prediction Models for Short and Medium Range Agrohydrological Applications. *Water Resources Management* 24(5): 1005-1028.
- Gibson, LA, C Jarman, C, Su, Z, Eckardt, FE. 2013. Estimating evapotranspiration using remote sensing and the Surface Energy Balance System – A South African perspective. *Water SA* 39(4): 477-484.
- Gibson, LA, Munch, Z, Engelbrecht, J. 2011. Particular uncertainties encountered in using a pre-packaged SEBS model to derive evapotranspiration in a heterogeneous study area in South Africa. *Hydrology and Earth System Sciences* 15: 295–310.
- Glenn, EP, Huete, AR, Nagler, PL, Hirschboeck, KK, Brown, P. 2007. Integrating Remote Sensing and Ground Methods to Estimate Evapotranspiration. *Critical Reviews in Plant Sciences* 26: 139–168.
- Hargreaves, GH, Samani, ZA. 1985. Reference crop evapotranspiration from ambient air temperature. *Applied Engineering in Agriculture* 1(2): 96-99.
- Jarman, C, Everson, C, Savage, M, Mengistu, M, Clulow, A, Walker, S, Gush, M. 2009. *Refining tools for evaporation monitoring in support of water resources management*. Report No. 1567/1/08 Water Research Commission, Pretoria, South Africa.
- Jia, K, Wei, X, Gu, X, Yao, Y, Xie, X, Lib, B. 2014. Land cover classification using Landsat 8 Operational Land Imager data in Beijing, China. *Geocarto International*.
- Jin, X, Guo, R, Xia, W. 2013. Distribution of Actual Evapotranspiration over Qaidam Basin, an Arid Area in China. *Remote Sensing* 5: 6976-6996.
- Jovanovic, N, Israel, S. 2012. Critical review of methods for the estimation of actual evapotranspiration in hydrological models.
- Lee, TS, Najim, MMM, Aminul, MH. 2004. Estimating evapotranspiration of irrigated rice at the West Coast of the Peninsular of Malaysia. *Journal of Applied Irrigation Science* 39(1): 103 - 111.

- Li, Z, Tang, R, Wan, Z, Bi, Y, Zhou, C, Tang, B, Yan, G, Zhang, X. 2009. A review of current methodologies for regional evapotranspiration estimation from remotely sensed data. *Sensors* 9: 3801-3853.
- Lott, RB, Hunt, RJ. 2001. Estimating evapotranspiration in natural and constructed wetlands. *Wetlands* 21(4): 614–628.
- Maeda, EE, Wiberg, DA, Pellikka, PKE. 2011. Estimating reference evapotranspiration using remote sensing and empirical models in a region with limited ground data availability in Kenya. *Applied Geography* 31: 251-258.
- Makkink, G. 1957. Testing the Penman formula by means of lysimeters. *Journal of the Institution of Water Engineers* 11(3): 277-288.
- Mauck, BA, Warburton, M. 2013. Mapping areas of future urban growth in the Mgeni catchment. *Journal of Environmental Planning and Management*: 1-17.
- McCabe, MF, Wood, EF. 2006. Scale influences on the remote estimation of evapotranspiration using multiple satellite sensors. *Remote Sensing of Environment* 105(4): 271-285.
- Mengistu, MG, Everson, CS, Moyo, NC, Savage, MJ. 2014. *The Validation of the Variables (Evaporation and Soil Moisture) in Hydrometeorological Models*. 2066/1/13 Pretoria, South Africa.
- Molden, D, Sakthivadivel, R. 1999. Water Accounting to Assess Use and Productivity of Water. *Water Resources Development* 15(1/2): 55-71.
- Monteith, J. 1965. Evaporation and environment. *Symp. Soc. Exp. Biol.*
- Mutiga, JK, Su, Z, Woldai, T. 2010. Using satellite remote sensing to assess evapotranspiration: Case study of the upper Ewaso Ng'iro North Basin, Kenya. *International Journal of Applied Earth Observation and Geoinformation* 12, Supplement 1(0): S100-S108.
- Pahlevan, N, Schott, J. 2013. Leveraging EO-1 to Evaluate Capability of New Generation of Landsat Sensors for Coastal/Inland Water Studies. *IEEE Journal of selected topics in applied earth observation and remote sensing* 6(2): 360-374.
- Penman, HL. 1948. Natural Evaporation from Open Water, Bare Soil and Grass. *Proceedings of the Royal Society of London. Series A. Mathematical and Physical Sciences* 193(1032): 120-145.
- Priestley, CHB, Taylor, RJ. 1972. On the Assessment of Surface Heat Flux and Evaporation Using Large-Scale Parameters. *Monthly Weather Review* 100(2): 81-92.
- Rahman, H, Dedieu, G. 1994. SMAC: a simplified method for the atmospheric correction of satellite measurements in the solar spectrum. *Remote Sensing* 15(1): 123-143.
- Roerink, GR, Su, Z, Menenti, M. 2000. S-SEBI: A Simple Remote Sensing Algorithm to Estimate the Surface Energy Balance. *Physics and Chemistry of the Earth* 25(2): 147-157.
- Ruhoff, AL, Paz, AR, Collischonn, W, Aragao, LEOC, Rocha, HR, Malhi, YS. 2012. A MODIS-based energy balance to estimate evapotranspiration for clear-sky days in Brazilian Tropical Savannas. *Remote Sensing* 4: 703-725.
- Savenije, HHG. 2004. The importance of interception and why we should delete the term evapotranspiration from our vocabulary. *Hydrological Processes* 18: 1507–1511.
- Su, Z. 2002. The Surface Energy Balance System (SEBS) for estimation of turbulent heat fluxes. *Hydrology and Earth System Sciences* 6(1): 85-99.
- Sugita, F, Kishii, T. 2002. Effect of roughness distribution on evaporation processes over non-homogeneous sand surfaces: a wind tunnel investigation. *Hydrological Processes* 16: 2141–2153.

- Summerton, M, Schulze, RE, Graham, PL. 2010. Impacts of a changing climate on hydrology and water supply in the Mgeni catchment, South Africa. *Third International Symposium, Managing Consequences of a Changing Global Environment*. Newcastle.
- Thornthwaite, CW. 1948. An Approach toward a Rational Classification of Climate. *Geographical Review* 38(1): 55-94.
- Vinukollu, RK, Wood, EF, Ferguson, RC, Fisher, JB. 2011. Global estimates of evapotranspiration for climate studies using multi-sensor remote sensing data: Evaluation of three process-based approaches. *Remote Sensing of Environment* 115: 801–823.
- Warburton, ML, Schulze, RE, Jewitt, GPW. 2010. Confirmation of ACRU model results for applications in land use and climate change studies. *Hydrology and Earth System Sciences* 14(12): 2399-2414.
- Wildlife, KE. 2011. *KwaZulu-Natal Land Cover*. . Biodiversity Conservation Planning Division, Ezemvelo KZN Wildlife, Pietermaritzburg.

5. ESTIMATING SPATIAL VARIATIONS OF TOTAL EVAPORATION USING MULTISPECTRAL SENSORS WITHIN THE UMNGENI CATCHMENT, SOUTH AFRICA

C Shoko*, DJ Clark, H Bulcock and MG Mengistu

Centre for Water Resources Research, University of KwaZulu-Natal, Private Bag X01, Scottsville, Pietermaritzburg 3209, South Africa

Abstract

This study investigated the feasibility of using multispectral remote sensing data to estimate spatial variations of total evaporation at a catchment scale. Total evaporation is of importance in assessing and managing long-term water use, especially in water-limited environments. In South Africa, increasing demand for water threatens long-term water supply sustainability. Therefore, there is a need to account for water utilization by different land uses for well-informed water resources management and future planning, in order to meet the growing demand, due to population growth and economic development. The aim of this study was to determine spatial variations of total evaporation, within the uMngeni Catchment in KwaZulu-Natal, South Africa, from Landsat 8 and MODIS images, using the SEBS model. The results indicate that Landsat 8 is more suitable for spatial representation of seasonal and annual total evaporation estimates, when compared to the MODIS dataset. In addition, when compared to mean monthly ground-based eddy covariance measurements, Landsat-based estimates have a high R^2 of 0.72 and a low RMSE of 32.34 mm (30.30% of the monthly mean), whereas MODIS-based estimates have a low R^2 of 0.44 and a high RMSE of 93.63 mm (87.74% of the monthly mean). Spatial variations of total evaporation have shown that different sensors, with varying spatial resolutions, have different abilities to show spatial variations of total evaporation, especially with regard to the characteristics of the land cover types at catchment level. It was also found that not only the land cover type within a catchment, but also the spatial characteristics (*i.e.* area, patchiness), have an effect on total evaporation estimates. The findings of this study underscore the importance of the

sensor type and land cover characteristics in deriving accurate and reliable spatial variations of total evaporation at a catchment scale.

Keywords: total evaporation, remote sensing, land cover characteristics, patchiness, areal extent

5.1 Introduction

Water availability is an issue of concern on a local and global scale and its management is becoming more challenging, particularly in semi-arid areas. In South Africa, the increasing water scarcity compounded by population growth and economic development (New, 2002), requires more accurate budgeting, so that the available water resources may be better allocated. In addition, the science community agrees that climate change may profoundly affect the hydrological cycle, particularly precipitation patterns and temperature, which all have a bearing on water availability (Dore, 2005; McCarthy, 2001). Consequently, there is a need for better water management to meet demand by various consumers. Total evaporation, which includes water consumption by plants and the loss of water from open water surfaces, soil moisture and non-vegetated surfaces, is one of the key component of the water balance to be considered in water resources management (McCabe and Wood, 2006; Xu *et al.*, 2006). Total evaporation depends on both climatic and land surface characteristics, and reflects the variations in water consumption, in response to climatic and land use changes (Mutiga *et al.*, 2010; Wang *et al.*, 2013). Therefore, understanding spatial variations of total evaporation will aid the proper planning and allocation of water.

There are different approaches which have been applied for the estimation of total evaporation. The most widely used include those of Penman-Monteith (Allen *et al.*, 1998; Jia *et al.*, 2014a; Penman, 1948), Thornthwaite (Thornthwaite, 1948) and Priestley-Taylor (Priestley and Taylor, 1972), as well as the use of micro-meteorological methods, such as the eddy covariance (Clulow *et al.*, 2011; Mengistu *et al.*, 2014; Scott, 2010), surface renewal (Mengistu and Savage, 2010; Spano *et al.*, 2000), scintillometry (Menenti *et al.*, 2003) and lysimeters (Gowda *et al.*, 2013; Makkink, 1957; Morton, 1983). Although these methods have been successfully applied to

derive total evaporation across different land cover types, ranging from forests to agricultural areas, they lack one of the key aspects, which is the spatial representation of total evaporation. Liou and Kar (2014) describes these approaches as lacking the spatial representation of the total evaporation across a heterogeneous landscape, hence they cannot be up-scaled for large-scale mapping and estimation.

The advent of remote sensing technologies, therefore, provides a valuable alternative to address the important and challenging task of estimating the spatial variations of total evaporation across varying land cover types in a cost-effective manner, when compared to meteorological or micro-meteorological methods (Dube *et al.*, 2014; Nouri *et al.*, 2014; Wilson *et al.*, 2003). Although remote sensing cannot directly quantify total evaporation from space, satellite data provides inputs for its estimation, especially when combined with ground-based meteorological observations (Liu *et al.*, 2003). Consequently, different remote sensing-based approaches have been developed to estimate spatial variations of total evaporation, including the use of energy balance models. These models include the Surface Energy Balance Index (SEBI) (Roerink *et al.*, 2000), the Surface Energy Balance System (SEBS) (Su, 2002), the Surface Energy Balance Algorithm for Land (SEBAL) (Bastiaanssen *et al.*, 1998) and the Mapping EvapoTranspiration at high Resolution with Internalized Calibration (METRIC) (Allen *et al.*, 2007). However, the SEBS model is regarded as the most widely-used and effective model in deriving total evaporation estimates. This is because it estimates aerodynamic resistances more explicitly than other models (Elhag *et al.*, 2011; Jia *et al.*, 2003; Ma *et al.*, 2012; Ma *et al.*, 2011; Rwasoka *et al.*, 2011; van der Kwast *et al.*, 2009), it is applicable on various spatial scales and it has also been validated in several studies for different land cover types (Su *et al.*, 2007).

Although the SEBS model has a proven track record for the accurate spatial estimation of total evaporation, the use of this model, together with varying satellite datasets, across varying land uses, within a heterogeneous catchment, has not been widely researched. For instance, different studies that have estimated variations of total evaporation using SEBS, have focused mainly on individual or specific land cover types, such as wetlands (Chen *et al.*, 2002; Jia *et al.*, 2009), forest (Goodrich *et al.*, 2000; Xu *et al.*, 2006) or agricultural fields (Ray and Dadhwal, 2001;

Senay *et al.*, 2007). However, few studies have focused on the potential of using multispectral data for estimating the spatial variations of total evaporation, within a heterogeneous catchment. The spatial heterogeneity of land cover characteristics within a catchment results in variations in water use patterns and subsequent total evaporation; hence, for better management of water resources, there is a need to understand such variations. Land cover heterogeneity, characterized by varying spatial characteristics, imposes challenges for estimating the spatial variation in total evaporation, using point-based measurements or local micro-meteorological observations. In this study, the use of multispectral remote sensing data, Landsat 8 at 30 m and MODIS at 1000 m spatial resolution, is investigated, to determine spatial variations of total evaporation across the uMngeni Catchment, in KwaZulu-Natal, South Africa. Specifically, this study aims to determine; (i) how total evaporation estimates vary across the heterogeneous catchment over a season or year, and (ii) the effect of varying land cover characteristics (*i.e.* land cover type, areal extent, patchiness and roughness length) in relation to the spatial resolution of the sensor in estimating variations of total evaporation.

5.2 Materials and Methods

The spatial and temporal variability of total evaporation estimates across a catchment with varying land cover characteristics was examined in the uMngeni Catchment, using the 30 m Landsat 8 and 1000 m MODIS data, over a period of one year (*i.e.* May 2013 to April 2014). Total evaporation estimates over a long period of time (one year), including dry (May to October) and wet (November to April) season are necessary for accurate water accounting purposes and management purposes at catchment scale.

5.2.1 Study site

The uMngeni Catchment in the Province of KwaZulu-Natal, South Africa, shown in Figure 5.1, is responsible for the provision of water to the Durban and Pietermaritzburg areas (Summerton *et al.*, 2010). The catchment is characterized by spatial and temporal variations in climatic conditions. For instance, it receives rainfall in summer, which ranges from 700 mm in the drier

interiors to above 1 500 mm in the western parts. Generally, rainfall has a west-east and north-south gradient (Figure 5.1). This implies that the eastern and southern most parts of the catchment receive low rainfall. The catchment has a mean annual temperature ranging from 12°C in the west 20°C towards the coast (Warburton *et al.*, 2010). It has also been highlighted that the uMngeni catchment is vulnerable to heavy floods and sporadic droughts (Schulze, 1997; Schulze and Perks, 2000). This makes total evaporation monitoring vital for many applications, such as climate change modelling, water quality deterioration and land use/cover changes. The major land cover types within the uMngeni Catchment include built-up areas, commercial irrigated agriculture, wetlands, grasslands, natural forest, plantations, orchards, sugarcane, water bodies and natural bush.

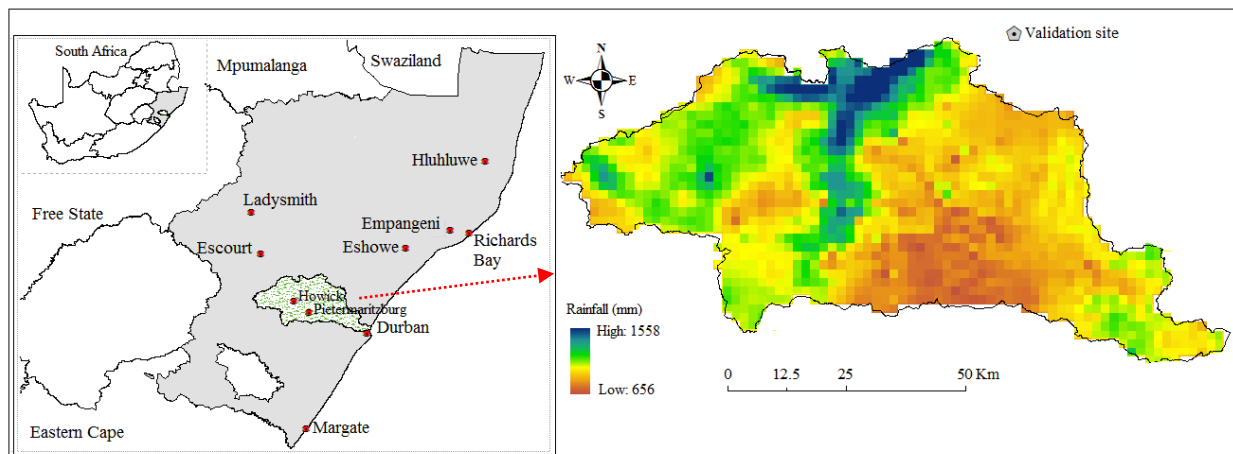


Figure 5.1 Location of the study area and mean annual rainfall (Schulze *et al.*, 2008)

5.2.2 Data acquisition and pre-processing

To assess the spatial and temporal variations of total evaporation across the uMngeni Catchment with varying land cover characteristics, Landsat 8 and MODIS datasets were used, based on the SEBS model as explained in Chapter 4. Continuing from the study in Chapter 4, (Shoko *et al.*, 2014), which is a comparison of total evaporation from a few images for a few discrete days in time, this section (Chapter 5), estimates total evaporation over a period of one year (from May 2013 to April 2014), as well as investigate the effect of land cover spatial distribution relative to sensor spatial resolution. The period covered coincided with the availability of Landsat 8 images,

since its launch on the 11th of February 2013. The one-year period covered the main dry and wet seasons within the uMngeni Catchment. It is important to note that the same data (*i.e.* remote sensing, meteorological and ancillary) and preprocessing techniques applied in this section were similar to those in Chapter three, therefore, no further detail is provided in this section.

5.2.3 Determination of monthly and annual total evaporation estimates

Monthly total evaporation estimates from the two sensors are derived based on daily estimates from MODIS and Landsat 8. However, the computation of seasonal and annual total evaporation from Landsat 8 datasets is challenging because of its 16-day temporal resolution and the potential lack of cloud-free images. To obtain seasonal and annual total evaporation estimates, Landsat 8-based estimates were up-scaled (gap filling) to monthly estimates, by applying a representative coefficient and daily reference evaporation, as applied by previous studies (Allen and Bastiaanssen, 2002; Singh *et al.*, 2014; Tasumi *et al.*, 2005). The cloudy-free images used to derive representative coefficients were the images for 23/05/2013, 08/06/2013, 24/06/2013, 23/07/2013, 11/08/2013 and 23/03/2014. In the case of missing images for some months, due to cloud cover, available images for the previous or closest month were used to derive representative coefficient. The final seasonal or annual total evaporation estimates was therefore derived as:

$$ET = \sum_{i=1}^n (ET_{oi} \times ET_{fi}) \quad (5.1)$$

where:

- ET = seasonal /annual total evaporation estimates (mm),
- ET_{oi} = reference total evaporation estimates (mm) for period i (days), and
- ET_{fi} = representative total evaporation coefficient (-) for period i .

For this study, the ET_{fi} used were estimated, using the actual total evaporation derived from Landsat 8 (mm) and reference total evaporation (mm) using the following function:

$$ET_{fi} = \frac{ET_{Landsat8}}{ET_{oi}} \quad (5.2)$$

where

- ET_{fi} = representative total evaporation coefficient (-) for period i ,
- $ET_{Landsat8}$ = actual total evaporation derived from Landsat 8 (mm), and
- ET_{oi} = reference total evaporation estimates (mm) for period i (days).

Reference total evaporation was derived from meteorological data, using an inbuilt function in the ILWIS software (<http://52north.org>). The required inputs include wind speed, humidity and temperature. Additional inputs include a Digital Elevation Model (DEM), average shortwave transmissivity of the study area, as well as the Julian day. The average short wave transmissivity was derived from the DEM, using the formula after Allen and Bastiaanssen (2002) as:

$$\tau_{sw} = 0.75 + 2 \times 10^{-5} \times Z \quad (5.3)$$

where

- τ_{sw} = average short wave transmissivity (-), and
- Z = DEM (m).

5.2.4 Statistical Analysis

To assess the reliability and performance of MODIS and Landsat 8, total evaporation estimates from the two datasets were statistically compared, using a paired T-test and the Analysis of Variance (ANOVA). To further assess how close estimates from remote sensing data were to ground-based measurements, the r-square (R^2) and the root mean square error (RSME) were determined.

5.2.5 Determining spatial characteristics of different land cover types

The spatial and temporal variability of total evaporation estimates across a catchment is hypothesized to vary with varying land cover characteristics (*i.e.* land cover type, areal extent, patchiness). Therefore, the spatial variations in land cover characteristics were generated, using the landscape configuration metrics analysis tool in ArcView 3.3 software. Different landscape configuration metrics have been developed and implemented to understand the spatial characteristics of a landscape for various applications (Fiener *et al.*, 2011; Kowe *et al.*, 2014; McGarigal and Marks, 1995; Seto and Fragkias, 2005; Turner, 1989; Turner, 2001). In this study, four primary measures of landscape characteristics were used: (i) number of patches (NP), (ii) mean patch size (MPS), (iii) total edge (TE), and roughness length (Z_{om}). The number of patches (NP), which determines the number of patches for a specific land cover type and measures the extent of fragmentation of the land cover type within the catchment. The greater the number of patches for a particular land cover type, the more fragmented it is (Herold *et al.*, 2003). Mean patch size determines the average area of each patch for a particular land cover type. Generally, high values of MPS indicate that the majority of patches for a particular land cover type had a larger areal extent (Gustafson, 1998). The total edge is a measure of the extent of the fragmentation of a particular land cover. A high TE reflects more fragmentation of the land cover type (Kowe *et al.*, 2014). However, to assess the effect of roughness length on total evaporation across the catchment, the land cover map, MODIS and Landsat derived roughness lengths were compared. The land cover map based roughness length was generated based on individual land cover values obtained from the literature (Su, 2006), which coincided with the uMngeni land cover types (highlighted in Chapter 3, Section 3.6).

5.3 Results

To understand the spatial variations of total evaporation across the uMngeni Catchment, different land cover types and their characteristics (*i.e.* area, patchiness) were determined. In addition, total evaporation estimates at a longer temporal scale (one year) were also determined.

5.3.1 Land cover types and distribution within the uMngeni Catchment

The spatial variations in land cover types within the uMngeni Catchment are shown in Figure 5.2, based on the EKZNW (2013) land cover database. Grassland is the most dominant land cover (28.42%), followed by natural forest (20.70%), built-up areas (11.39%), sugarcane (10.59%), subsistence agriculture (8.43%), plantations (8.38%), natural bush (6.60%), waterbodies (3.87%), wetlands (1.13%), orchards (0.24%) and commercial irrigation had the lowest areal coverage (0.23%), as shown in Figure 5.3.

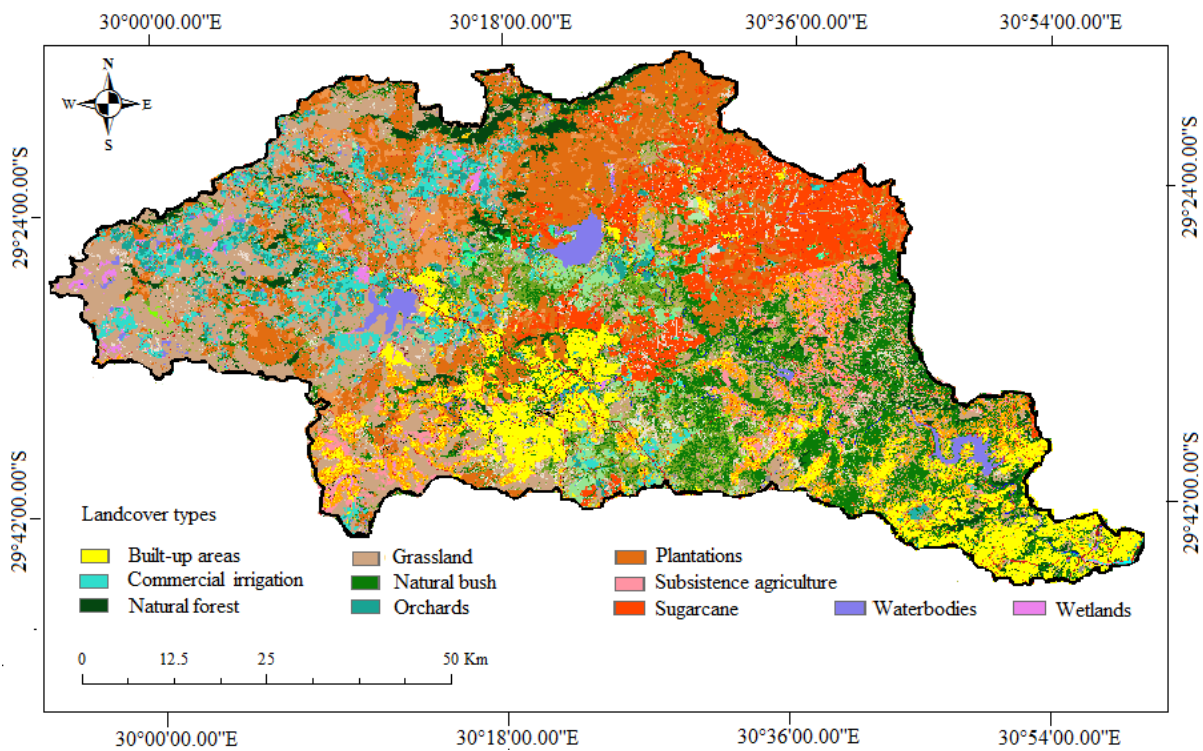


Figure 5.2 Main land cover types within the uMngeni Catchment, EKZNW (2013)

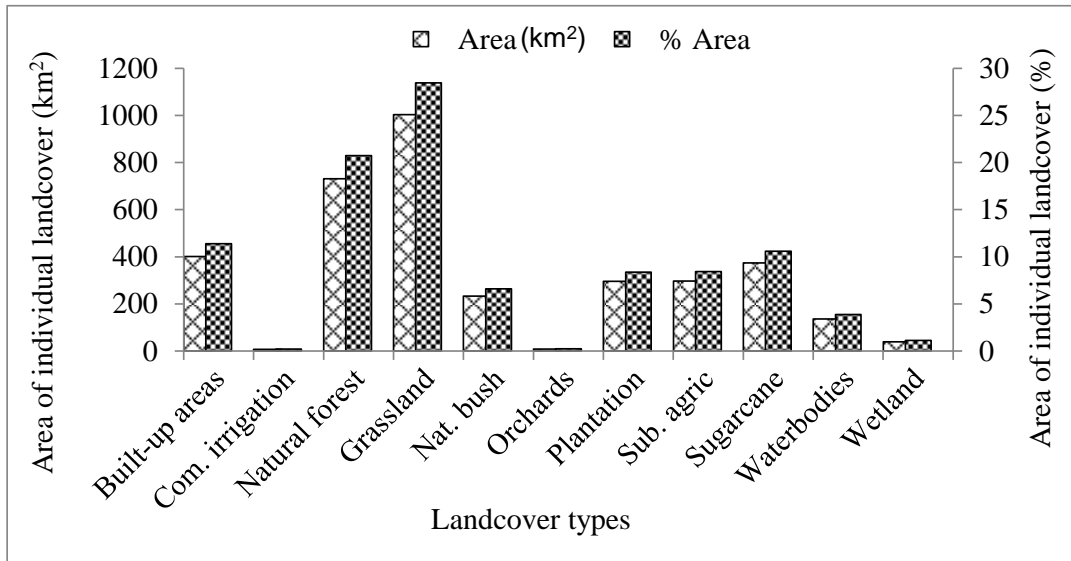


Figure 5.3 Land cover types areal extent, EKZNW (2013)

5.3.2 Spatial characteristics of different land cover types

Measures of the spatial characteristics for different land cover types within the uMngeni Catchment were derived and are shown in Table 5.1. Generally, different land cover types exhibit different spatial characteristics, which have an effect on spatial variations in total evaporation estimates across the catchment. It can be observed that grasslands have the highest number of patches (2538), followed by built-up areas (1866). Commercial irrigation had the lowest number of patches (44), followed by orchards (64). In terms of the mean patch size, built-up areas have the largest mean patch size (0.73 km²), followed by sugarcane (0.65 km²). On the other hand, commercial irrigation and water bodies had the lowest mean patch size (0.12 km²), followed by orchards (0.13 km²). All the different land cover types have mean patch sizes that are smaller than the spatial resolution of the MODIS sensor (1 km²). However, the mean patch sizes of all the different land cover types were larger than the spatial resolution of Landsat 8 sensor (0.0009 km²). Consequently, most of the patches for the different land cover types and subsequent total evaporation estimates are more likely to be detected by the Landsat 8 sensor than the MODIS sensor. Grassland was the most fragmented, compared to any other land cover type (shown by the highest total edge of 9.58), followed by natural forest (4.89). Commercial

irrigation was the least fragmented (shown by the lowest total edge length of 0.09), followed by orchards (0.12).

Table 5.1 Spatial characteristic of different land cover types

Land cover	No. of patches (-)	Mean patch size (km ²)	Total edge (-)
Built-up areas	1866	0.73	3.45
Com. irrigation	44	0.12	0.09
Natural forest	1700	0.43	4.89
Grassland	2538	0.39	9.58
Nat. bush	1182	0.20	3.18
Orchards	64	0.13	0.12
Plantation	1410	0.21	3.16
Sub. agric	194	0.56	1.08
Sugarcane	572	0.65	2.45
Waterbodies	1122	0.12	1.27
Wetland	218	0.18	0.53

The results in Figure 5.4 indicate the various roughness length of momentum (Z_{0m}) for uMngeni Catchment derived from: (a) Landsat 8, (b) MODIS and (c) uMngeni land cover map respectively. General values from literature (Brutsaert, 2005; Pardalos *et al.*, 2014; Ramli *et al.*, 2009; Su, 2006; WMO, 2008) were used to determine Z_{0m} for the land cover types represented in the uMngeni land cover map. It can be observed that the MODIS and Landsat derived Z_{0m} maps indicate a similar spatial variation across the catchment, when compared to the land cover derived Z_{0m} . The landcover-based Z_{0m} also show higher values, as compared to those derived from remote sensing. This might be attributed to the fact that published Z_{0m} values are not always available for every landcover type, hence they show a general representation. In contrast, remote sensing-based values correspond exactly with the characteristics of the land cover types at satellite overpass time; therefore remain attractive in estimating total evaporation.

Figure 5.5 (a and b) illustrates the Landsat 8 and MODIS total evaporation estimates resulting from the use of roughness length according to SEBS for the 23rd of May 2013. In addition, Figure 5.5 (c and d) shows the Landsat 8 and MODIS estimates based on roughness length generated from uMngeni landcover map for the same day. It can be observed that SEBS derived

roughness length resulted in slightly higher total evaporation estimates, when compared to the land cover derived roughness length.

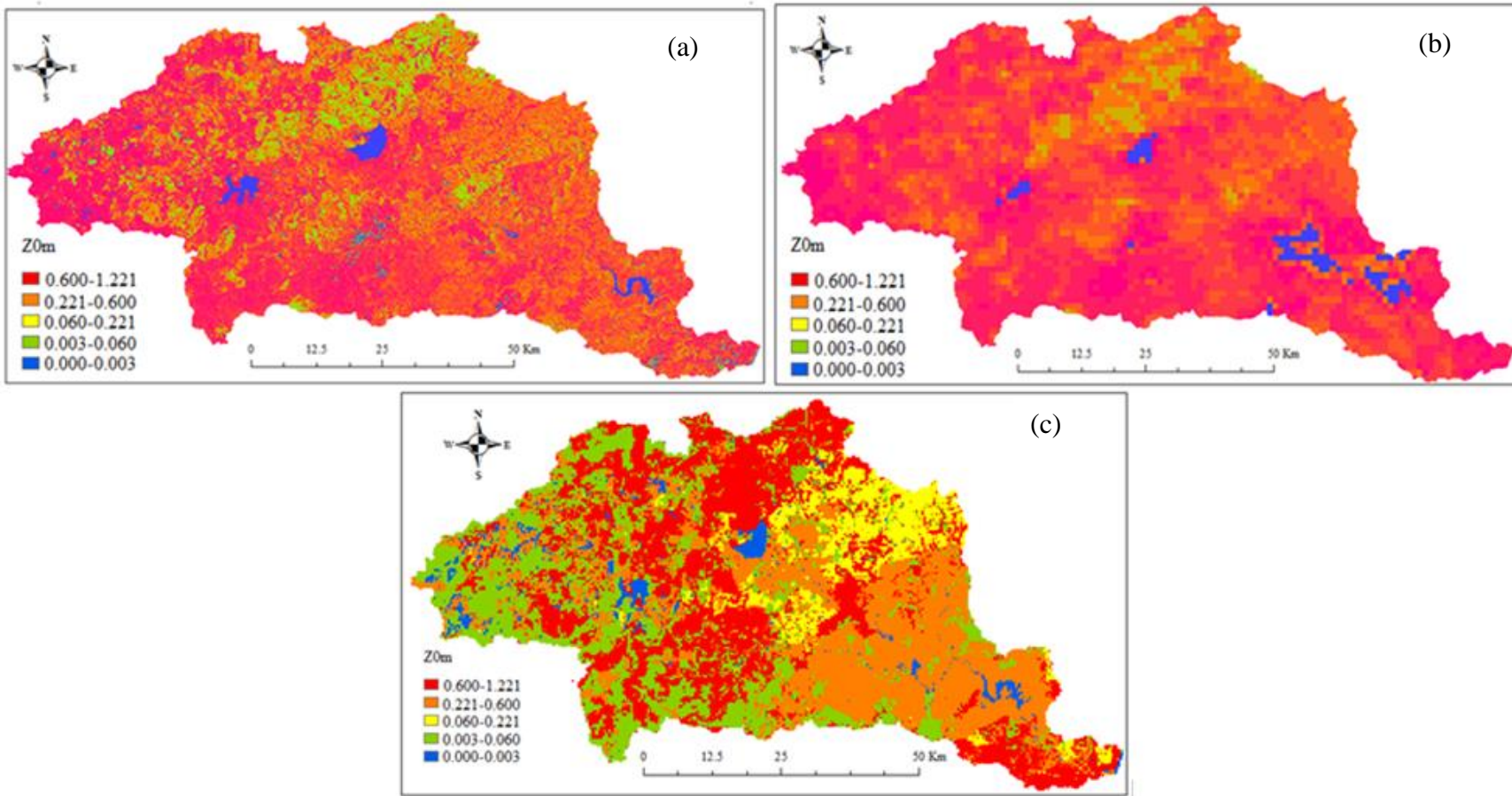


Figure 5.4 Z_{0m} for uMngeni Catchment, derived on the 23rd of May 2013 from: (a) Landsat 8, (b) MODIS and (c) land cover map

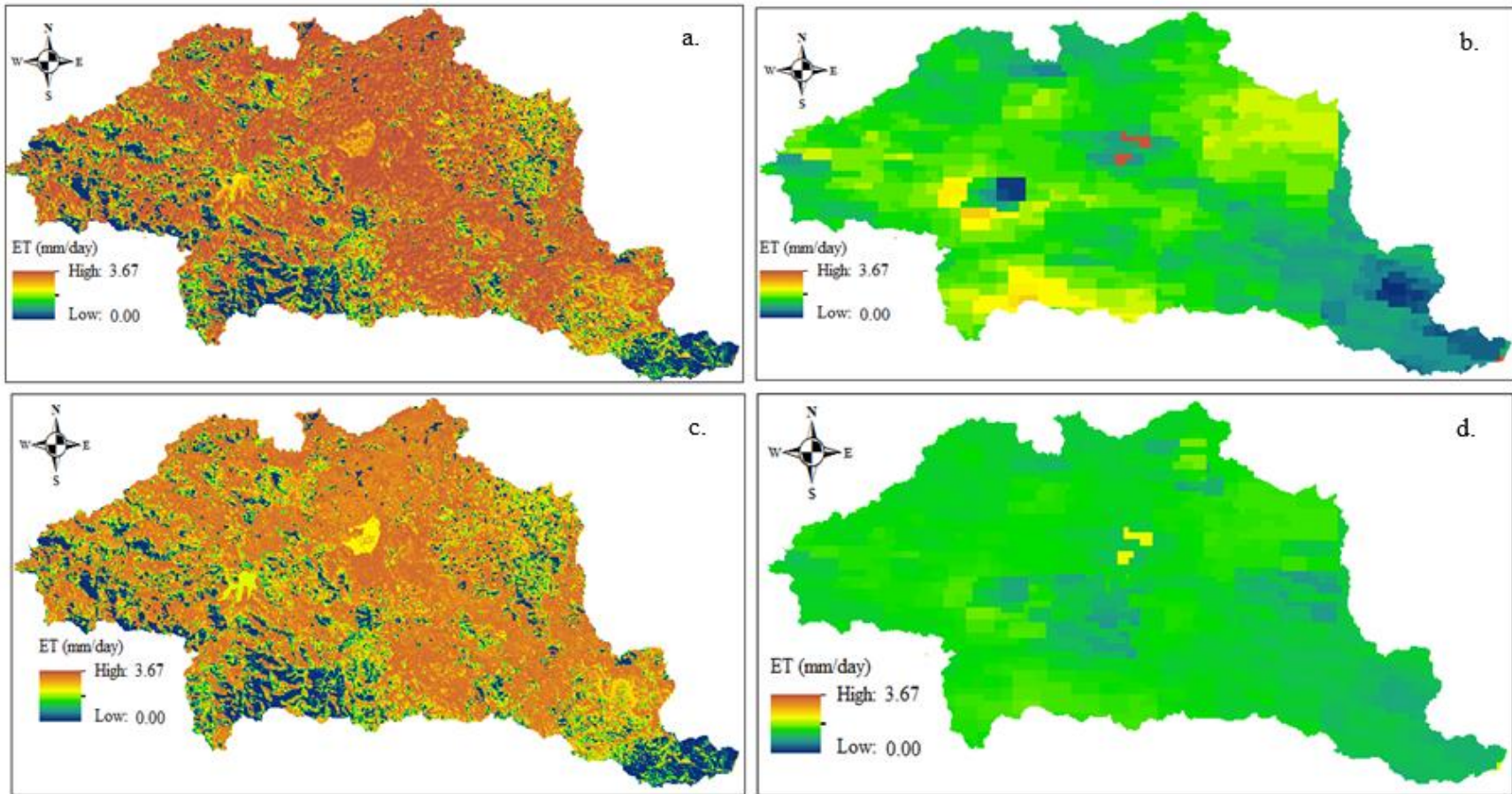


Figure 5.5 Landsat 8 (a) and MODIS (b) total evaporation estimates for the 23rd of May 2013 using Z_{om} derived by SEBS, and Landsat (c) and MODIS (d) total evaporation estimates using Z_{om} derived from uMngeni land cover map

5.3.3 Monthly total evaporation estimates

Monthly mean total evaporation estimates derived from upscaled Landsat 8 and MODIS daily datasets for the uMngeni Catchment for the period of May 2013 to April 2014 are shown in Figure 5.6. The calculation of total evaporation was done based on SEBS derived estimates of roughness length rather than land cover-based values, as published values are not always available for all land cover classes, whereas remote sensing-based values correspond exactly with the characteristics of the land cover types at satellite overpass time; therefore remain attractive in estimating total evaporation. It can be observed that both sensors show a similar trend of total evaporation. However, Landsat 8 shows higher mean monthly total evaporation estimates, compared to MODIS. During the course of the year, monthly total evaporation followed the expected variations in seasonal meteorological conditions, with low total evaporation estimates in the dry months of May, June, July, August and September, which constitute the dry period. The total evaporation estimates were high in the months of October to January, reached a maximum in December with 186 mm and 133 mm for Landsat 8 and MODIS respectively. Also, the results from a paired T-test show that the Landsat 8 and MODIS-derived mean monthly estimates of total differed significantly for the entire period (T-test; $F_{1,796} = 2.200$, $p < 0.05$).

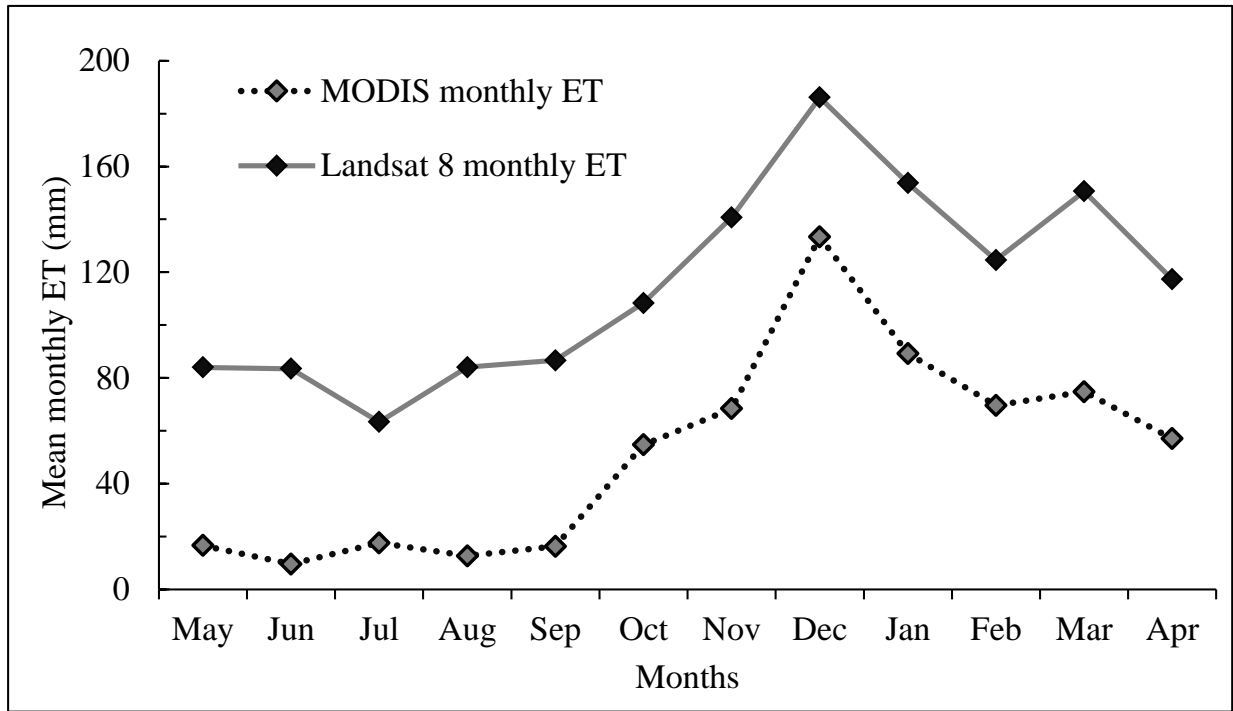


Figure 5.6 Monthly mean total evaporation estimates for the catchment for the hydrological year 2013/14

5.3.4 Spatial variation of seasonal and annual total evaporation

The spatial variation of seasonal and annual total evaporation estimates derived from MODIS and Landsat 8 datasets for the uMngeni Catchment are shown in Figure 5.7. Generally, it can be observed that both sensors show a similar spatial distribution of total evaporation for the wet and dry seasons. The western and northern parts, which are mainly, dominated by plantations, natural forests, commercial irrigated agriculture, water bodies and wetlands, show higher total evaporation estimates, when compared to the eastern- and southern-most parts, which are mainly occupied by urban areas. In addition both sensors indicated that total evaporation varies with the season, with high and low values in the wet and dry seasons respectively. The results further highlighted the advantage of using the 30 m spatial resolution Landsat 8 sensor to map the spatial variations of total evaporation across a heterogeneous catchment, compared to the 1000 m MODIS sensor.

The seasonal and annual statistics of total evaporation from MODIS and Landsat for the whole catchment were extracted and the results are summarized in Table 5.2. Landsat 8 yielded higher seasonal and annual total evaporation estimates, when compared to MODIS. For instance, in the wet season, the 30 m Landsat 8 sensor recorded a maximum of 1629 mm with an average of 770 and standard deviation of 309 mm. In contrast, MODIS recorded lower estimates, with a maximum of 820 mm and an average of 432 mm. The standard deviation of annual total evaporation ranged between 202 and 449 in the dry and wet seasons respectively for Landsat, whereas the MODIS sensor shows a low standard deviation ranging from 51 mm in the dry season to 109 mm in the wet season.

Table 5.2 Summary of seasonal and annual total evaporation statistics (mm)

Period	Landsat 8				MODIS			
	Min.	Max.	Mean	Stdev	Min.	Max.	Mean	Stdev
Wet season	0	1629	770	309	96	820	432	109
Dry season	0	787	306	202	1	439	78	51
Annual	0	2384	1053	449	101	1233	510	150

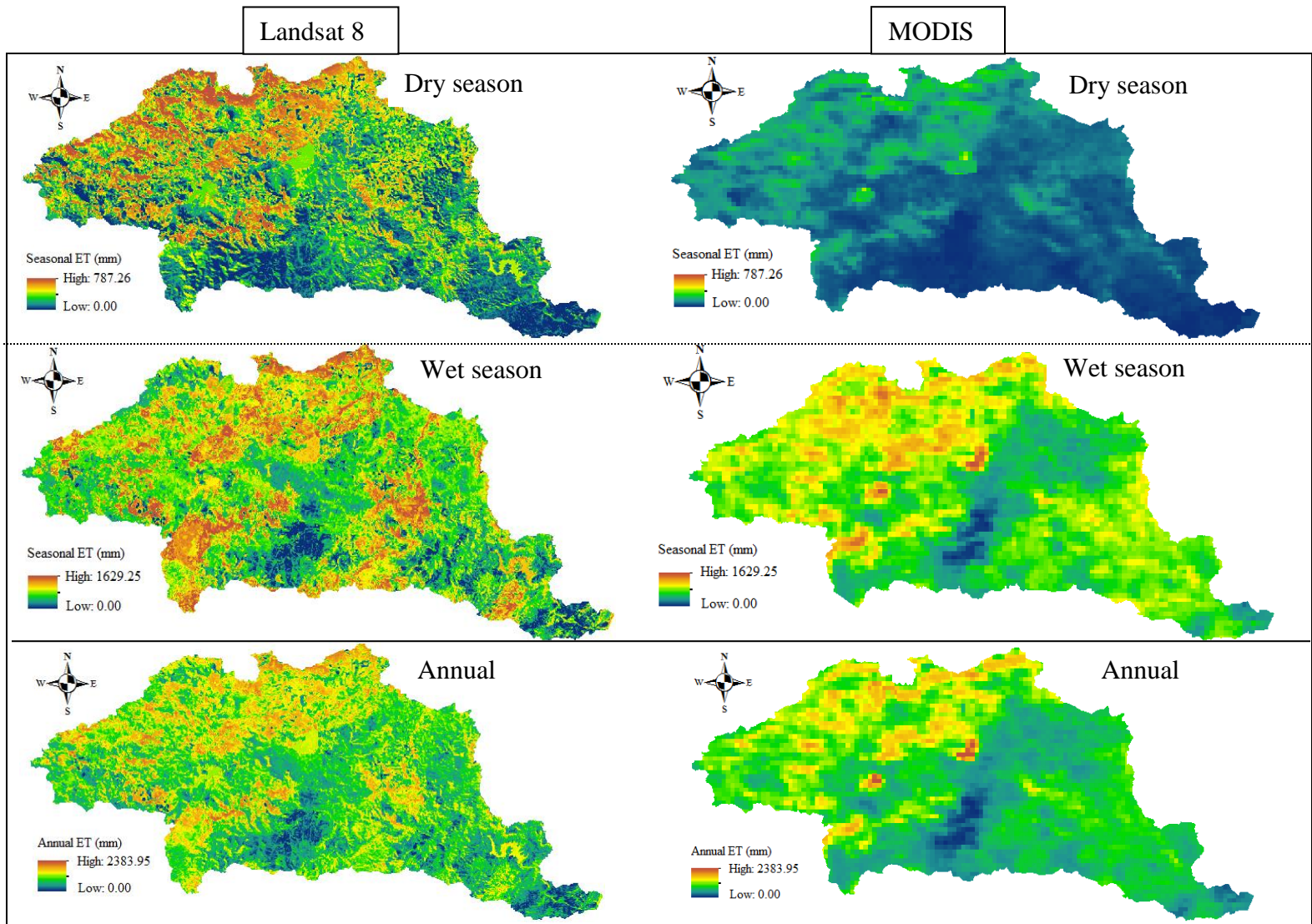
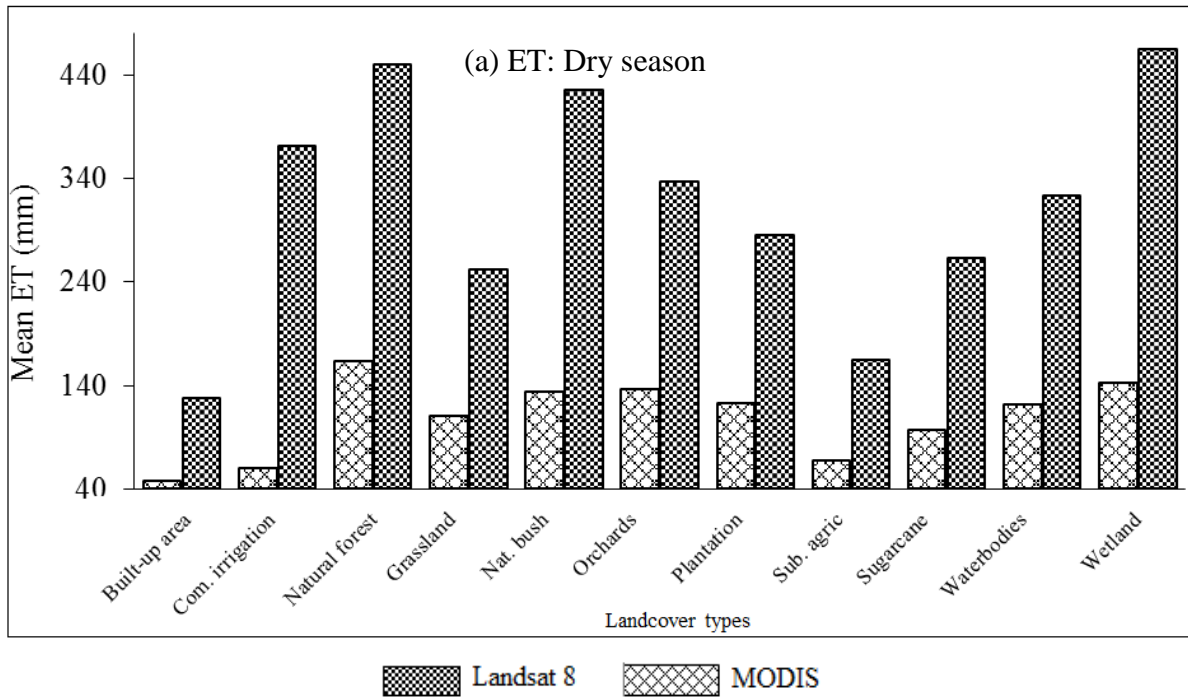


Figure 5.7 Spatial variation of seasonal and annual total evaporation

5.3.5 Seasonal total evaporation from different land cover types

Seasonal total evaporation estimates for different landcover types for dry and wet seasons (2013/2014) are shown Figure 5.8 (a) and (b), respectively. Landsat 8 showed higher estimates for all the different land cover types, when compared to MODIS. It was observed that for both sensors the lowest total evaporation estimates were for built-up areas for both the wet and the dry seasons. However, for MODIS, the highest total evaporation estimates were observed from natural forest in both seasons, while for Landsat 8 the highest estimates were from commercial irrigation in the wet season and wetlands in the dry season.



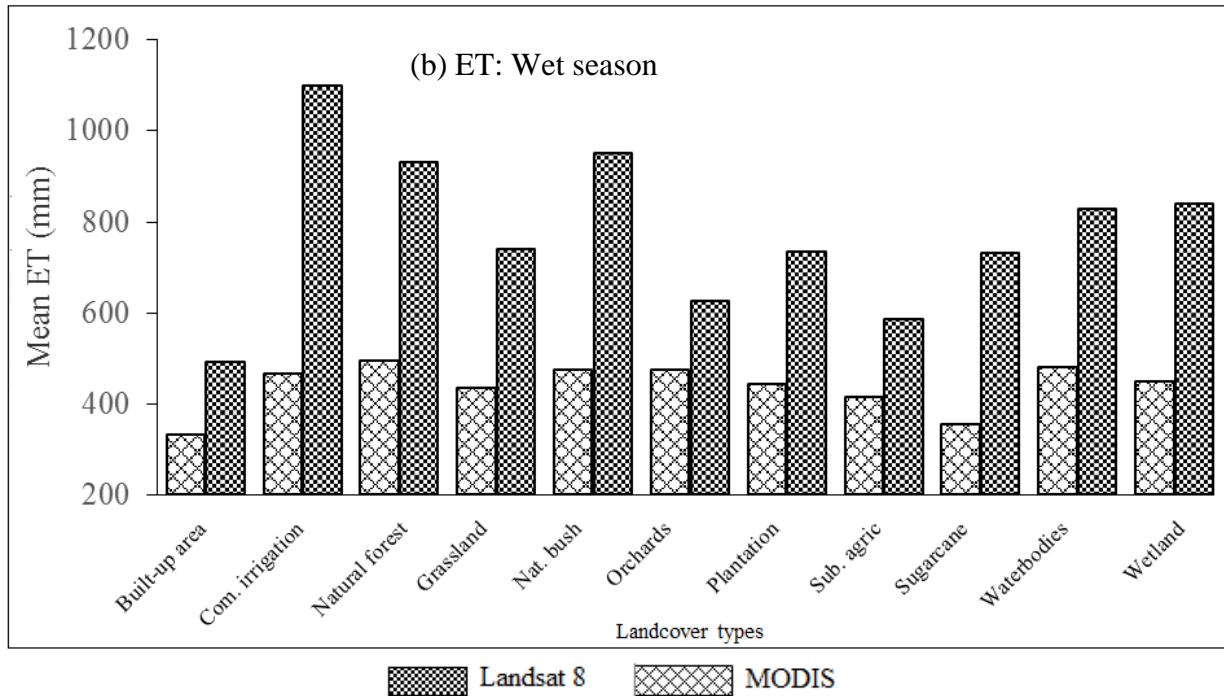


Figure 5.8 Land cover-based mean seasonal total evaporation estimates from the two sensors a) Dry season (2013) and (b) Wet season (2013/14)

5.3.6 Annual total evaporation from different land cover types

Annual total evaporation estimates per land cover type within the uMngeni Catchment are shown in Figure 5.9. Annual estimates show that total evaporation varies with sensor, as well as with land cover type. As can be seen, the Landsat 8 annual estimates were higher than those for MODIS for all the land cover types. It can also be observed that both sensors show lowest mean annual total evaporation estimates from built-up areas. The results in Table 5.3 further indicate detailed annual total evaporation statistics for different land cover types. It was found that Landsat 8 shows lower minimum total evaporation estimates (less than one) as compared to MODIS. This might be attributed to the 30 m spatial resolution which enables Landsat 8 to detect small variations in total evaporation, as compared to the 1000 m MODIS resolution which fails to differentiate the existence of mixed land cover types within a particular pixel. The highest mean annual total evaporation estimates using Landsat 8 were from commercial irrigation (1472 mm), followed by natural forest (1381 mm). For MODIS, natural forest had the highest mean

annual total evaporation (657 mm), followed by orchards (612 mm) (Table 5.3) and its standard deviation ranged from 33 mm (commercial irrigation) to 176 mm (orchards).

Overall, the One Way ANOVA results also reported that MODIS land cover-based seasonal and annual mean estimates were significantly different from Landsat 8 land cover-based estimates (One way ANOVA; $F_{1.812} = 2.22$, $p < 0.05$). However, annual and seasonal mean total evaporation estimates for the different land cover types obtained from MODIS data showed no significant differences (One way ANOVA; $F_{2.853} = 0.125$, $p = 0.998$). In contrast, Landsat 8 yielded significantly different mean total evaporation estimates for all land cover types (One Way ANOVA; $F_{4.964} = 87.011$, $p < 0.05$).

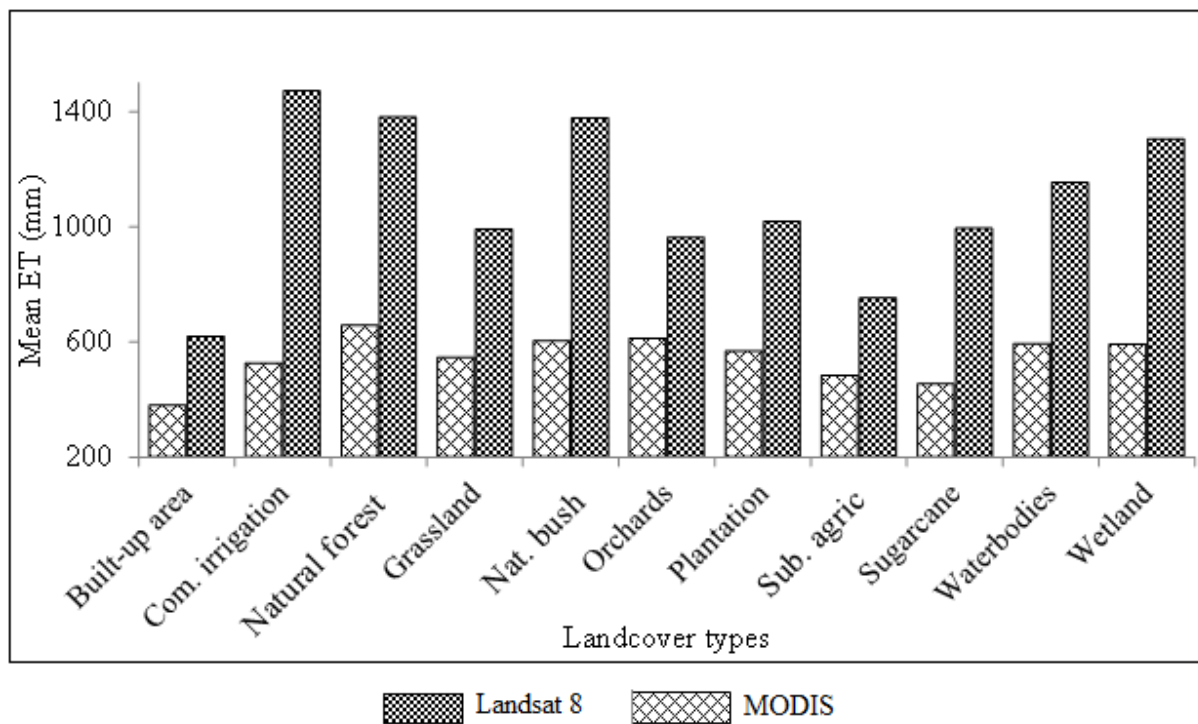


Figure 5.9 Land cover-based mean annual total evaporation from the two sensors for the period 2013-2014

Table 5.3 Summary of land cover-based annual total evaporation statistics (mm)

Land cover	Landsat 8				MODIS			
	Min.	Max.	Mean	Stdev	Min.	Max.	Mean	Stdev
Built-up areas	< 0.5	2226	618	401	101	1106	380	151
Com. irrig.	437	2011	1472	312	432	539	525	33
Nat. forest	< 0.5	2384	1381	428	125	1222	657	152
Grassland	< 0.5	2356	991	398	101	1232	546	162
Nat. bush	< 0.5	2346	1378	480	101	1039	604	175
Orchards	< 0.5	1954	963	326	225	978	612	176
Plantation	< 0.5	2259	1019	357	102	1222	567	162
Sub. agric	< 0.5	2149	751	355	113	983	483	99
Sugarcane	< 0.5	2134	994	308	142	971	453	110
Waterbodies	< 0.5	2350	1154	382	108	1233	593	173
Wetland	249	2330	1306	324	255	913	592	123

Histograms of annual total evaporation estimates from MODIS and Landsat 8, based on pixel coverage, for some of the land cover types, are shown in Figure 5.10. Generally, it can be observed that the two sensors have different capabilities in determining spatial variations of total evaporation, even within a particular land cover type. Landsat 8 managed to produce total evaporation estimates in a wider range (*i.e.* from < 250 mm to > 1500 mm) for the different land cover types. However, MODIS failed to detect total evaporation from some of the pixels with less than 250 mm and pixels exceeding 1000 mm. It can be noted that Landsat 8 and MODIS detected different pixel coverage for different total evaporation ranges. For instance, Landsat 8 total evaporation estimates showed that the majority of the grassland pixels (43.99%) had an annual total evaporation between 500-1000 mm, and very few pixels (2.27%) of less than 250 mm. In contrast, more than half (59.66%) of the grassland pixels for MODIS had an annual total evaporation between 250-500 mm, and 3.5% with less than 250 mm. In addition, about half of the natural forest pixels (49.65%) from Landsat 8 exceeded 1500 mm of total evaporation and 1.56% with less than 250 mm. In contrast, the majority of natural forest pixels (64.85%) for MODIS had annual estimates between 500-1000 mm, and 0.28% with less than 250 mm. For the sugarcane land cover type, Landsat 8 detected almost half of the pixels (47.78%) between 500-1000 mm and a few pixels (0.53%) with less than 250 mm, whereas MODIS detected the majority of pixels (88.7%) between 250-500 mm. Landsat 8 at 30 m spatial resolution managed to capture the small variations of total evaporation within a particular land cover type better than the MODIS sensor with 1000 m spatial resolution.

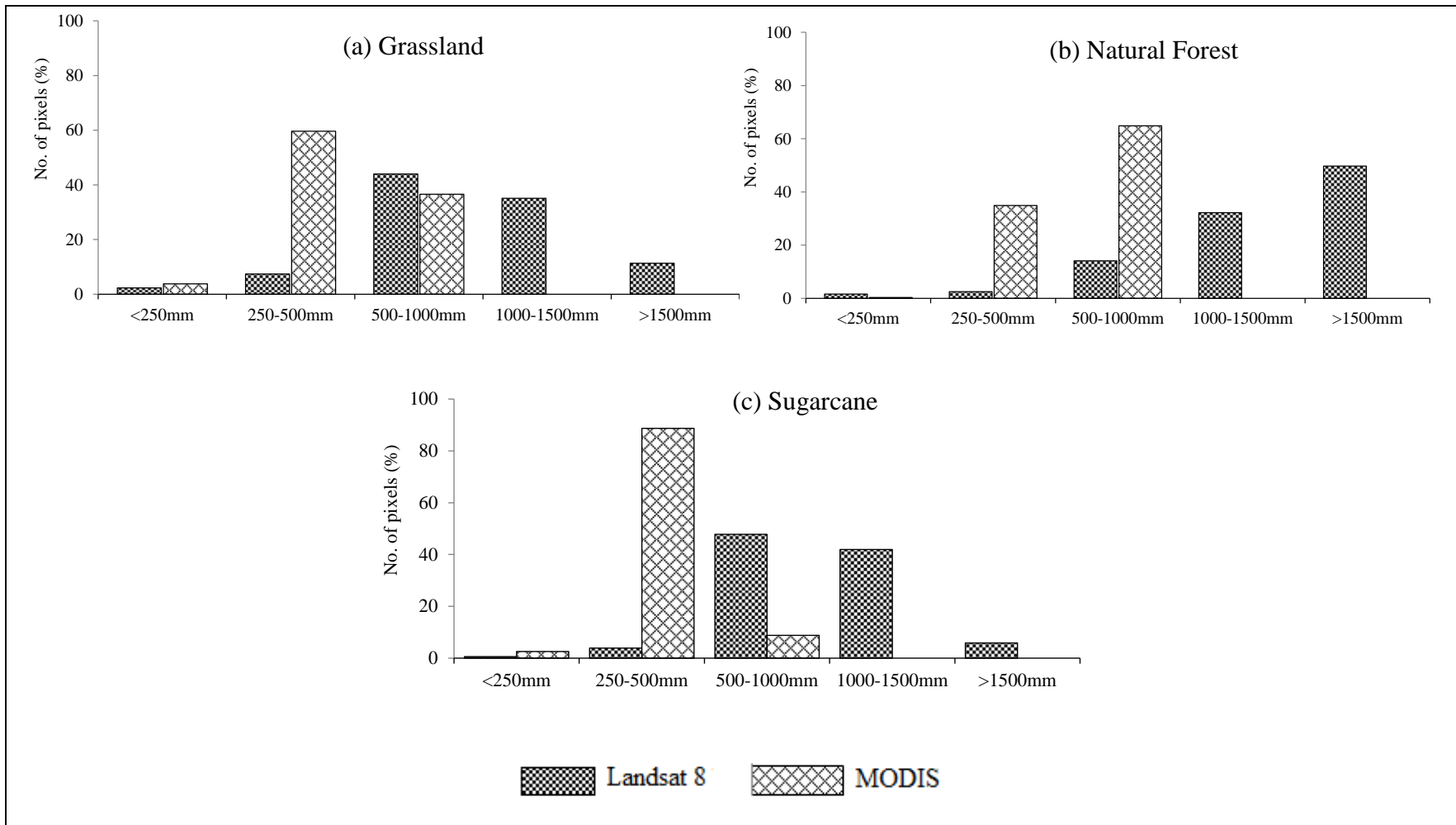


Figure 5.10 Mean annual total evaporation for selected land cover types from the two sensors

5.3.7 Validation results

A comparison of monthly mean total evaporation measured by eddy covariance against Landsat 8 and MODIS-based monthly mean estimates is shown in Figure 5.11 for the Two Streams validation site, dominated by wattle plantation. The data used for this analysis was monthly mean measurements and monthly mean remote sensing estimates corresponding to the station for six months, from May to October 2013. Overall, the Landsat-based estimates correlated well ($R^2 = 0.72$) with a RMSE of 32.34 mm per month (30.30% of the mean), with ground-based measurements. In contrast, MODIS performed poorly ($R^2 = 0.44$), with a RMSE of 93.63 mm per month (87.74% of the mean) in the variations of mean monthly total evaporation estimates.

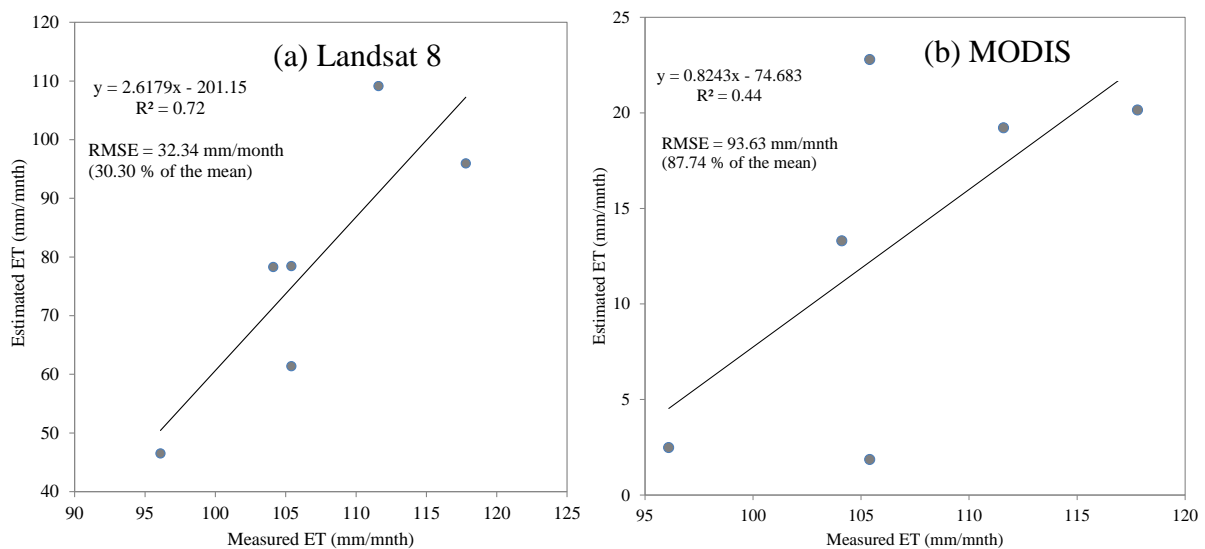


Figure 5.11 Validation of remotely-sensed mean monthly total evaporation with eddy covariance

5.4 Discussion

There have been various remote sensing studies aimed at estimating total evaporation at different spatial scales, using different sensors (Che-sheng *et al.*, 2011; Gómez *et al.*, 2005; Hafeez *et al.*, 2002; Jia *et al.*, 2003; Sobrino *et al.*, 2007; Verstraeten *et al.*, 2005). More recently, advances in remote sensing products, such as Landsat 8, have attracted even more attention in monitoring the earth surface characteristics. This is due to their better spatial resolution and refined spectral properties, which have the enhanced potential of

distinguishing the small variations in surface features (El-Askary *et al.*, 2014; Jia *et al.*, 2014b; Pahlevan and Schott, 2013). This study highlights the potential of using multispectral images (*i.e.* Landsat 8 and MODIS) in mapping the spatial variations of total evaporation, within a heterogeneous catchment, for more informed management of water resources, especially in water-scarce environments. Specifically, the study investigated how total evaporation varies within a heterogeneous catchment characterized by varying land cover types, with different spatial characteristics.

5.4.1 Seasonal and annual total evaporation estimates

Total evaporation for the uMngeni Catchment exhibits temporal and spatial variations, which reflect the combined effects of climatic conditions and land cover characteristics. It was observed that the western- and northern-most parts experienced high total evaporation estimates across the whole period, when compared to the eastern- and southern-most parts of the catchment. This may be due to variations in the climatic conditions, which vary seasonally across the Catchment. For instance, the uMngeni Catchment has a west-east and north-south gradient rainfall, thus more rainfall is received in the western and northern most parts of the Catchment. Moreover, high rainfall (above 1500 mm) is received in the western parts, whereas the drier eastern interiors receive an annual of 656 mm (Figure 5.1). Moreover, there are dams in the upper and middle parts of the catchment, which supplies water for irrigation (Warburton *et al.*, 2010); this contribute to total evaporation. The results also confirmed that seasonal variations result in variations of total evaporation, with high total evaporation estimates in the wet season and low estimates in the dry season. Higher rainfall in the wet season, results in more water being available for evaporation. In the dry season, low total evaporation estimates may be attributed to lower rainfall, so that croplands and areas with natural vegetation might have less soil moisture available to be evaporated, compared to the wet season.

5.4.2 Spatial variations of total evaporation across the catchment

Spatial variations in seasonal and annual total evaporation estimates highlighted the effect of land cover characteristics on variations of total evaporation. It was observed that for both sensors the lowest estimates were from built-up areas, with Landsat 8 showing higher

estimates than MODIS. The low estimates observed from built-up areas may be due to their hydrological and spatial characteristics across the Catchment. Built-up areas, with extensive impervious surfaces, generally generate more surface runoff, which drains quickly and, in the long run, less surface water remains for evaporation (Taha, 1997; Walsh *et al.*, 2012). The two sensors show different land cover type with the highest annual total evaporation estimates. For Landsat 8, the highest estimates were for commercial irrigation. High mean total evaporation estimates from commercial irrigation may be due to increased water availability for evaporation from the combined effects of rainfall and irrigation (Uddin *et al.*, 2013). Contrary to Landsat 8, MODIS produced the highest mean total evaporation estimates from natural forests. This can possibly be explained by their physiological and spatial characteristics (large patch size and number, areal coverage (see Table 5.1), among other factors within the Catchment. The physiological characteristics of forests allow them to evapotranspire, even in the dry season, due to their capability to access relatively deeper soil water by their roots (Rwasoka *et al.*, 2011). The contrast in highest mean total evaporation between Landsat 8 and MODIS may be attributed to the fact that commercial irrigation constitutes the smallest number of patches (44) and have the smallest mean patch size (0.12 km²) (Table 5.1), which might be difficult to detect with the 1000 m spatial resolution of MODIS.

When considering the effect of varying land cover characteristics, it was observed that the spatial characteristics of the land cover types affect the estimation of total evaporation across the catchment. This was confirmed by grassland, which occupies the highest land area (approx. 28.42%) within the Catchment, but did not result in highest estimates. Lower estimates from grasslands may be attributed to its spatial and physiological characteristics. Grasslands had the highest patch number and the highest total edge length, which all reflect more fragmentation (Table 5.1) and this may result in patches being incorporated within neighboring pixels of major land cover type, among other factors. This was confirmed by Ellis-Cockcroft and Cotter (2014), who reported that fragmentation or isolated patches for a particular land cover type reduce estimates of total evaporation loss within a landscape. In addition, the physiological characteristics of grass (small surface area) provide a limited area through which soil water is lost. Both sensors detect the lowest seasonal and annual total evaporation estimates from built up areas, which constitute the third largest area (approx. 11.4%) within the catchment. In addition, it was observed that the roughness length (Z_{0m})

derived from MODIS and Landsat show a similar spatial pattern, as compared to the land cover based. The use of roughness length shows a similar pattern with MODIS and Landsat 8, although it has resulted in lower estimates. The results in Figure 5.10 also show that MODIS has a low ability to capture the variations of total evaporation on a pixel basis for the different land cover types, as it only detects total evaporation between 250 and 1000 mm for the different land cover types. This may be attributed to the effect of its 1000 m resolution in relation to patch size of different land cover types, which the sensor failed to discriminate (Roerink *et al.*, 2000). The sensor reflects the predominant land cover type characteristics within the pixel, thereby missing its variation. Recent studies (Guerschman *et al.*, 2009; Ha *et al.*, 2011; He *et al.*, 2007) have also highlighted the inability of the MODIS sensor to differentiate the small variations in land cover characteristics, especially when applied on a small scale.

Although Landsat 8 has the potential to detect smaller spatial variations of total evaporation estimates at catchment scale, its temporal resolution and the possibility of cloud cover is of major concern. In contrast, although MODIS performs poorly in the spatial representation of total evaporation, its daily temporal resolution still remains attractive. It provides temporal estimates, for better time series analysis, which are required for well-informed water accounting and subsequent management and allocation.

5.5 Conclusion

The main essence of this study was to determine spatial variations of total evaporation from multispectral Landsat 8 and MODIS data and the effect of land cover characteristics (*i.e.* area, patchiness) for the uMngeni Catchment, using the SEBS model. The results show that:

- a) Landsat 8 with a 30 m spatial resolution is a promising dataset for the better spatial representation of total evaporation at catchment scale, when compared to MODIS with 1000 m resolution;
- b) The spatial characteristics of each land cover type in relation to the sensor spatial resolution affect spatial variations of total evaporation across the catchment;
- c) MODIS at 1000 m resolution has a low detection ability of total evaporation estimates within a particular land cover type for the entire period, when compared to Landsat 8

at 30 m spatial resolution, which managed to detect all the variations of total evaporation ranges; and

- d) Temporal and spatial variations in climatic conditions, among other factors, have a considerable effect on total evaporation estimation at a catchment scale.

On the basis of this research it can be concluded that the Landsat 8 dataset could be useful for a better spatial representation of total evaporation in accounting for water loss at a catchment scale. However, despite useful results on the spatial variations of total evaporation from Landsat 8, its 16-day temporal resolution is a cause for concern besides limited validation data for the catchment. For the better long-term and sustainable management of water resources, daily total evaporation estimates at finer resolution are required. Although the MODIS datasets are less suitable for determining the spatial variations of total evaporation within a heterogeneous catchment, its daily temporal resolution still remains attractive in the monitoring of total evaporation for water accounting and planning. There is the need for further research to investigate the possible integration of Landsat 8 and MODIS datasets to estimate total evaporation for more comprehensive and well-informed water accounting at a catchment scale.

5.6 References

- Allen, R, Bastiaanssen, W. 2002. SEBAL Expert Training. . The University of Idaho and Idaho State University, Pocatello, USA.
- Allen, R, Tasumi, M, Trezza, R. 2007. Satellite-Based Energy Balance for Mapping Evapotranspiration with Internalized Calibration (METRIC)-Model. *Journal of Irrigation and Drainage Engineering* 133(4): 380-394.
- Allen, RG, Pereira, LS, Raes, D, Smith, M. 1998. *Crop evapotranspiration - Guidelines for computing crop water requirements- FAO Irrigation and Drainage Paper 56*. Food and Agriculture Organization of the United Nations, Rome, Italy, pp. 15-64.
- Bastiaanssen, WGM, Menentia, M, Feddesb, RA, Holtslagc, AAM. 1998. A remote sensing surface energy balance algorithm for land (SEBAL) 1. Formulation. *Journal of Hydrology* 212: 198–212.
- Che-sheng, Z, Jie, Z, Hui-xiao, W, Jian, Y. 2011. Quantitative estimation of land surface evapotranspiration in Taiwan based on MODIS data. *Water Science and Engineering* 4(3): 237-245.
- Chen, J-H, Kan, C-E, Tan, C-H, Shih, S-F. 2002. Use of spectral information for wetland evapotranspiration assessment. *Agricultural Water Management* 55(3): 239-248.
- Clulow, A, Everson, C, Gush, M. 2011. *The long-term impact of Acacia mearnsii trees on evaporation, streamflow and ground water resources*. Report No. TT505/11 Water Research Commission, Pretoria, South Africa.
- Dore, MH. 2005. Climate change and changes in global precipitation patterns: what do we know? *Environment international* 31(8): 1167-1181.

- Dube, T, Mutanga, O, Elhadi, A, Ismail, R. 2014. Intra-and-Inter Species Biomass Prediction in a Plantation Forest: Testing the Utility of High Spatial Resolution Spaceborne Multispectral RapidEye Sensor and Advanced Machine Learning Algorithms. *Sensors* 14(8): 15348-15370.
- El-Askary, H, Abd El-Mawlad, SH, Li, J, El-Hattab, MM, El-Raey, M. 2014. Change detection of coral reef habitat using Landsat-5 TM, Landsat 7 ETM+ and Landsat 8 OLI data in the Red Sea (Hurghada, Egypt). *International Journal of Remote Sensing* 35(6): 2327-2346.
- Elhag, M, Psilovikos, A, Manakos, I, Perakis, K. 2011. Application of the Sebs Water Balance Model in Estimating Daily Evapotranspiration and Evaporative Fraction from Remote Sensing Data Over the Nile Delta. *Water Resources Management* 25: 2731–2742.
- Ellis-Cockcroft, I, Cotter, J. 2014. *Tropical Forest Fragmentation; Implications for Ecosystem Function*. School of Biosciences, Innovation Centre Phase 2, University of Exeter, UK.
- Fiener, P, Auerswald, K, Van Oost, K. 2011. Spatio-temporal patterns in land use and management affecting surface runoff response of agricultural catchments—A review. *Earth-Science Reviews* 106(1): 92-104.
- Gómez, M, Oliso, A, Sobrino, JA, Jacob, F. 2005. Retrieval of evapotranspiration over the Alpillles/ReSeDA experimental site using airborne POLDER sensor and a thermal camera. *Remote Sensing of Environment* 96(3–4): 399-408.
- Goodrich, D, Scott, R, Qi, J, Goff, B, Unkrich, C, Moran, M, Williams, D, Schaeffer, S, Snyder, K, MacNish, R. 2000. Seasonal estimates of riparian evapotranspiration using remote and in situ measurements. *Agricultural and Forest Meteorology* 105(1): 281-309.
- Gowda, PH, Howell, TA, Paul, G, Colaizzi, PD, Marek, TH, Su, B, Copeland, KS. 2013. Deriving Hourly Evapotranspiration Rates with SEBS: A Lysimetric Evaluation. *Vadose Zone Journal* 12(3): 1-40.
- Guerschman, JP, Van Dijk, AI, Mattersdorf, G, Beringer, J, Hutley, LB, Leuning, R, Pipunic, RC, Sherman, BS. 2009. Scaling of potential evapotranspiration with MODIS data reproduces flux observations and catchment water balance observations across Australia. *Journal of Hydrology* 369(1): 107-119.
- Gustafson, EJ. 1998. Quantifying landscape spatial pattern: what is the state of the art? *Ecosystems* 1(2): 143-156.
- Ha, W, Gowda, PH, Howell, TA. 2011. A review of downscaling methods for remote sensing-based irrigation management: part I. *Irrigation Science*: 1-20.
- Hafeez, M, Chemin, Y, Van De Giesen, N, Bouman, B. 2002. Field Evapotranspiration Estimation in Central Luzon, Philippines using different sensors: Landsat 7 ETM+, Terra Modis and Aster. *ISPRS/CIG conference July*.
- He, YB, Z, S, L, J, Wang, SL. 2007. Regional evapotranspiration of different land covers based on remote sensing. *Journal of Applied Ecology* 18(2): 288-296.
- Herold, M, Liu, X, Clarke, KC. 2003. Spatial metrics and image texture for mapping urban land use. *Photogrammetric Engineering & Remote Sensing* 69(9): 991-1001.
- Jia, K, Wei, X, Gu, X, Yao, Y, Xie, X, Li, B. 2014a. Land cover classification using Landsat 8 Operational Land Imager data in Beijing, China. *Geocarto International (ahead-of-print)*: 1-11.
- Jia, L, Su, Z, van den Hurk, B, Menenti, M, Moene, A, De Bruin, HAR, Yrisarry, JJB, Ibanez, M, Cuesta, A. 2003. Estimation of sensible heat flux using the Surface Energy

- Balance System (SEBS) and ATSR measurements. *Physics and Chemistry of the Earth* 28(1–3): 75-88.
- Jia, L, Xi, G, Liu, S, Huang, C, Yan, Y, Liu, G. 2009. Regional estimation of daily to annual regional evapotranspiration with MODIS data in the Yellow River Delta wetland. *Hydrology and Earth System Sciences* 13(10): 1775-1787.
- Kowe, P, Pedzisai, E, Gumindoga, W, Rwasoka, D. 2014. An analysis of changes in the urban landscape composition and configuration in the Sancaktepe District of Istanbul Metropolitan City, Turkey using landscape metrics and satellite data *Geocarto International*(just-accepted): 1-30.
- Liou, Y-A, Kar, SK. 2014. Evapotranspiration Estimation with Remote Sensing and Various Surface Energy Balance Algorithms—A Review. *Energies* 7(5): 2821-2849.
- Liu, J, Chen, J, Cihlar, J. 2003. Mapping evapotranspiration based on remote sensing: An application to Canada's landmass. *Water Resources Research* 39(7): 56-78.
- Ma, W, Hafeez, M, Rabbani, U, Ishikawa, H, Ma, Y. 2012. Retrieved actual ET using SEBS model from Landsat-5 TM data for irrigation area of Australia. *Atmospheric Environment* 59: 4080-4414.
- Ma, W, Ma, Y, Su, B. 2011. Feasibility of retrieving land surface heat fluxes from ASTER data using SEBS: a case study from the Namco area of the Tibetan plateau. *Arctic, Antarctic, and Alpine Research* 43(2): 239-245.
- Makkink, G. 1957. Testing the Penman formula by means of lysimeters. *Journal of the Institution of Water Engineers* 11(3): 277-288.
- McCabe, MF, Wood, EF. 2006. Scale influences on the remote estimation of evapotranspiration using multiple satellite sensors. *Remote Sensing of Environment* 105(4): 271-285.
- McCarthy, JJ. 2001. *Climate change 2001: impacts, adaptation, and vulnerability: contribution of Working Group II to the third assessment report of the Intergovernmental Panel on Climate Change*. Cambridge University Press.
- McGarigal, K, Marks, BJ. 1995. Spatial pattern analysis program for quantifying landscape structure. *Gen. Tech. Rep. PNW-GTR-351. US Department of Agriculture, Forest Service, Pacific Northwest Research Station*.
- Menenti, M, Jia, L, Su, H. 2003. On SEBI-SEBS validation in France, Italy, Spain, USA and China. *Proceedings of the workshop on use of remote sensing of crop evapotranspiration for large regions. International Commission on Irrigation and Drainage (ICID)*. Montpellier, France.
- Mengistu, M, Savage, M. 2010. Surface renewal method for estimating sensible heat flux. *Water SA* 36(1): 9-18.
- Mengistu, MG, Everson, CS, Moyo, NC, Savage, MJ. 2014. *The Validation of the Variables (Evaporation and Soil Moisture) in Hydrometeorological Models*. 2066/1/13 Pretoria, South Africa.
- Morton, FI. 1983. Operational estimates of areal evapotranspiration and their significance to the science and practice of hydrology. *Journal of Hydrology* 66(1–4): 1-76.
- Mutiga, JK, Su, Z, Woldai, T. 2010. Using satellite remote sensing to assess evapotranspiration: Case study of the upper Ewaso Ng'iro North Basin, Kenya. *International Journal of Applied Earth Observation and Geoinformation* 12, Supplement 1(0): S100-S108.
- New, M. 2002. Climate change and water resources in the southwestern Cape, South Africa. *South African Journal of Science* 98(7 & 8): p. 369-376.

- Nouri, H, Beecham, S, Anderson, S, Hassanli, AM, Kazemi, F. 2014. Remote sensing techniques for predicting evapotranspiration from mixed vegetated surfaces. *Urban Water Journal*(ahead-of-print): 1-14.
- Pahlevan, N, Schott, J. 2013. Leveraging EO-1 to Evaluate Capability of New Generation of Landsat Sensors for Coastal/Inland Water Studies. *IEEE Journal of selected topics in applied earth observation and remote sensing* 6(2): 360-374.
- Penman, HL. 1948. Natural Evaporation from Open Water, Bare Soil and Grass. *Proceedings of the Royal Society of London. Series A. Mathematical and Physical Sciences* 193(1032): 120-145.
- Priestley, CHB, Taylor, RJ. 1972. On the Assessment of Surface Heat Flux and Evaporation Using Large-Scale Parameters. *Monthly Weather Review* 100(2): 81-92.
- Ray, S, Dadhwal, V. 2001. Estimation of crop evapotranspiration of irrigation command area using remote sensing and GIS. *Agricultural Water Management* 49(3): 239-249.
- Roerink, GR, Su, Z, Menenti, M. 2000. S-SEBI: A Simple Remote Sensing Algorithm to Estimate the Surface Energy Balance. *Physics and Chemistry of the Earth* 25(2): 147-157.
- Rwasoka, DT, Gumindoga, W, Gwenzi, J. 2011. Estimation of actual evapotranspiration using the Surface Energy Balance System (SEBS) algorithm in the Upper Manyame catchment in Zimbabwe. *Physics and Chemistry of the Earth* 36(14–15): 736-746.
- Schulze, R. 1997. Impacts of global climate change in a hydrologically vulnerable region: challenges to South African hydrologists. *Progress in Physical Geography* 21(1): 113-136.
- Schulze, R, Perks, L. 2000. Assessment of the impact of climate change on hydrology and water resources in South Africa. *ACRUcons report* 33.
- Schulze, R, Maharaj, M, Warburton, M, Gers, C, Horan, , MJC, K, RP, , Clark, D. 2008. *South African Atlas of Climatology and Agrohydrology*. WRC Report 1489/1/06, DVD-ROM, Pretoria, South Africa.
- Scott, RL. 2010. Using watershed water balance to evaluate the accuracy of eddy covariance evaporation measurements for three semiarid ecosystems. *Agricultural and Forest Meteorology* 150: 219–225.
- Senay, GB, Budde, M, Verdin, JP, Melesse, AM. 2007. A coupled remote sensing and simplified surface energy balance approach to estimate actual evapotranspiration from irrigated fields. *Sensors* 7(6): 979-1000.
- Seto, KC, Fragkias, M. 2005. Quantifying spatiotemporal patterns of urban land-use change in four cities of China with time series landscape metrics. *Landscape ecology* 20(7): 871-888.
- Shoko, C, Clark, D, Bulcock, H, Mengistu, M. 2014. The use of remote sensing for estimating variations in total evaporation in the uMgeni Catchment. *The 17th SANCIAHS National Hydrology Symposium* Cape Town, South Africa.
- Singh, RK, Senay, GB, Velpuri, NM, Bohms, S, Scott, RL, Verdin, JP. 2014. Actual Evapotranspiration (Water Use) Assessment of the Colorado River Basin at the Landsat Resolution Using the Operational Simplified Surface Energy Balance Model. *Remote Sensing* 6(1): 233-256.
- Sobrino, JA, Gómez, M, Jiménez-Muñoz, JC, Olioso, A. 2007. Application of a simple algorithm to estimate daily evapotranspiration from NOAA–AVHRR images for the Iberian Peninsula. *Remote Sensing of Environment* 110: 139–148.
- Spano, D, Snyder, RL, Ducec, P, U.K.T., P. 2000. Estimating sensible and latent heat flux densities from grapevine canopies using surface renewal. *Agricultural and Forest Meteorology* 104: 171–183.

- Su, H, Wood, EF, McCabe, M, F., Su, Z. 2007. Evaluation of remotely sensed Evapotranspiration over the CEOP EOP-1 Reference Sites. *Journal of the Meteorological Society of Japan* 85A: 439-459.
- Su Z 2006. 'An introduction to the surface energy balance system (SEBS)', Lecture notes, ESA TIGER Capacity Building Facility 1st Training Course on "Advanced optical remote sensing", Cape Town, 22-25 November 2006.
- Su, Z. 2002. The Surface Energy Balance System (SEBS) for estimation of turbulent heat fluxes. *Hydrology and Earth System Sciences* 6(1): 85-99.
- Summerton, M, Schulze, RE, Graham, PL. 2010. Impacts of a changing climate on hydrology and water supply in the Mgeni catchment, South Africa. *Third International Symposium, Managing Consequences of a Changing Global Environment*. Newcastle.
- Taha, H. 1997. Urban climates and heat islands: albedo, evapotranspiration, and anthropogenic heat. *Energy and buildings* 25(2): 99-103.
- Tasumi, M, Trezza, R, Allen, RG, Wright, JL. 2005. Operational aspects of satellite-based energy balance models for irrigated crops in the semi-arid US. *Irrigation and Drainage Systems* 19(3-4): 355-376.
- Thornthwaite, CW. 1948. An Approach toward a Rational Classification of Climate. *Geographical Review* 38(1): 55-94.
- Turner, MG. 1989. Landscape ecology: the effect of pattern on process. *Annual review of ecology and systematics*: 171-197.
- Turner, MG. 2001. *Landscape ecology in theory and practice: pattern and process*. Springer.
- Uddin, J, Hancock, N, Smith, R, Foley, J. 2013. Measurement of evapotranspiration during sprinkler irrigation using a precision energy budget (Bowen ratio, eddy covariance) methodology. *Agricultural Water Management* 116: 89-100.
- van der Kwast, J, Timmermans, W, Gieske, A, Su, Z, Oliso, A, Jia, L, Elbers, J, D. Karssenber, D, S. de Jong, S. 2009. Evaluation of the Surface Energy Balance System (SEBS) applied to ASTER imagery with flux-measurements at the SPARC 2004 site (Barrax, Spain). *Hydrology and Earth System Sciences* 13: 1337-1347.
- Verstraeten, WW, Veroustraete, F, Feyen, J. 2005. Estimating evapotranspiration of European forests from NOAA-imagery at satellite overpass time: Towards an operational processing chain for integrated optical and thermal sensor data products. *Remote Sensing of Environment* 96(2): 256-276.
- Walsh, C, Fletcher, T, Burns, M. 2012. Urban stormwater runoff: a new class of environmental flow problem. *PloS one* 7(9): 458-479.
- Wang, S, Yang, Y, Luo, Y, Rivera, A. 2013. Spatial and seasonal variations in evapotranspiration over Canada's landmass. *Hydrology and Earth System Sciences Discussions* 10(5): 6107-6151.
- Warburton, ML, Schulze, RE, Jewitt, GPW. 2010. Confirmation of ACRU model results for applications in land use and climate change studies. *Hydrology and Earth System Sciences* 14(12): 2399-2414.
- Wildlife, KE. 2011. *KwaZulu-Natal Land Cover*. . Biodiversity Conservation Planning Division, Ezemvelo KZN Wildlife, Pietermaritzburg.
- Wilson, JS, Clay, M, Martin, E, Stuckey, D, Vedder-Risch, K. 2003. Evaluating environmental influences of zoning in urban ecosystems with remote sensing. *Remote Sensing of Environment* 86(3): 303-321.
- Xu, C-y, Gong, L, Jiang, T, Chen, D, Singh, V. 2006. Analysis of spatial distribution and temporal trend of reference evapotranspiration and pan evaporation in Changjiang (Yangtze River) catchment. *Journal of Hydrology* 327(1): 81-93.

6. SYNTHESIS AND RECOMMENDATION

6.1 Introduction

Accurate information on the spatial variation of total evaporation across a heterogeneous catchment is critical for a wide range of applications, including irrigation management (Timmermans *et al.*, 2013), drought monitoring (Rana and Katerji, 2000), climate change modelling (McVicar *et al.*, 2012), hydrological modelling (Weiß and Menzel, 2008) and landuse/change management (Zhang *et al.*, 2001). Ground-based methods of estimating total evaporation, although they have been widely-used, cannot estimate the spatial variations that occur at a catchment scale. The advancement of remote sensing offers an alternative method, which enables a better spatial representation of total evaporation from local to global scales. The aim of this research was to estimate the variations of total evaporation across a heterogeneous uMngeni Catchment, using remote sensing. The specific objectives were: (a) to determine the effect of sensor spatial resolutions on estimating total evaporation across the uMngeni Catchment, and (b) to determine spatial variations of total evaporation estimates, using multispectral remote sensing data within the heterogeneous uMngeni Catchment. Total evaporation estimates for the catchment were derived, using the SEBS model, based on multispectral Landsat 8 (30 m) and MODIS (1000 m) model input datasets.

6.2 The Effect of Sensor Spatial Resolution on Estimating Total Evaporation

In order to accurately estimate total evaporation in uMngeni Catchment, it was necessary to first assess the effect of varying sensor spatial resolution (*i.e.* pixel size). This research evaluated two readily available multispectral sensors namely; the 30 m spatial resolution Landsat 8 sensor and the 1000 m spatial resolution MODIS sensor in estimating spatial variations in total evaporation across a heterogeneous catchment using the SEBS model.

The results of this study have shown that sensor spatial resolution plays a critical role in the accurate estimation of total evaporation across a heterogeneous catchment. For example, it was observed that remote sensing datasets with a smaller pixel, such as Landsat (30 m) is

capable of mapping the small spatial variations in total evaporation input parameters and subsequent estimates that occurred between landcover types. However, remote sensing datasets with a large pixel size, such as MODIS (1000 m), have problems in mapping spatial variations in total evaporation across varying land cover types at catchment scale. For instance, MODIS input parameters, such as LST, NDVI show less variability, compared to Landsat 8. This was further confirmed by the spatial variations of total evaporation, where MODIS estimates showed less variability, compared to Landsat 8. This suggests that large spatial resolution datasets are too coarse to distinguish variations in biophysical parameters and energy fluxes across different landcover types. The sensor detects such variations within a single pixel as an aggregation, without distinguishing mixed coverage from different landcover types. This further resulted in aggregation of energy fluxes with less variability. This is supported by Kustas and Norman (2000) who found that coarse spatial resolution sensors invariably result in pixel-averaged heat flux estimation for surfaces with significant variability in vegetation cover. They concluded that aggregation of sub-pixel variability can cause a significant error of the energy fluxes.

Overall, the findings of this study provides the necessary insight and basis for future total evaporation estimation at catchment scale using remote sensing, particularly the ability of fine resolution sensors in discriminating biophysical parameters and energy fluxes. This provides a better representation of water loss from different landcover types, which is crucial for water management purposes, especially in water-scarce environments.

6.3 Estimating the Spatial Variations in Total Evaporation across a Heterogeneous Catchment using Multispectral Remote Sensing Data

Although great improvements have been made in estimating spatial variations of total evaporation, most research focuses on estimating total evaporation on specific land cover types using either remote sensing or meteorological-based methods. However, the results of this study showed that for accurate and reliable total evaporation estimation, incorporating different land cover characteristics (*i.e.* type, areal extent, patchiness *etc.*) is necessary if better water allocation, management and proper planning are to be achieved.

The findings from this study have also shown the potential of using the Landsat 8 sensor to determine spatial variations in total evaporation at a catchment scale. The sensor managed to capture variations in total evaporation at a wider range from different land cover types for the entire period. In contrast, the MODIS sensor, at 1000 m resolution, failed to detect variations in total evaporation ranges from some of the pixels within a particular land cover type across the catchment. This confirms the inability of coarse resolution satellite sensors, with their large pixel size to detect variations in land cover types which affects estimates of total evaporation. This is in agreement with Allen *et al.* (2008), who used MODIS and Landsat 7 images to estimate total evaporation using the METRIC model. They stated that the spatial fidelity of the landscape was highly degraded, when using the MODIS sensor. This resulted in low total evaporation estimates. They concluded that Landsat-based estimates are highly preferred, when compared to those of MODIS, because of their better resolution (30 m).

Results from this study have further highlighted the importance of inputs and energy fluxes in remote sensing estimates of total evaporation. For instance, the spatial variations of Rn play a critical role in determining the spatial and temporal variations of total evaporation. This is in agreement with the study by Sobrino *et al.* (2007), which showed that the spatial variations of total evaporation estimates followed that of Rn . They found that lower estimates of Rn and total evaporation occur in the dry season, whereas high estimates occurred during the wet season. This is primarily as a result of variations in climatic conditions, among other factors. For instance, in the wet season, an increase in solar radiation and rainfall results in more water and energy available for total evaporation to occur. Furthermore, total evaporation estimates were influenced by surface characteristics, where higher estimates were obtained from vegetated areas (as indicated by high NDVI, FVC and LAI parameters), as compared to less vegetated areas. The effect of seasonal variations in climatic variables on total evaporation was also indicated. Similar seasonal variations of total evaporation estimates were observed by Boronina and Ramillien (2008) in Chad. In addition, variations in total evaporation are determined by various bio-physical variables, rather than individual variables, such as LST (Glenn *et al.*, 2007; Glenn *et al.*, 2010; Jin *et al.*, 2013).

With regard to land cover heterogeneity, it is critical to determine variations in land cover types, including area and patchiness, especially in relation to the scale of remote sensing products. This might have an influence on the effectiveness of the satellite sensor to

discriminate land cover specific characteristics. This might also influence the ability of the sensor to derive total evaporation inputs and subsequent estimates. For instance, if the areas of land cover patches are smaller than the pixel resolution of the sensor, it is most likely that most of the patches are aggregated by the sensor. The sensor fails to differentiate the existence of mixed patches within a particular pixel, as well as variations in total evaporation inputs. This might lead to lower and less variability of input parameters resulting in the underestimation of total evaporation across heterogeneous catchments.

Based on the findings from this study, it was confirmed that the 30 m Landsat 8 dataset has greater potential than the 1000 m MODIS in estimating spatial variations in total evaporation. Quantification of total evaporation is required at finer spatial and temporal resolution, for well-informed water accounting and subsequent management and allocation to different consumers. Although Landsat 8 produced better spatial variations in total evaporation, its 16-day temporal resolution and the possibility of cloudy cover is a major problem. In contrast, despite poor spatial representation of total evaporation from MODIS, its daily temporal resolution still plays a fundamental role in the long-term analysis of total evaporation. It is however important to note that the availability of validation data for the catchment was a major challenge and concern of the study.

Overall, this study confirms the feasibility of using multispectral remote sensing data to understand the spatial variations of total evaporation within a catchment, characterized by various land cover characteristics, for water accounting purposes. This approach enables the estimation of water use by different land cover types in a spatially distributed manner at a catchment scale. Furthermore, information on water use by different landcover types could serve to assess the effects of land use changes on hydrological processes. Remote sensing will continue to play a fundamental role in quantifying the surface energy budget and providing information, at a low cost, for improving water consumption estimates, especially in water scarce environments.

6.4 Recommendations for Future Studies

In general, the findings from this study contribute to and support the ongoing research into understanding spatial variations of total evaporation for water resources management across the globe. Consequently, these findings may possibly lay a foundation for the better management and allocation of water resources, especially in water-limited areas.

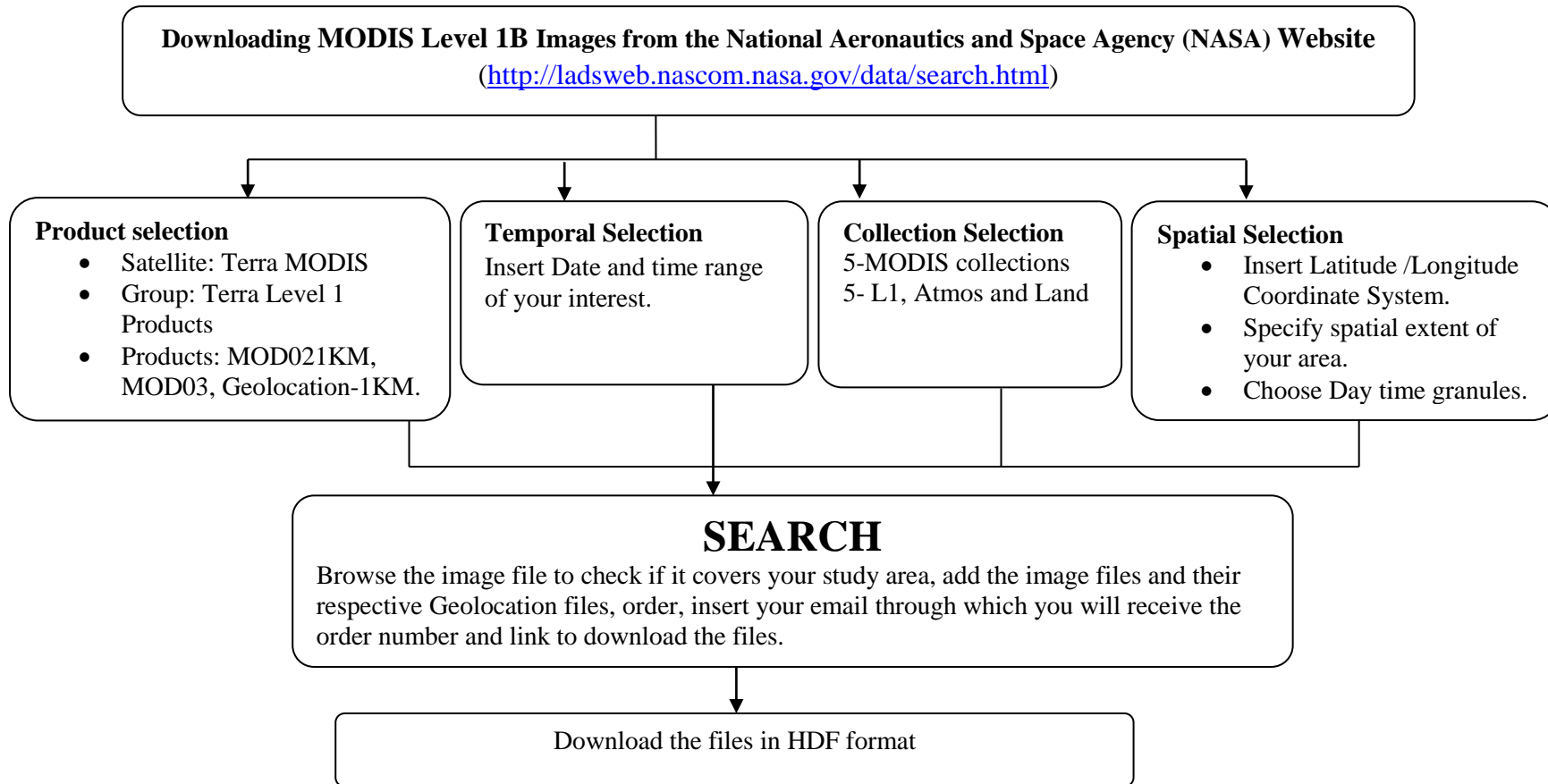
Although this study has highlighted the importance of sensor spatial resolution and land cover characteristics in understanding the spatial variations of total evaporation within a heterogeneous catchment in South Africa, further investigations are required. The following recommendations are therefore suggested for future studies:

- a) To fully understand the potential of using multispectral Landsat 8 datasets in spatial representation of total evaporation estimates, further studies should be undertaken over various bio-climatic regions.
- b) Future research should also consider integrating Landsat 8, which has low temporal and moderately high spatial resolution, with high temporal and low spatial resolution images, such as MODIS, to increase the utility of satellite products in water resources management.
- c) Successful water resources management requires the application of high spatial resolution remotely sensed data. Therefore, there is a need for future researchers to develop approaches for downscaling of daily low spatial resolution MODIS datasets.
- d) The present study used two multispectral sensors namely; the 30 m spatial resolution Landsat 8 and the 1000 m MODIS data. It would be interesting for future research to compare Landsat 8-based estimates with those obtained using Landsat 7 ETM.
- e) In-situ measurements of total evaporation for the different land cover types in a catchment are very important for validating the remote sensing estimates. Therefore future studies should also focus on ground based techniques with better spatial resolution, such as scintillometry.
- f) Further validation of total evaporation estimates from Landsat 8 and MODIS within uMngeni catchment may be possible indirectly through the use of stream flow data together with simplified water balance calculations.

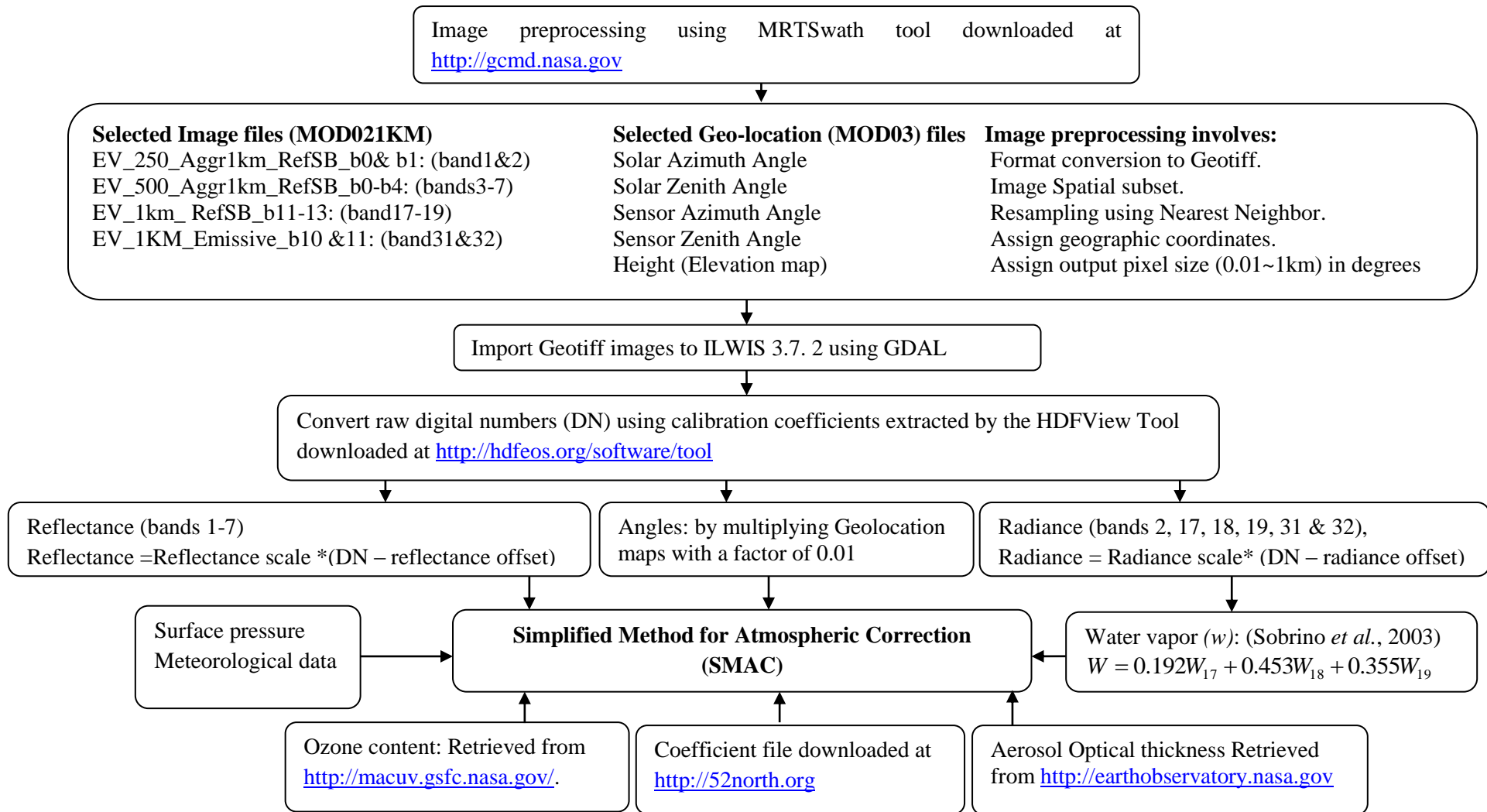
6.5 References

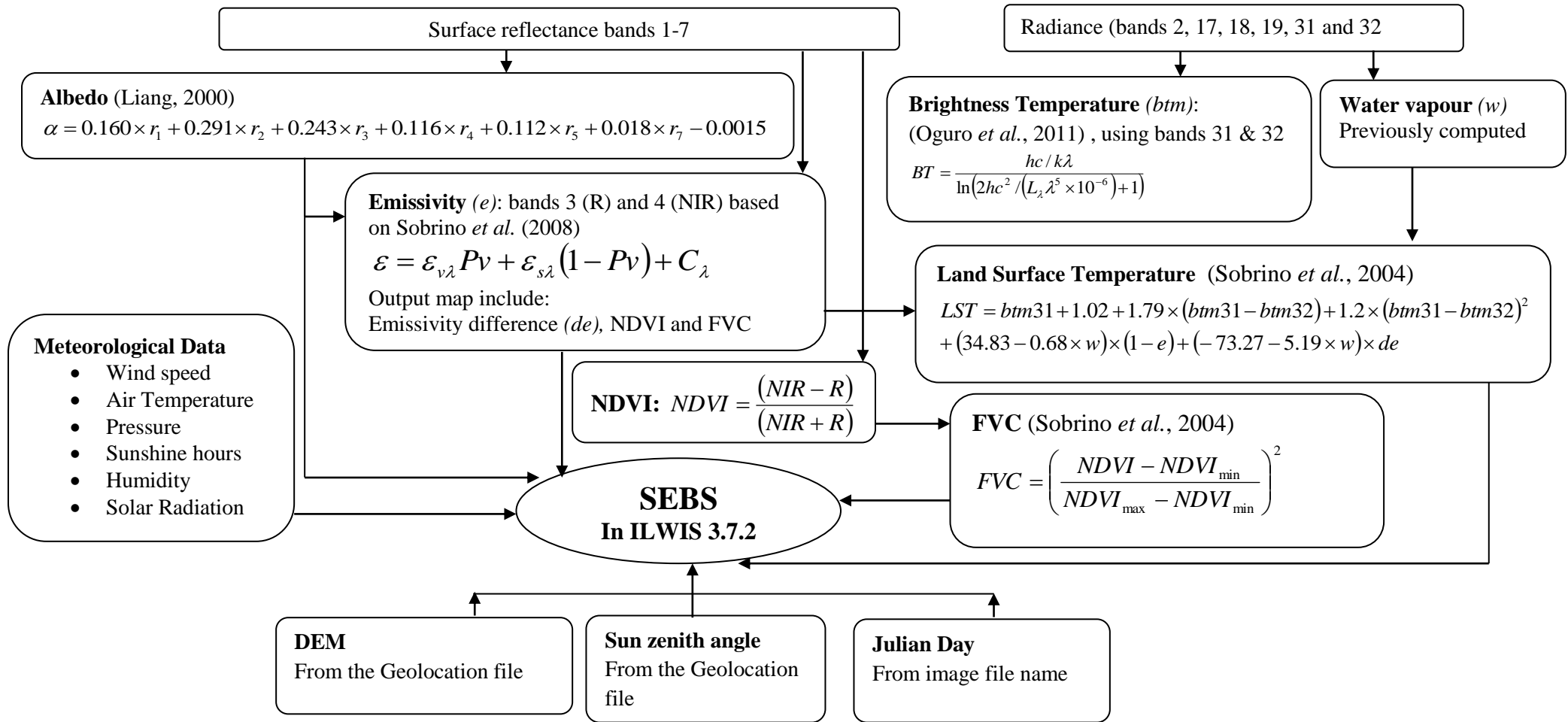
- Allen, RG, Robison, CW, Trezza, R, Garcia, M and Kjaersgaard, J. 2008. Comparison of Evapotranspiration Images from MODIS and Landsat along the Middle Rio Grande of New Mexico.in: *The 17th William T. Pecora Memorial Remote Sensing Symposium Proceedings*, Denver, Colorado.
- Glenn, EP, Huete, AR, Nagler, PL, Hirschboeck, KK, Brown, P. 2007. Integrating Remote Sensing and Ground Methods to Estimate Evapotranspiration. *Critical Reviews in Plant Sciences* 26: 139–168.
- Glenn, EP, Nagler, PL, Huete, AR. 2010. Vegetation index methods for estimating evapotranspiration by remote sensing. *Surveys in geophysics* 31(6): 531-555.
- Irmak, A, Ratcliffe, I, Ranade, P, Hubbard, K and Singh, KR. 2011. Estimation of Land Surface Evapotranspiration with a Satellite Remote Sensing Procedure. *Great Plains Research* 21: 73-88.
- Jiang, L and Islam, S. 1999. A methodology for estimation of surface evapotranspiration over large areas using remote sensing observations. *Geophysical Research Letters* 26(17): 2773-2776.
- Jin, X, Guo, R, Xia, W. 2013. Distribution of Actual Evapotranspiration over Qaidam Basin, an Arid Area in China. *Remote Sensing* 5: 6976-6996
- McVicar, TR, Roderick, ML, Donohue, RJ, Li, LT, Van Niel, TG, Thomas, A, Grieser, J, Jhajharia, D, Himri, Y, Mahowald, NM, Mescherskaya, AV, Kruger, AC, Rehman, S and Dinpashoh, Y. 2012. Global review and synthesis of trends in observed terrestrial near-surface wind speeds: Implications for evaporation. *Journal of Hydrology* 416–417(0): 182-205.
- Rana, G and Katerji, N. 2000. Measurement and estimation of actual evapotranspiration in the field under Mediterranean climate: a review. *European Journal of Agronomy* 13(2–3): 125-153.
- Ruhoff, AL, Paz, AR, Collischonn, W, Aragao, LEOC, Rocha, HR and Malhi, YS. 2012. A MODIS-based energy balance to estimate evapotranspiration for clear-sky days in Brazilian Tropical Savannas. *Remote Sensing* 4: 703-725.
- Sobrino, JA, Gómez, M, Jiménez-Muñoz, JC, Olioso, A. 2007. Application of a simple algorithm to estimate daily evapotranspiration from NOAA–AVHRR images for the Iberian Peninsula. *Remote Sensing of Environment* 110: 139–148.
- Su, H, Wood, EF, McCabe, M, F, and Su, Z. 2007. Evaluation of remotely sensed Evapotranspiration over the CEOP EOP-1 Reference Sites. *Journal of the Meteorological Society of Japan* 85A: 439-459.
- Su Z 2006. ‘An introduction to the surface energy balance system (SEBS)’, Lecture notes, ESA TIGER Capacity Building Facility 1st Training Course on “Advanced optical remote sensing”, Cape Town, 22-25 November 2006.
- Teluguntla, P, Ryu, D, George, B and Walker, JP. 2011 Impact of Spatial Scale on Remotely Sensed Evapotranspiration Estimates from Heterogeneous Land Surfaces.in: *19th International Congress on Modelling and Simulation* Perth, Australia.
- Timmermans, J, Su, Z, van der Tol, C, Verhoef, A and Verhoef, W. 2013. Quantifying the uncertainty in estimates of surface–atmosphere fluxes through joint evaluation of the SEBS and SCOPE models. *Hydrol. Earth Syst. Sci.* 17(4): 1561-1573.
- Vinukollu, RK, Wood, EF, Ferguson, RC and Fisher, JB. 2011. Global estimates of evapotranspiration for climate studies using multi-sensor remote sensing data: Evaluation of three process-based approaches. *Remote Sensing of Environment* 115: 801–823.

APPENDIX A Total evaporation estimation flowcharts using MODIS L1B images

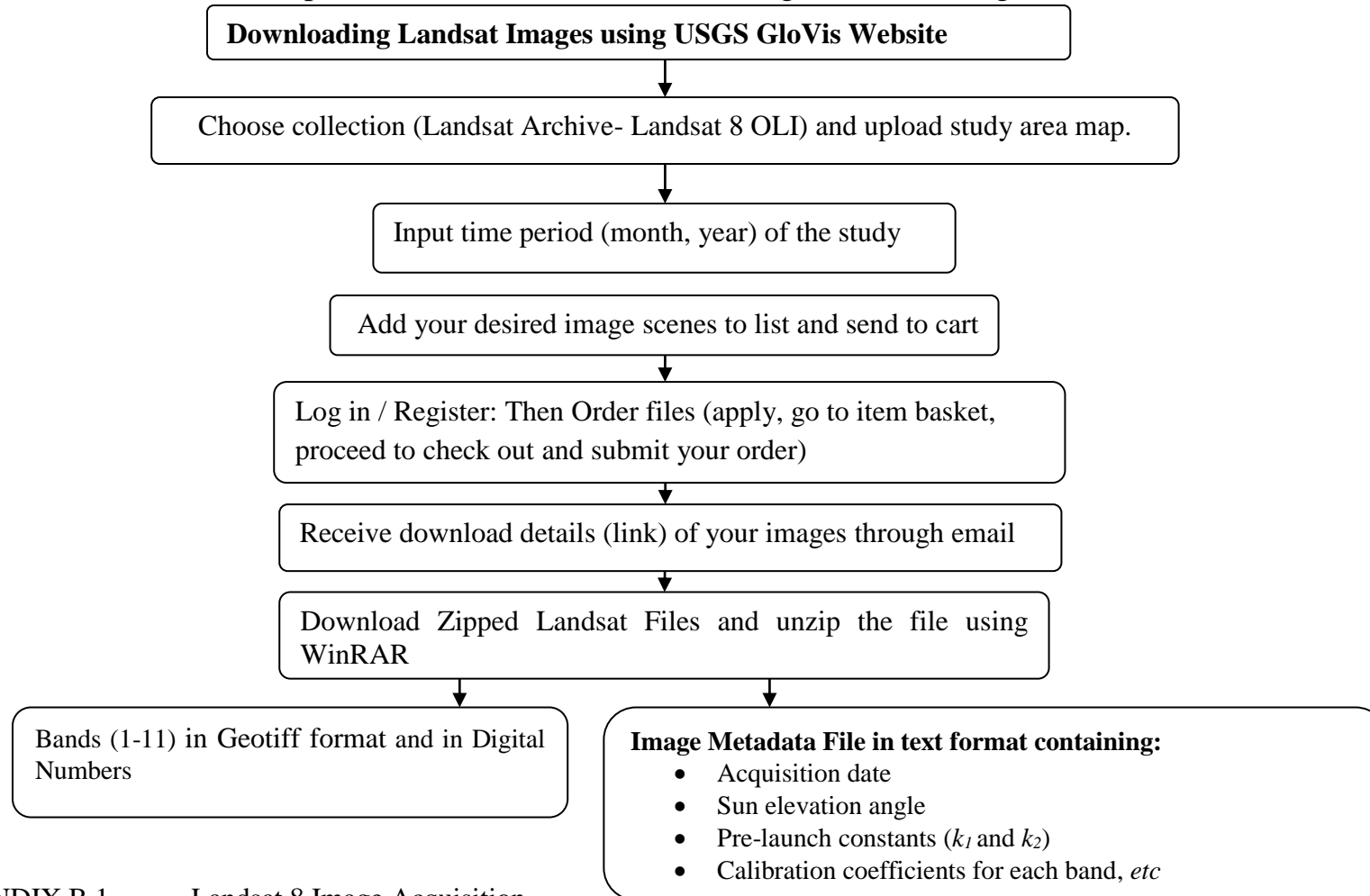


Appendix A. 1 MODIS L1B image acquisition

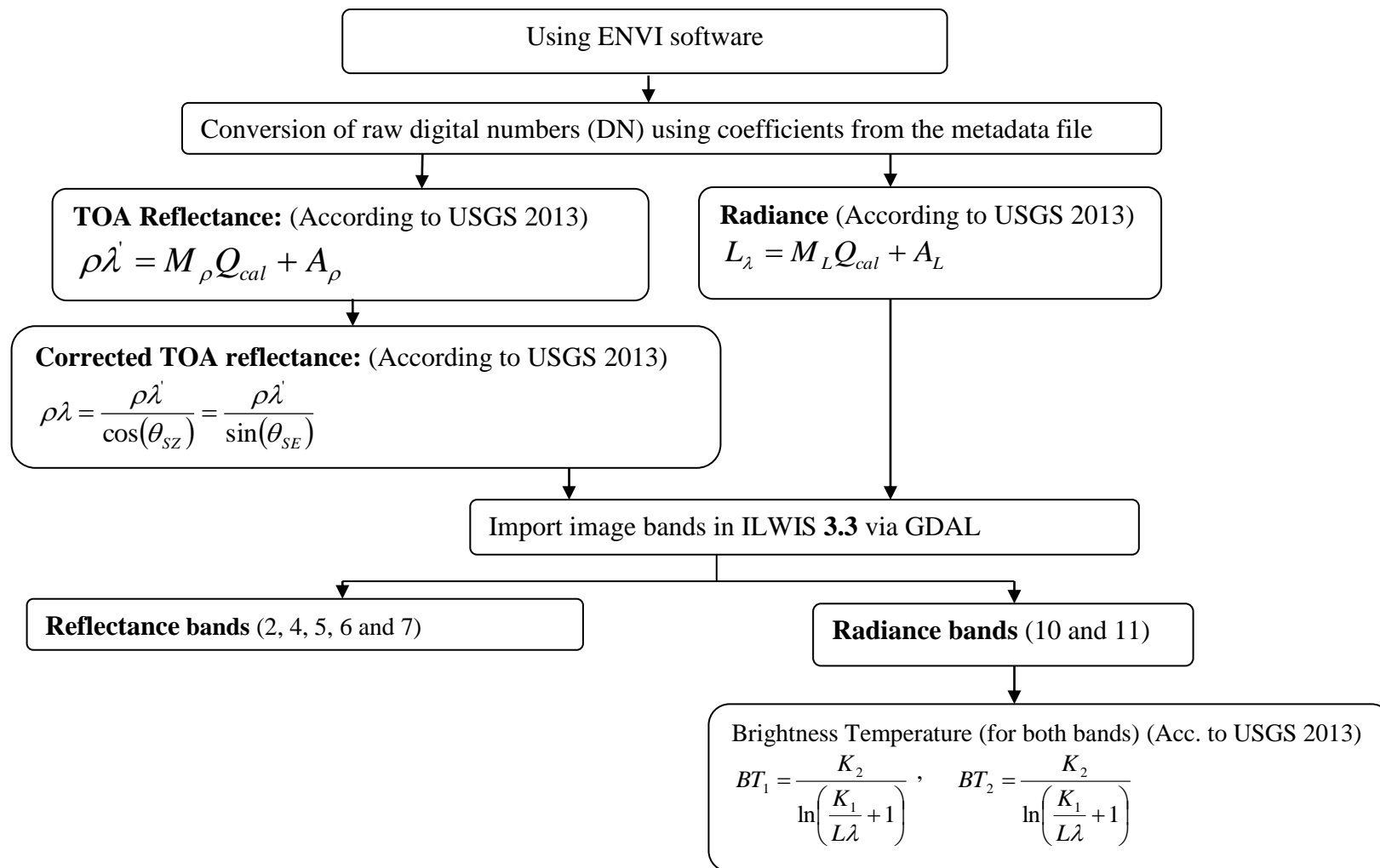


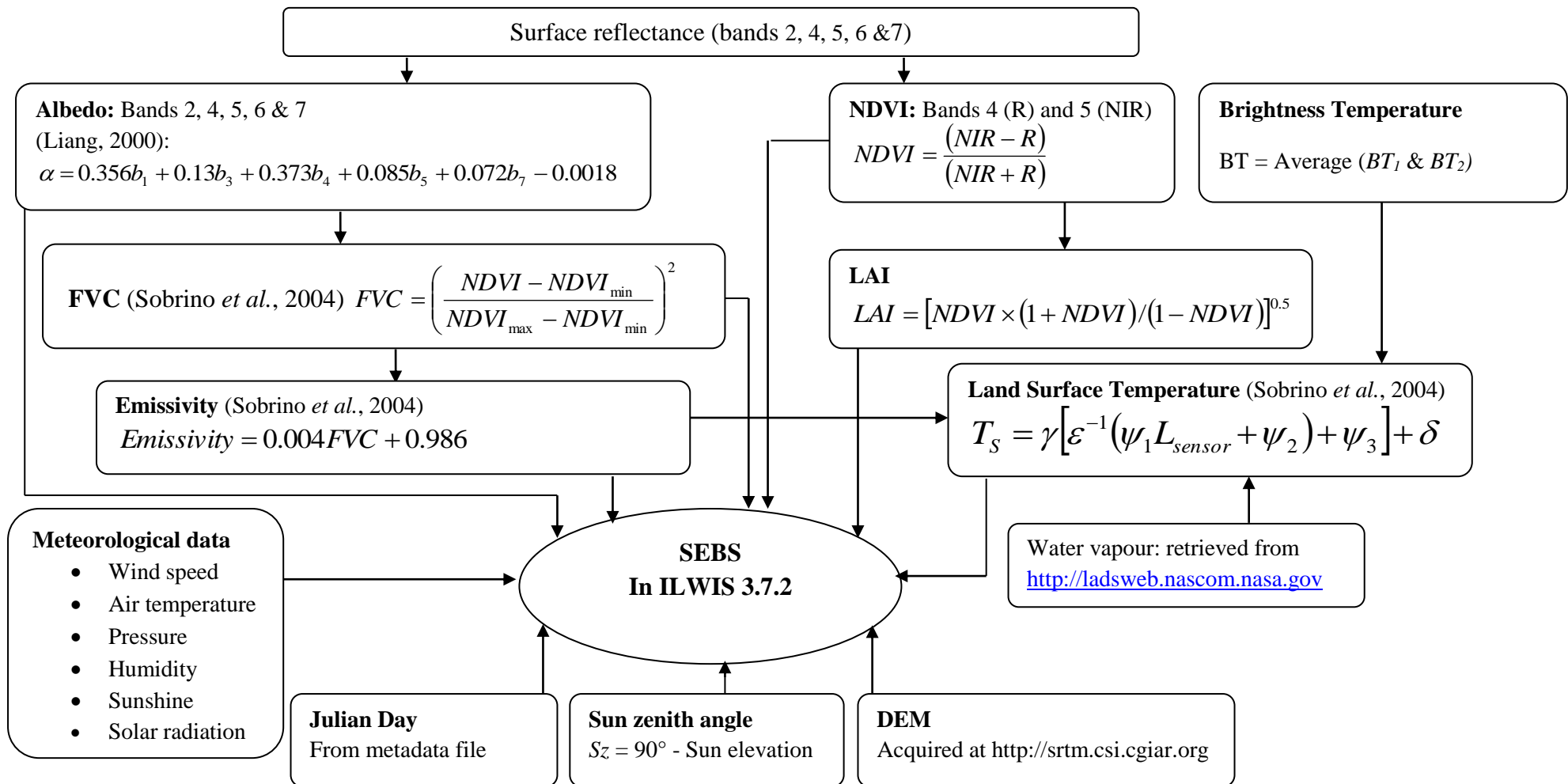


APPENDIX B Total evaporation estimation flowcharts using Landsat 8 images



APPENDIX B.1 Landsat 8 Image Acquisition





APPENDIX B.3 SEBS Computation using Landsat 8 Images